

ABSTRACT

Title of Document:

A SUNLIGHT TO MICROWAVE POWER
TRANSMISSION MODULE PROTOTYPE
FOR SPACE SOLAR POWER

Paul Iven Jaffe, Doctor of Philosophy, 2013

Directed By:

Professor Victor L. Granatstein,
Department of Electrical and Computer
Engineering

The prospect of effectively limitless, continuous electricity from orbiting satellites for use on earth has captured many people's interest for decades. The proposed approach typically entails collection of solar energy, its conversion to microwave energy, and the wireless transmission of the microwaves to the earth. This offers the benefit of providing baseload power while avoiding diurnal cycle and atmospheric losses associated with terrestrial solar power. Proponents have contended that the implementation of such systems would offer energy security, environmental, and broad technological advantages to those who would undertake their development, while critics have pointed out economic, political, and logistical barriers. Niche applications, such as provision of power to remote military bases, might better tolerate the higher energy costs associated with early operational systems.

Among recent implementations commonly proposed for solar power satellites, highly modular concepts have received considerable attention. Each employs an array

of modules for performing conversion of sunlight into microwaves for transmission to earth. This work details results achieved in the design, development, integration, and testing of photovoltaic arrays, power electronics, microwave conversion electronics, and antennas for 2.45 GHz microwave-based "sandwich" module prototypes. Prototypes were fabricated and subjected to the challenging conditions inherent in the space environment, including solar concentration levels in which an array of modules might be required to operate. This testing of sandwich modules for solar power satellites in vacuum represents the first such effort.

The effort culminated with two new sandwich module designs, "tile" and "step", each having respectively area-specific masses of 21.9 kg/m^2 and 36.5 kg/m^2 , and mass-specific power figures of 4.5 W/kg at minimum one sun and 5.8 W/kg at minimum 2.2 suns (AM0) simulated solar illumination. The total combined sunlight to microwave efficiency of the modules was shown to be on the order of 8% and 7% for vacuum operation in the 10^{-6} torr regime. These represent the highest reported combined sandwich module efficiencies under either ambient or vacuum conditions, nearly quadrupling the previous efficiency record. The novel "step" concept was created to address thermal concerns and resulted in a patent publication.

Results from module characterization are presented in context and compared with figures of merit, and practical thresholds are formulated and applied. The results and discussion presented provide an empirical basis for assessment of solar power satellite economic models, and point to several opportunities for improvements in area-specific mass, mass-specific power, and combined conversion efficiency of future prototypes.

A SUNLIGHT TO MICROWAVE POWER TRANSMISSION MODULE
PROTOTYPE FOR SPACE SOLAR POWER

By

Paul Iven Jaffe

Dissertation submitted to the Faculty of the Graduate School of the
University of Maryland, College Park, in partial fulfillment
of the requirements for the degree of
Doctor of Philosophy
2013

Advisory Committee:

Professor Victor L. Granatstein, Chair/Advisor
Professor Martin C. Peckerar
Professor John Melngailis
Professor Jeremy Munday
Professor David Akin

Dedication

This work is dedicated to my wife, Rachael Schoenbaum, and our two young sons, Jules and Elliott. Without their unflagging support, it surely would not have been possible.

Acknowledgements

First and foremost, I thank my advisor, Professor Victor Granatstein. His sustained encouragement and confidence in my efforts buoyed me through many challenging times when I might otherwise have faltered. The debt I owe him I will strive to pay forward by assisting others in their own research and academic pursuits.

The outstanding and engaged faculty and staff in the graduate office of the University of Maryland were key enablers of my work and studies, including Professor Martin Peckerar, Dr. Tracy Chung, Melanie Prange, and Maria Hoo.

My journey and interest in this research area might never have started were it not for the inspiration and comprehensive technical overview supplied by John Mankins, former manager of Advanced Concepts Studies at NASA. His infectious enthusiasm, persistence, and tremendous depth and breadth of knowledge should serve as examples to researchers and program managers everywhere.

The creation of the climate conducive for my study of this topic is traceable to the efforts of Dr. Gerry Borsuk, and the encouragement in the initial development of the proposal came from Dr. Jill Dahlburg and Dr. Rob Walters.

I had the good fortune of receiving selfless and extensive comments on the original research proposal, as well as feedback during the course of the project and the thesis development process from luminaries in the field, notably Dr. James McSpadden, Professor Nobuyuki Kaya, and Dr. Frank Little.

This endeavor could never have commenced without the opportunities afforded by my employer, the U. S. Naval Research Laboratory (NRL). My supervisor, Mark Johnson, and my organization's management have been steadfast and accommodating

in their support of my development and of the project itself, including Bob Towsley, Bill Raynor, Jerry Golba, John Schaub, Pete Wilhelm, and Dr. John Montgomery. Key administrative support was provided by Nancy Peaper and Arthur Espanta. The funding for this work came from an NRL Base Program 6.2 research effort.

The NRL team that supported the development and testing effort is large and accomplished. Jason Hodkin supplied critical RF design prowess, Dr. Mike Nurnberger provided the antenna design, Clark Person delivered the highly efficient power electronics, Forest Harrington drafted the many iterations of the mechanical design, Bang Nguyen performed detailed thermal analyses, Susie LaCava managed the essential solar array development and carefully proofread this thesis, Dave Scheiman was invaluable in the creation and understanding of the solar simulation approach, Kathy Seymour assembled and reworked the module electronics, Mike Freeman guided our thermal feature and instrumentation implementation, and Trevor Specht and Ray Dixon aided the interfacing of all our test equipment to the facility's electrical mains. Additional invaluable assistance came from Mike Brown, Kwok Cheung, Sheleen Spencer, Matthew Long, and Jim Pirozzoli.

Phil Jenkins, Maria Gonzalez, Dr. John Pasour, Dr. Baruch Levush, George Flach, Dr. Kieran Carroll, Doug Sinclair, Sean Lynch, and Professor Kameswara Rao Bhamidipaty provided subject matter expertise, sage and vital inputs, and valuable advice at crucial points in the project.

Numerous fabrication and test facility technicians played imperative parts in helping everything come together safely and effectively, including Mike Van Herpe,

Chris Calder, Paul Peffers, Tim Wilson, Bernie Lafrance, Paul Stencel, Mickey Dougherty, Frank Trimble, Mike Derosa, and others.

Mark Kanawati and Dr. Dino Lorenzini of SpaceQuest, Ltd. were incredibly knowledgeable, patient, and flexible as our solar array needs evolved, and they delivered outstanding hardware that from any other source likely would not have met the technical requirements or would have exceeded the available resources.

Many students performed indispensable roles during the project: Andrew Han was instrumental from its inception to completion, Grant Stewart was unparalleled in his ability to simply get things done, Karina Hemmendinger diligently kept the integrated testing on track, Ethan Hettwer developed and executed test scripts for the earliest RF environmental testing, Owen Nugent contributed rectenna work, Kate Aplin aided with background research and proposal review, Daniel Rhoades developed the original light field characterization methods, Sanjeet Das executed the pathfinding power beaming demonstration, Michael Long worked through endless solar panel geometries, and many others assisted as well, including but not limited to: Rashaad Patterson, Donald Thomas, Evan Siefring, Kanyetta Washington, Mike Taylor, Brad Segelhorst, Thanh Pham, Magda Moses, and Ben Adducci.

I've gleaned tremendous knowledge and insights from other young researchers in the field, including Dr. Martin Leitgab, Ian McNally, Corey Bergsrud, and Bea Adkins. Dr. Seth Potter and Dr. Peter Schubert have also provided great professional inspiration.

Colleagues who provided support and who were patient with me as I was consumed by this project and other responsibilities include Dr. Rich Fischer,

Professor Steve Blank, Professor Reza Zekavat, Darel Preble, Steve Leete, and Bert Murray.

I would be remiss if I did not acknowledge just a few of the many influential and inspirational teachers I've had over the years, including Professor Dan Jablonski, Professor Dan Dockery, Professor Chuan Sheng Liu, Professor Leonard Taylor, Professor Kazuo Nakajima, Judy Parsons, Ursula Alexander, Diane Albertini, and Barbara Case.

While the outstanding staff at Joint Base Anacostia Bolling Child Development Center II provided first-rate childcare, the librarians of the community library provided a quiet place to think and write for countless hours, and free popcorn on some Fridays.

Though I'm sure I've forgotten many others who made it possible, I will never forget my family, parents, and grandparents, who in large part made me who I am today by instilling and nurturing within me an insatiable curiosity and a love of learning.

Table of Contents

Dedication	ii
Acknowledgements	iii
Table of Contents	vii
List of Tables	ix
List of Figures	x
Chapter 1: Introduction	1
Motivation	1
Historical Perspective	3
Solar Power Satellite “Reference System”	7
Modular Implementation Concepts	9
The Sandwich Module	10
Goals	16
Chapter 2: Sandwich Module Prototype Development	18
Thermal Analysis	18
Step Module Concept	23
Critical Tradeoffs	27
Photovoltaics	27
DC-to-RF conversion	32
Antenna Elements	38
Module Architectures	41
Thermal Control Methods	41
Design Iteration	43
Module Fabrication	43
Chapter 3: Prototype Testing	45
Progressive Testing	45
Sun Simulation	47
Xenon Light Source	47
Light Attenuating Screens	50
Light Field Characterization	52
Space Environment Simulation	58
Fused Silica Window	59
Thermal Vacuum Chamber	62
Summary Comparison of Space, Simulated Space, and Ambient Environments	69
Supporting Equipment and Configuration for Module Testing	70
Chapter 4: Results and Discussion	75
Overview	75
Effects of Varying Illumination Conditions and Vacuum	75
Ambient Testing with Varying Illumination	75

Vacuum Testing with Varying Illumination	77
Key Figures of Merit and Results	81
Collect/Transmit Area-Specific Mass [kg/m ²].....	81
Mass-Specific Transmitted Power [W/kg].....	84
Combined Conversion Efficiency.....	85
Additional Figures of Merit and Module Qualities of Interest	88
 Chapter 5: Potential Economic Thresholds.....	90
Generalized Comparison of Energy Sources	90
Economic Analyses for Solar Power Satellites.....	91
 Chapter 6: Conclusions	102
Summary	102
Implications of Present Work	103
Future Work	103
Specialized Test Facility Development	103
Antenna Characterization.....	105
Mass Reduction.....	106
Thermal Management Improvements	107
Thermal Instrumentation Improvements.....	110
Efficiency Enhancement	111
Additional Module Functionality.....	112
Alternative Sandwich Module Approaches	112
 Appendix A: Microwave Power Transmission.....	115
Appendix B: SPS System Design	123
References.....	125

List of Tables

Table 1: Projected RF signal and efficiency chain performance for tile module.	35
Table 2: Screen designations with blockage and throughput percentages from manufacturer specifications.	50
Table 3: Screen designations and sun concentrations for initial tile module testing focus settings.....	52
Table 4: Comparison of Space and Simulated Space Environments for Sandwich Module Operation	70
Table 5: Tile module mass breakdowns.....	83
Table 6. Efficiencies for the 2.45 GHz prototype tile module in vacuum at about one sun illumination (117W input over 0.087m ²).	87
Table 7: Minimal inputs for a space solar power cost model	92
Table 8: Four cases with varying assumptions to generate Levelized Cost of Energy values for solar power satellites.....	97
Table 9: Comparison of simple solar power satellite Levelized Cost of Energy cases with conventional sources in \$/MWh. Conventional energy data from the U. S. Energy Information Administration.....	98
Table 10: Comparison of fully burdened cost of fuel kWh kerosene-based jet fuel equivalents to solar power satellite levelized cost of energy model results.	100
Table 11. Comparison of selected means of amplification and DC to RF conversion.	120
Table 12: System designs examined by the URSI report	124

List of Figures

Figure 1: Space Solar Power segments and efficiency figures adapted and updated from the DOE/NASA studies.....	6
Figure 2: A recent 5.8 GHz derivative by the Solar High Study Group of the original 1978 DOE/NASA SPS Reference System concept.....	8
Figure 3: Modular Symmetric Concentrator concept, circa 2007.....	10
Figure 4: Depiction of the functional layers of the sandwich module.....	11
Figure 5: Sandwich module layers showing subfunctions.....	12
Figure 6: The subset of sandwich module functions implemented in this research effort.....	16
Figure 7: Solar power intercepted at one sun (AM0) by a 28 cm by 28 cm module and combined module efficiency with notional layer efficiency estimates.....	19
Figure 8: Radiator area required to maintain temperature equilibrium for a 28 cm by 28 cm module at 23% efficiency	20
Figure 9: Temperature of a 28 cm by 28 cm module with both sides as black body radiators for various module efficiencies.....	21
Figure 10: Thermal Desktop® simulation of a sandwich module under 3 suns of illumination	22
Figure 11: Photovoltaics and transmit antenna comprised of tile modules.	24
Figure 12: Photovoltaics and transmission antenna comprised of step modules.....	24
Figure 13: Thermal Desktop® simulation of a step module under 3 suns of illumination.....	26
Figure 14: Layer stackup and I-V curve for the Spectrolab UTJ photovoltaic cells from the datasheet.....	28
Figure 15: Conversion module solar panel for a tile module.....	29
Figure 16: Conversion module solar panel for a step module.	29
Figure 17: Representative array string I-V and power data plot collected with direct sun-simulated illumination.....	30
Figure 18: I-V curves showing the effect of temperature on panel open circuit voltage with lamp output attenuated by screens to produce about one sun.....	31
Figure 19. DC power and RF electronics baseplate for the tile module.	33
Figure 20. Characterization of Power Added Efficiency performance of final stage amplifier.....	34
Figure 21: Step module prototype with antenna mockup, electronics shown at left. .	36
Figure 22: A representative spectrum analyzer screen capture from monitoring of the RF bandwidth, harmonics, and center frequency. This capture is for the step module while powered by a solar array simulator.	37
Figure 23: Simulated surface currents of short backfire antenna	39
Figure 24: Simulated gain pattern for a short backfire antenna at 2.45 GHz	40
Figure 25: Integrated tile module showing from top to bottom: solar array, conversion electronics with multilayer thermal blankets and black Kapton® tape, and antenna mockup.....	42
Figure 26: Tile module integration and test flow overview.....	46
Figure 27: 4,000W xenon light source with power supply.....	48

Figure 28: Spectrum of 4,000W L.P. Associates xenon lamp.....	49
Figure 29: The five light attenuating screens labeled with percent open area.....	51
Figure 30: BeamGage software screen capture.....	53
Figure 31: A light field portion matching the solar array size that has been processed to show the number of suns of intensity incident on each cell area, adapted from ...	55
Figure 32: Two lamp beam mapping showing equivalent number of suns of intensity over solar cell areas, adapted from	56
Figure 33: UV Grade Fused Silica Transmission Curve	59
Figure 34: Solar Radiation Spectrum	60
Figure 35: The fused silica window used with the vacuum chamber.....	61
Figure 36: DC and RF electronics in thermal vacuum chamber with fused silica window sealing chamber opening.....	62
Figure 37: Thermal vacuum chamber prior to fused silica window installation.	63
Figure 38: Module prototype in thermal vacuum chamber with fused silica window sealing chamber opening and vacuum chamber internals visible.....	64
Figure 39: Liquid nitrogen shroud cooling apparatus.....	66
Figure 40: Depiction of step module in vacuum chamber configuration	68
Figure 41: Step module installed in vacuum chamber for testing prior to installation of the fused silica window.	69
Figure 42: DC and RF electronics test support equipment.....	71
Figure 43: Subset of tile module temperature points collected during a representative vacuum test.	72
Figure 44: Insertion loss measurement of the step module RF power measurement configuration.	73
Figure 45: Test configuration for vacuum testing with illumination for the tile module	74
Figure 46: Tile module RF conversion efficiency and solar array temperature during testing at ambient pressure under various illumination conditions.....	76
Figure 47: Tile module RF conversion efficiency, solar array power, and RF output power vs. time with various illumination conditions at ambient pressure.....	77
Figure 48: Tile module electronics efficiency, solar array output power, solar array voltage, and RF output power as a function of different operating conditions. Each cluster of three points represents the mean, minimum, and maximum.	78
Figure 49: Tile module temperatures as a function of different operating conditions	80
Figure 50: Mass contributions of major categories of tile sandwich module parts. ...	84
Figure 51: NRL RF Anechoic Chamber	106
Figure 52. Power collection efficiency as a function of τ with optimum power taper over the transmitting aperture	117
Figure 53. One-way sea level to zenith (straight up through the entire atmosphere) attenuations in clear sky conditions	118
Figure 54. Rectenna components	122

Chapter 1: Introduction

Motivation

Global climate change and the consequent need for energy sources that avoid further contributions to climate degradation loom as significant societal concerns. It is widely realized that many sources of fossil fuels are either at risk of depletion or increasingly undesirable because of their contributions to greenhouse gases and growing scarcity. While many carbon-free or nearly carbon-free energy alternatives exist, they often suffer from significant problems such as intermittency, lack of scalability, locale dependence, or safety risks.

One promising clean power source is the sun, which has an effectively unlimited energy supply. However, terrestrial collection of solar energy poses problems. The diurnal cycle, atmospheric attenuation, and weather effects all diminish access to solar power. Because of its intrinsic unpredictability, terrestrial solar power necessitates the implementation of some means of energy storage or use in conjunction with one or more predictable sources of power to achieve system viability.

Collection of solar energy in space via satellite coupled with its conversion to microwaves for transmission to the ground largely overcomes these limitations, but it poses formidable engineering challenges and serious questions of economic plausibility. Though solar energy provided to the earth from space had been principally been considered in the past only for utility grid cases, the past decade has

seen greater interest in niche applications that could tolerate the higher expenses that would likely be associated with an initial capability. Such instances include power provision to remote locations with minimal infrastructure, military bases in forward areas, and areas devastated by natural disasters. A premium cost for power could be justifiably borne in these and other cases, particularly if it is still less expensive, more reliable, or more sustainable than existing alternatives. If such an implementation were pursued, it could serve to aid in the development and refinement of the needed technologies to improve the economic viability for the utility grid case.

Solar power satellite (SPS) (also known as space solar power (SSP)) concepts have been examined in depth on several occasions in the past, and interest has been renewed in recent years in part because of improvements in a number of supporting technologies. These include: increased solar cell efficiency, increased solid state power amplifier efficiency, large space structures advances, and technology developments for robotic assembly in space. Recent solar power system studies have been significantly limited in their ability to accurately determine the costs and challenges of deploying an operational system by the small amount of actual hardware development that has been done to show the feasibility of key SPS technological elements.

Recent space solar power system designs of widespread interest capitalize on highly modular architectures. However, assessments of their technical soundness are hampered by a dearth of substantive efforts to identify and resolve concerns about their component technologies, most notably those pertaining to the sandwich module.

The motivation for this research was the need for a critical examination of the challenges associated with sandwich module development.

Historical Perspective

The prospect of collecting a continuous, massive amount of solar energy in orbit and transferring it via wireless power transmission for use on earth has held the interest of a significant group of advocates and researchers for decades. Light from the sun is more intense in space because it is not attenuated by clouds or the atmosphere, and a satellite in geosynchronous orbit is illuminated essentially year-round, whereas terrestrial solar power systems must contend with seasonal sunlight variation and nighttime. Widely recognized as physically possible but economically prohibitive, interest in space solar power has resurged in recent years as a consequence of increased media attention resulting from government and non-governmental organization reports, as well as through efforts by private companies and national space agencies to develop or stimulate the development of practical space solar power systems. Thoughtful and reasoned criticisms [1][2] and counter-criticisms [3] have offered excellent summary insights into some of the major issues.

Major funded studies were conducted by the U.S. Department of Energy (DOE) and the National Aeronautics and Space Administration (NASA) during the late 1970s [4], the National Research Council in 1981 [5], and again by NASA in 1995 and 1999 in the form of the “Fresh Look” study [6] and Space Solar Power Exploratory Research and Technology (SERT) program [7], respectively. Many other funded and unfunded studies have been undertaken by the European Space Agency (ESA) [8], the Japanese Space Agency (JAXA) [9], The International Union

of Radio Science (URSI) [10], the U.S. National Security Space Office (NSSO) [11], the U.S. Naval Research Laboratory (NRL) [12], and numerous other national and international organizations [13]. In late 2011, the International Academy of Astronautics published “Green Energy from Space Solar Power - The First International Assessment of Space Solar Power: Opportunities, Issues and Potential Pathways Forward” [14]. There have also been many books written about SSP, including the comprehensive text *Solar Power Satellites* [15] edited by Peter Glaser, the original patent holder of the SSP concept, and an excellent recently published introductory text by Flournoy [16]. As of August 2013, approximately half a dozen corporate entities are explicitly endeavoring to develop space solar power systems, including PowerSat [17], Mitsubishi Electric [18], Solaren Space [19], and Space Energy [20].

Several different approaches to SSP have been proposed. Fundamentally, each has a means of solar energy collection and a method for conveying the collected energy to the ground. For collection, photovoltaics and solar thermal have principally been considered. For transmission, microwave frequencies and lasers have been examined. Solar-pumped lasers and large spaceborne mirrors have been proposed as combined collection and transmission schemes. Each collection and transmission scheme offers distinct advantages and disadvantages. Photovoltaics (PV) are considered for their comparative reliability and simplicity, while solar thermal is advocated for its theoretical ability to achieve efficiencies transcending the Shockley–Queisser limit [21] that bounds photovoltaics. Laser transmission is cited for its ability to utilize smaller transmitter and receiver apertures, whereas microwave transmission is

favored for its greatly reduced susceptibility to attenuation from tropospheric effects. Microwave power transmission has been investigated extensively for space solar power applications and enjoys many decades of terrestrial demonstrations, as documented in detail by William Brown [22]. A discussion of microwave power transmission is included as Appendix A.

Common technical concerns for all SSP implementations include total space segment mass, transmitted energy density on the ground, conversion efficiencies of the space and ground segments, power beam pointing and control, interaction between the power beam and the ionosphere and troposphere, and electromagnetic compatibility with other satellites and terrestrial services. These concerns and many others were examined exhaustively in the DOE/NASA studies of the 1970s, and in many cases works performed in association with these studies or their derivatives remain the exemplars for any future efforts. One such instance is the reference system functional breakdown and efficiency chain for the photovoltaic collection/microwave transmission scheme, an adaptation of which can be seen in Figure 1, notionally at 2.45 GHz. The efficiency figures are largely unchanged from the original assessment, with the notable exception of the PV efficiency. These are now on the order of 30% for commercially available space-rated photovoltaic cells, versus the 15% figure used in the DOE/NASA study.

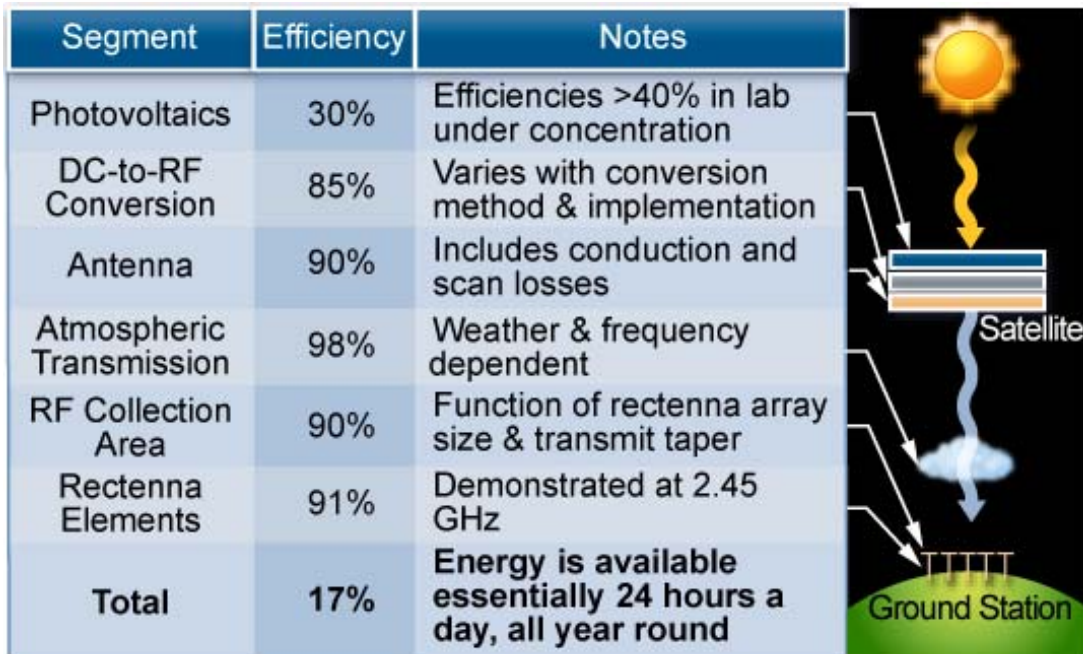


Figure 1: Space Solar Power segments and efficiency figures adapted and updated from the DOE/NASA studies [23].

In this work, the focus was principally on the development and testing of a prototype that implements the first three segments from Figure 1: photovoltaics, DC-to-RF conversion, and the antenna. The other segments are addressed only to provide context and illustrate some of the considerations that would go into a complete system.

Over a dozen major classes of solar power satellite (SPS) architectures have been proposed by different researchers. The most relevant to this work are those that employ photovoltaics for solar energy collection and microwave power transmission to deliver the energy to the earth, and in particular those that depend on the utilization of “sandwich” modules. The attraction to this specific approach can be appreciated by

examining some selected forerunners and understanding their limitations and challenges.

Solar Power Satellite “Reference System”

Any solar power satellite would have a large number of subsystems and design considerations. Though largely beyond the scope of this work, Appendix B: SPS System Design delves into general considerations such as space and ground aperture sizing and transmit frequency selection. For this discussion, focus is confined primarily to the DOE/NASA “Reference System” and its variants.

Figure 2 shows a recent derivative by the Solar High Study Group of the DOE/NASA “Reference System” that arose from the eponymous studies, and which features the combination of photovoltaics and microwave power transmission. It consists of an enormous satellite in geosynchronous orbit (GEO) with separate solar collection and power transmission surfaces. These are connected by wire harnessing and a slip ring mechanism that must transfer thousands of amps of current. The satellite would send many GWs of electricity to the utility grid via a microwave downlink operating at either 2.45 or 5.8 GHz, which would be collected by large rectifying antenna (rectenna) receiving stations [24].

This approach fits within the “perpendicular to orbital plane” class of SPS. For each perpendicular to orbital plane concept, the solar collection surface rotates on an axis perpendicular to the orbital plane in order to track the sun, and collected energy is routed to one or more transmission antennas that point at the earth to direct the energy beam.

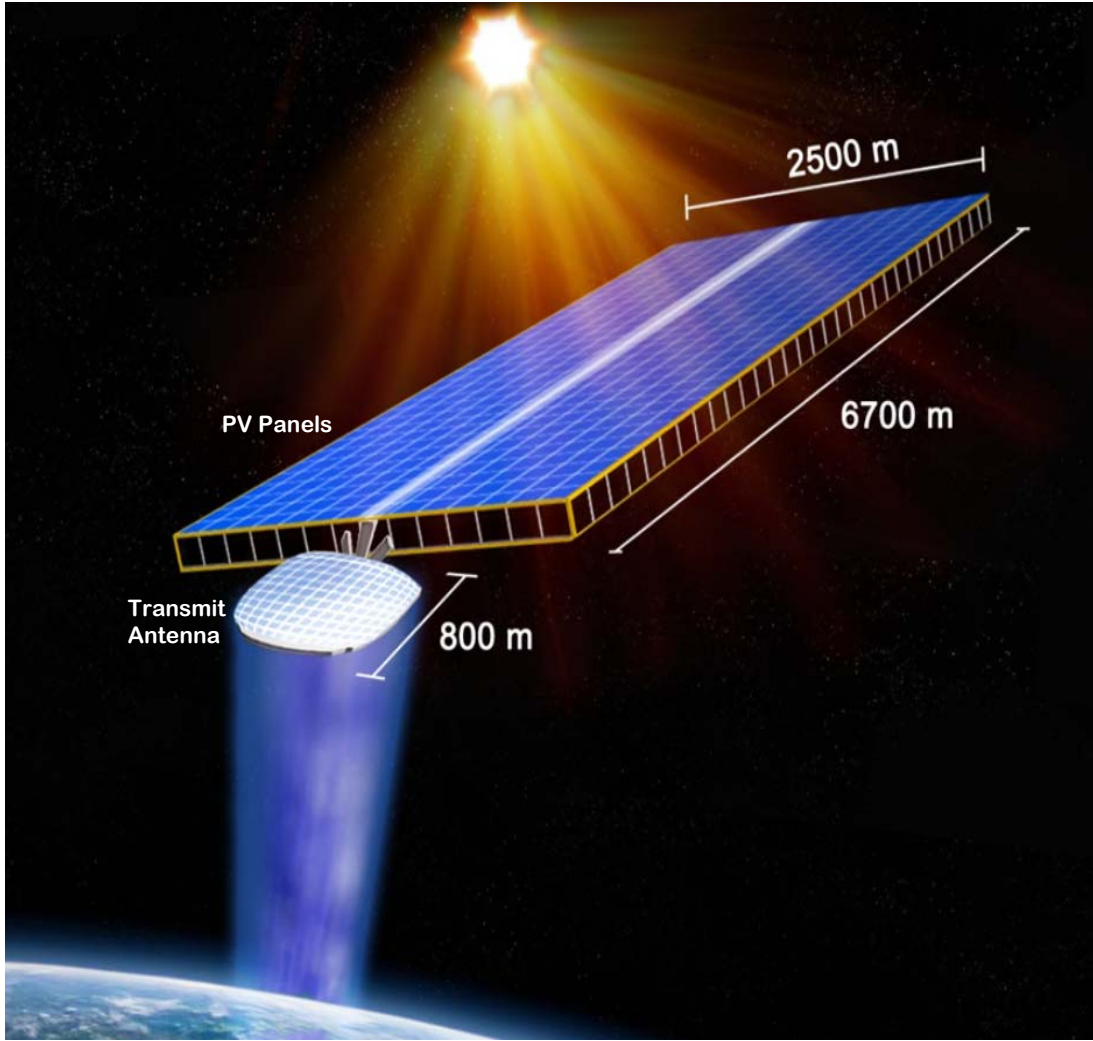


Figure 2: A recent 5.8 GHz derivative by the Solar High Study Group [25] of the original 1978 DOE/NASA SPS Reference System concept. A 525 m diameter transmit antenna version was also proposed.

The collection surface and the plane containing the antenna aperture must necessarily be pointed independently of each other, necessitating the aforementioned slip ring mechanism or some other means of energy redirection. Naturally, wiring to route the power around the satellite must be employed and this wiring undesirably contributes

to the overall spacecraft mass. The slip ring mechanism poses intrinsic reliability concerns due to its representing a potential single point of failure, especially at high operating powers. These shortcomings led researchers to investigate alternatives, like those that use sandwich modules, which address these possibly crippling problems.

Modular Implementation Concepts

Implementation schemes that avoid the mass and reliability failings of the Reference System and other previously proposed designs are those based heavily on modular system elements, such as the Modular Symmetrical Concentrator (MSC), a derivative of the Integrated Symmetrical Concentrator concept [26], and the SPS-Arbitrarily Large Phased Array (ALPHA) concept [27]. These approaches utilize optical energy routing and a microwave transmit aperture constructed from essentially identical elements. This avoids the need for a large, conductive rotating joint and limits wiring mass compared to historical reference concepts since the transmitters that relay the energy are located in close proximity to the photovoltaic cells that collect it. The use of modular elements offers the possibility of improved economy through mass production. Employing solar concentration could reduce the required launch mass and as a result lower the system cost, but it increases the magnitude of the thermal challenges. A depiction of a proposed MSC satellite is shown in Figure 3. Though this image shows a monolithic structure, it might also be possible to use several satellites flying in formation to dispense with the connecting structures.

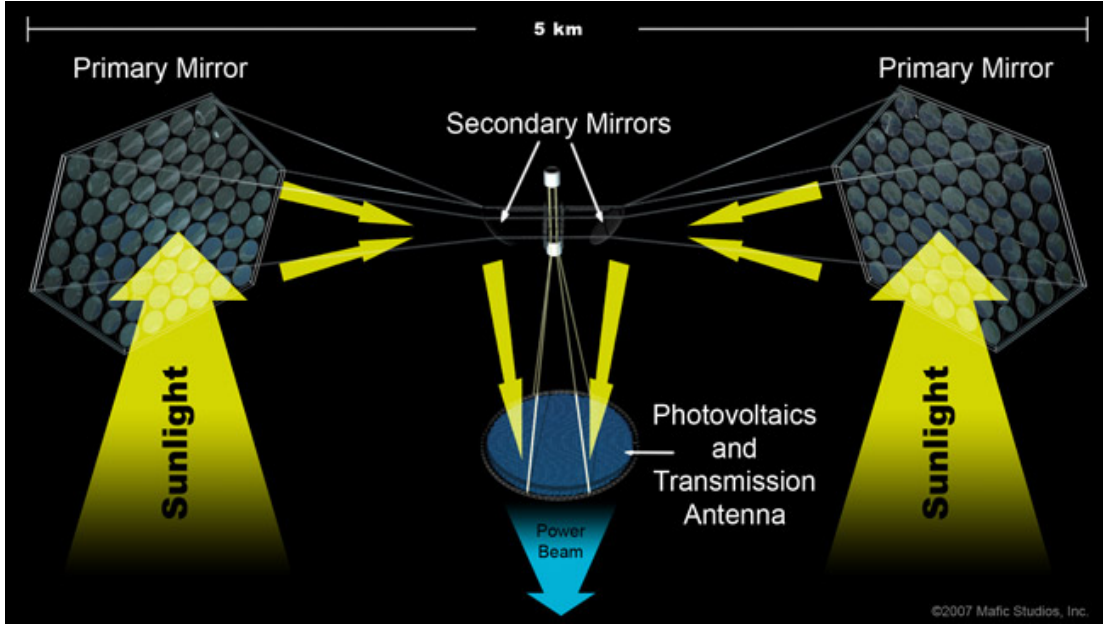


Figure 3: Modular Symmetric Concentrator concept [11], circa 2007.

The SPS-ALPHA concept takes modularity a step further and calls for effectively every element of the satellite to be modular. This concept is described in detail by Mankins in [27].

The Sandwich Module

The key element in most modular SSP architectures is the sandwich module, an idea which had first been seriously investigated in association with the original DOE/NASA studies [28]. The sandwich module as originally conceived performs functions separable into three layers: solar energy collection and conversion to direct current electricity, generation of a microwave signal of suitable frequency and amplitude for transmission, and transmission of the microwave energy. An array of modules is envisioned to be used in the formation of the immense spaceborne transmit antenna aperture that provides beam coupling sufficient to provide

meaningful energy transfer to the ground. Each sandwich module would act as an element or subarray in the large phased array antenna. A simple functional representation of a sandwich module appears in Figure 4.

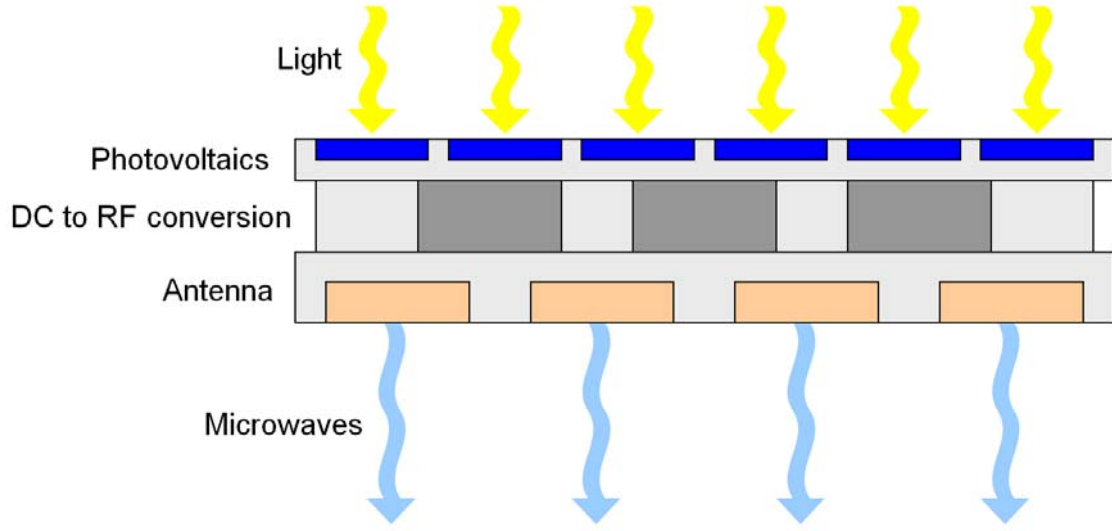


Figure 4: Depiction of the functional layers of the sandwich module.

The lower of these functional layers can be further decomposed into subfunctions that are anticipated to be needed for a module that would be deployed in practice. In the DC to RF conversion layer, the subfunctions include DC power conversion, incorporation of frequency and phase information for beam control, RF amplification and phase shifting, and output filtering. In the antenna layer, in addition to the elements to transmit the power beam, there would likely be separate elements to receive the pilot signal to be used to control beam pointing retrodirectively. This pointing method has been demonstrated safely and effectively on many occasions and is described in [29]. Figure 5 shows a depiction of the subfunctions in context. Note

that the input sunlight could be any of a range of concentrations, depending on the system implementation.

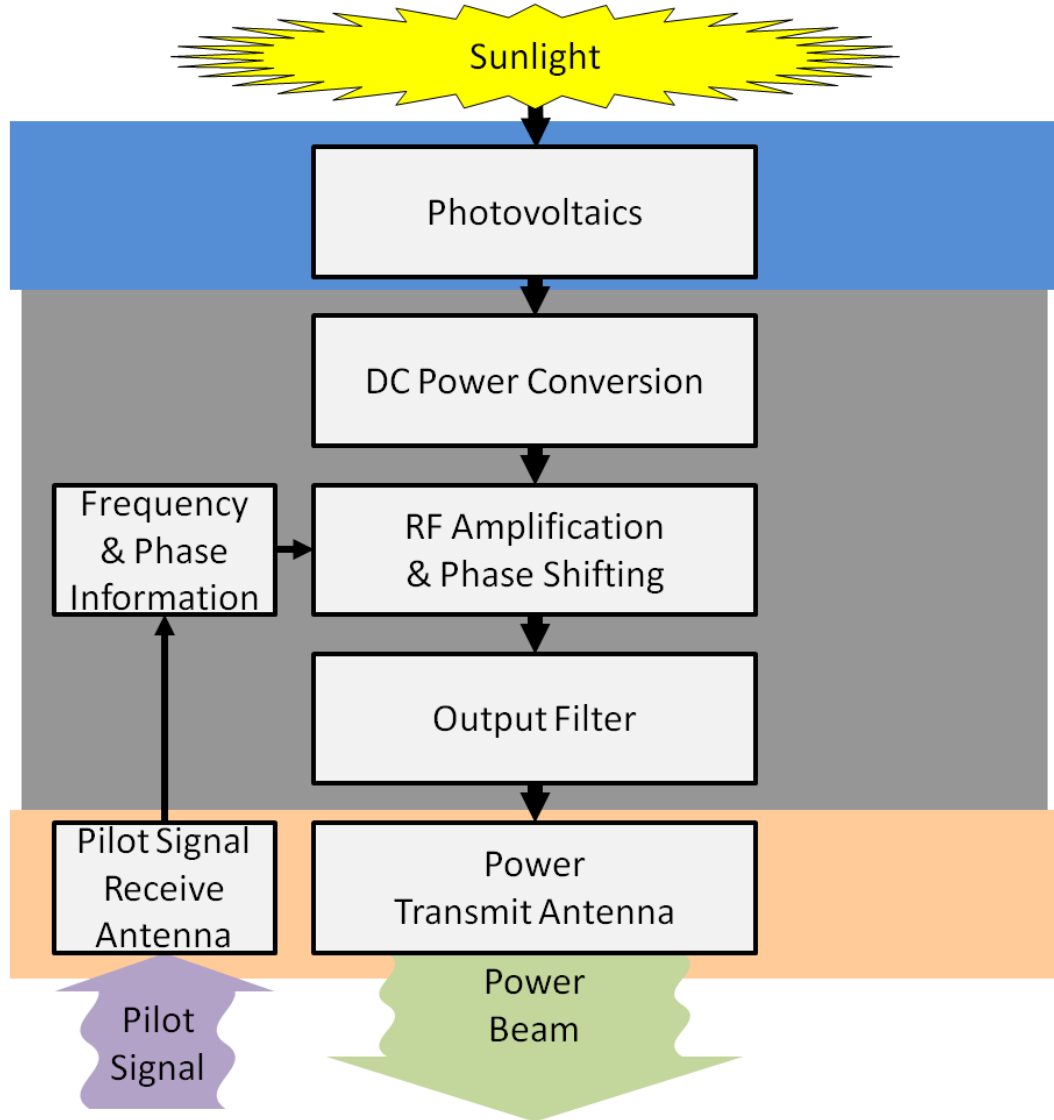


Figure 5: Sandwich module layers showing subfunctions.

Chief among the design challenges of a practical sandwich module are the integration of the various required elements and effective thermal management under adverse conditions. Although these aspects have received some attention from

researchers in the past, there had not been any characterization of a sandwich module prototype's performance in a realistic space environment scenario in conjunction with a comprehensive analysis of the limitations levied by heat transfer, materials, and specific power until this work.

The first exhaustive examination of the sandwich module concept was by Owen Maynard in 1980 [28]. His NASA report "Solid State SPS Microwave Generation and Transmission Study," outlines many of the obstacles and sensitivities associated with the sandwich design. Maynard proposed using solid state field-effect transistor (FET) amplifiers as an alternative to or in conjunction with the vacuum electronics microwave sources that had been suggested in much of the DOE/NASA study documentation. He identified the maintenance of low junction temperatures of the solid state amplifiers used in a sandwich approach as a key point in assuring that acceptable operating lifetimes would result. Solid state amplifier efficiency plays a major role in determining the amount of heat that must be dissipated, as does the efficiency of the adjacent solar cell layer. Lower efficiencies produce more waste heat and thus raise the junction temperature.

Maynard pointed out that an advantage of the solid state amplifiers over vacuum devices is that they do not require high voltages. The many thousands of volts needed for magnetrons and klystrons are difficult to manage in the space environment and necessitate the inclusion of high voltage power converters, introducing another source of conversion inefficiency. Among the issues and possible resolutions Maynard summarizes, charged particle radiation effects and topological considerations stand

out as some that specific part selection and module fabrication could address in a tangible fashion.

Since Maynard’s work, there has been renewed interest in the sandwich module for space solar power and for the modular symmetrical concentrator concept. Japanese researchers in particular have performed analyses and even constructed prototypes of sandwich modules. The first comprehensive prototype was developed in 2000 by Hiroshi Matsumoto of Kyoto University [30]. The effort, dubbed SPRITZ for “Solar Power Radio Integrated Transmitter,” culminated in hardware that included a solar illuminator, sandwich module prototype, and rectenna array for receiving the transmitted power. The solar cells used in the SPRITZ prototype were “about 15%” efficient, resulting in considerable waste heat [31]. The reported RF system efficiency at >25W radiated power output was also 15%, excluding the solar array contribution but including feeder network and phase shifter losses [32]. Because the module was only operated in ambient conditions in which the convective cooling effect of air could assist in the heat dissipation, its probable performance in space could not be accurately characterized. More recently, Nobuyuki Kaya’s group at Kobe University has also produced prototype sandwich modules as part of an ongoing and comprehensive microwave power transmission and SPS technology development campaign. Though the sandwich module development of Kaya’s group focuses primarily on the antenna design and retrodirective control attributes required in an ultimate implementation, attention is also given to amplifier selection and operating conditions. Thermal concerns and amplifier and antenna configuration at 2.4 GHz are outlined in [33].

Because of the complexities associated with addressing every possible functional aspect of a sandwich module, it was decided early on to focus on the most fundamental conversion elements. To this end, functions like implementing retrodirective beam control, phase shifting, output filtering, and actual antenna radiating were deferred for future possible prototypes so that resources could be focused on the photovoltaic conversion, DC-to-RF conversion, and to a lesser extent, antenna design and development. Figure 6 shows the subset of module functions which were implemented in this effort with the substitution of simulated sunlight for actual sunlight and a power measurement in lieu of antenna radiation.

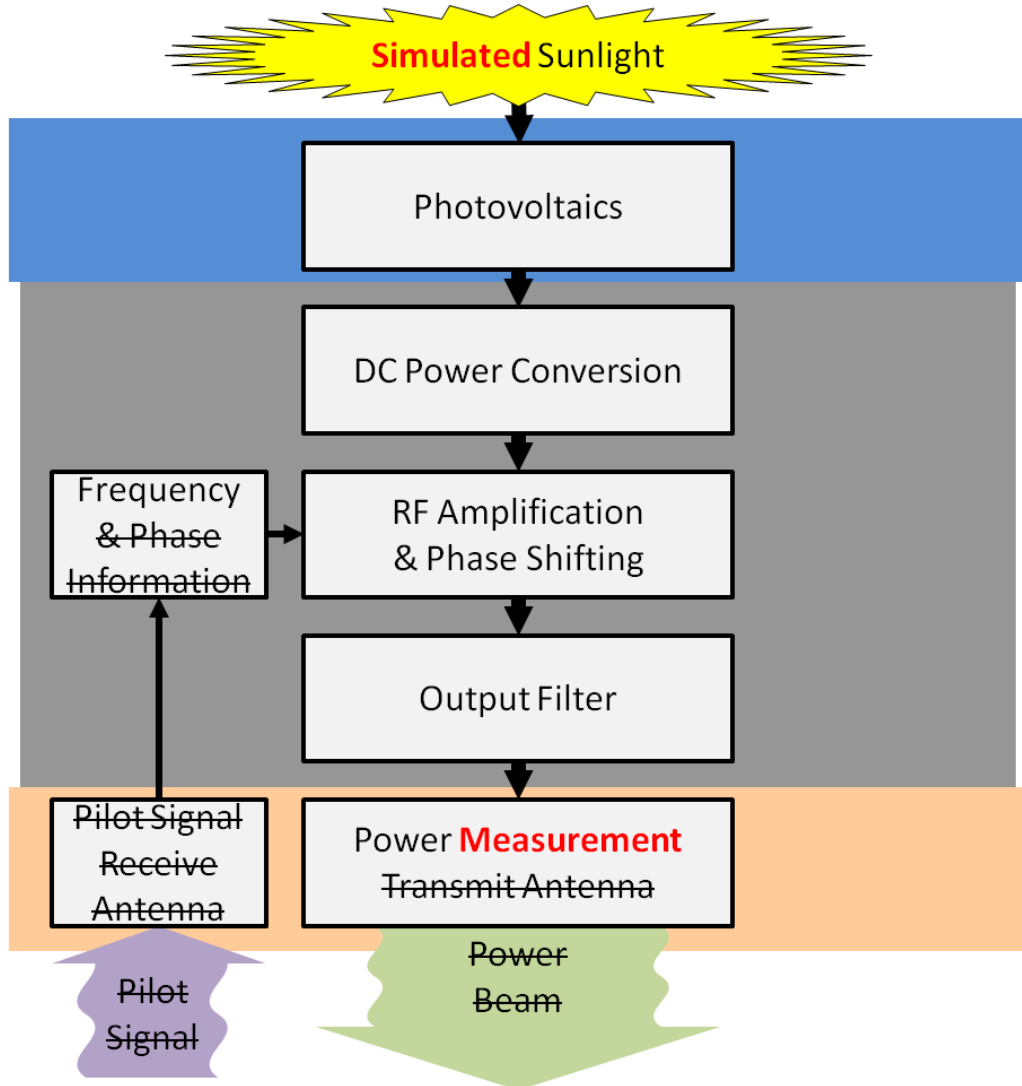


Figure 6: The subset of sandwich module functions implemented in this research effort. Strikethroughs are functions that were not included, and red text indicates a variation from the model in Figure 5.

Goals

For this effort, it was proposed to experimentally investigate, analyze, and address thermal and integration problems inherent in the development of a sandwich module

prototype for photovoltaic collection, DC-to-RF conversion, and wireless power transmission for space solar power so that a prototype could be constructed and tested in a simulated space environment. Specifically, it sought to:

- Design, fabricate, and test the highest mass-specific power, highest total combined efficiency sandwich module to date versus previous efforts.
- Perform the first test of a sandwich module for space solar power under space-like conditions of vacuum and temperature, and to characterize its performance.
- Contribute to an empirical foundation for informed debates on the technical and economic viability of a prominent class of proposed space solar power systems.

These goals were achieved, and the results are described in the remaining chapters.

Chapter 2: Sandwich Module Prototype Development

The module prototype development began with an assessment of the principal design drivers. Because every layer of the sandwich module contributed to and was affected by thermal concerns, this was addressed first.

Thermal Analysis

A first order study of the thermal problem for the sandwich module showed some of the limitations imposed by the radiative heat transfer relation:

$$P = \varepsilon\sigma AT^4 \quad (1)$$

where P is the heat power transmitted, ε is the emissivity of the material, σ is the Stefan-Boltzmann constant, A is the radiating area, and T is the absolute temperature in kelvin. A view factor of one to a non-radiating body is implied. By assuming that a flat sandwich module could only use its top and bottom for radiating heat, since it would be adjacent to other modules needing to also dissipate heat at its edges, bounds were established by specifying the desired operating temperature, which in turn were set to allow usage of commercially available electronic components. In practice, solar cells and antenna surfaces can be decent radiators, so having these respective top and bottom surfaces modeled as efficient radiating surfaces was not unreasonable.

The sun's yearly averaged power flux in space in earth orbit is approximately 1370 W/m², though the actual flux presented to a conversion module may vary as a result of a concentrator implementation and orbital position. For the first order study, the flux was assumed to be constant. Multiplying notional efficiencies of the component layers gave the rough total module efficiency shown in Figure 7. In this case, a square module made of four rows of seven cells with each cell measuring 4 cm x 7 cm was assumed for simplicity.

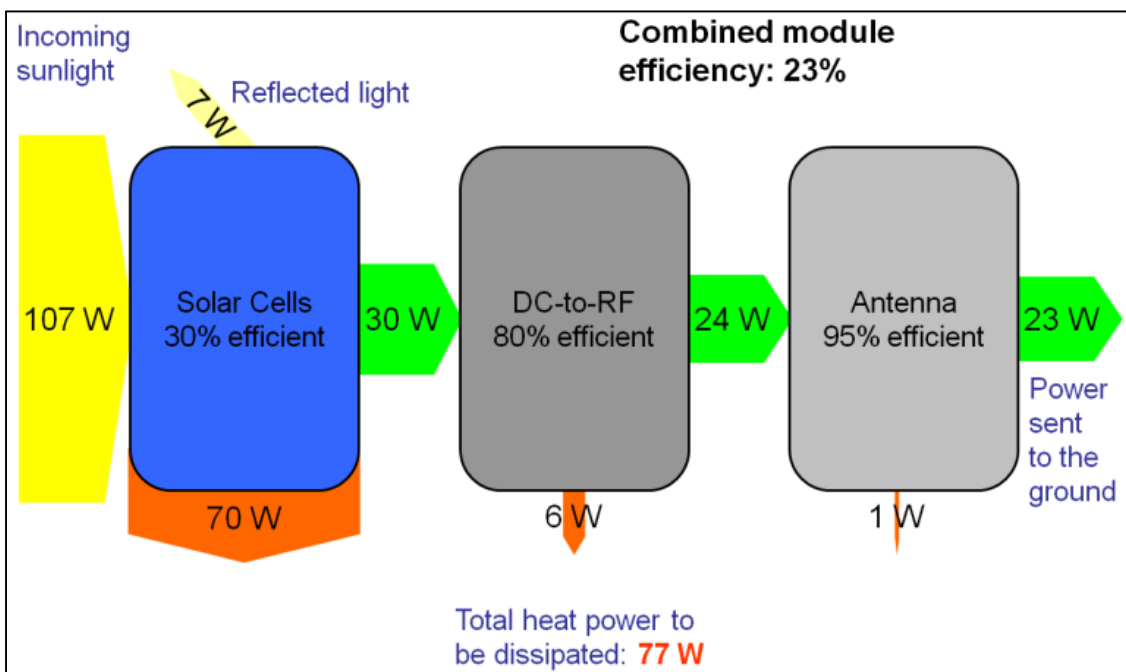


Figure 7: Solar power intercepted at one sun (AM0) by a 28 cm by 28 cm module and combined module efficiency with notional layer efficiency estimates.

The required radiator area was calculated for different sun concentrations and emissivities for modules at different desired operating temperatures, as shown in

Figure 8. Because this was an idealized model, the temperature effects on the efficiency of the layers, most notably the photovoltaic and DC-to-RF conversion layers, were not accounted for. The efficiencies of these two layers will tend to decrease with rising temperatures, in turn resulting in more heat that must be dissipated, further raising the module temperature.

Evident is that with the assumptions made, the available radiator area of a two-sided module will limit the solar illumination level to about two suns for an operating temperature of 100°C, and 6 suns for an operating temperature of 200°C.

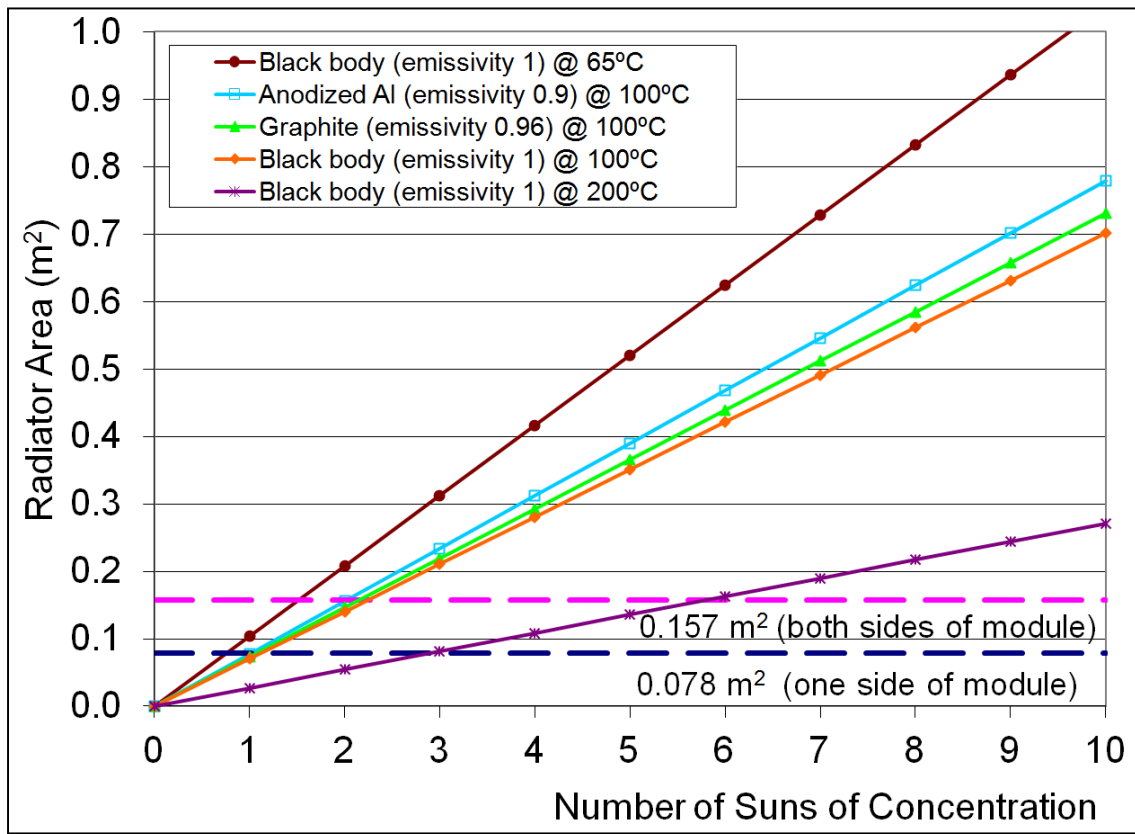


Figure 8: Radiator area required to maintain temperature equilibrium for a 28 cm by 28 cm module at 23% efficiency.

Inserting combined module efficiencies of varying levels of optimism allowed plotting the resulting temperatures as a function of sun concentration. This plot, seen in Figure 9, shows that to operate below 150°C with reasonable efficiency assumptions limits the sun concentration to about three suns. An increase in radiator area would necessitate a departure from the prototypical flat sandwich module.

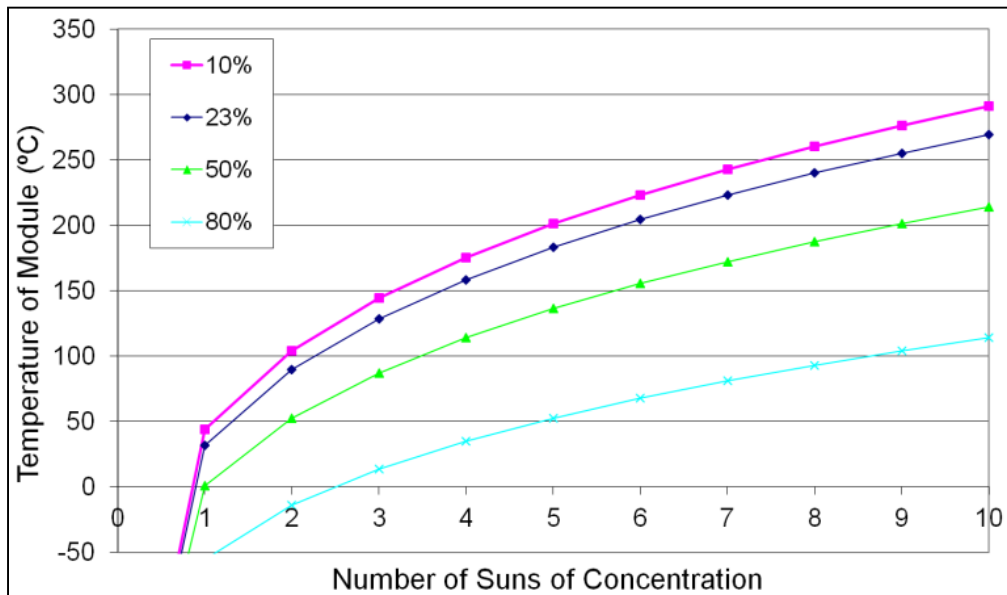


Figure 9: Temperature of a 28 cm by 28 cm module with both sides as black body radiators for various module efficiencies.

Keeping the target module temperature below 150°C helps limit the efficiency degradation resulting from the temperature of the photovoltaics and the DC-to-RF converters. In reality, individual efficiency degradations would be dependent on the local temperature, which varies across different parts of the module. A thermal analysis using Thermal Desktop® performed for a sandwich module design with

realistic efficiency assumptions operating under three suns [34] shows the peak temperature indeed surpasses 150°C, as seen in Figure 10.

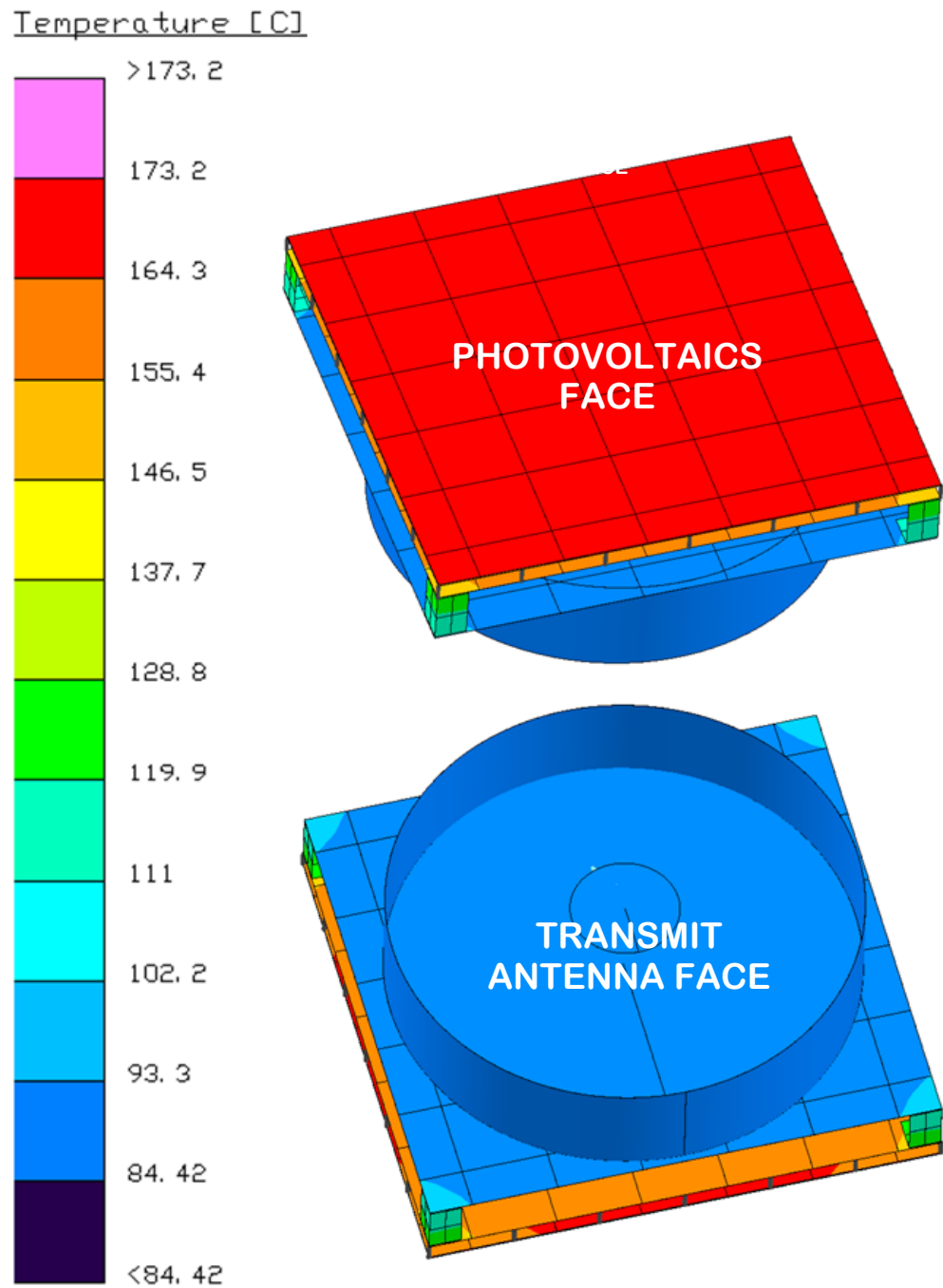


Figure 10: Thermal Desktop® simulation of a sandwich module under 3 suns of illumination [35].

The limits imposed by the thermal analyses presented here offered two possible paths to the creation of a sandwich module suitable for SSP: (1) a flat module at moderate sun concentration (below three suns), or (2) a departure from the traditional flat sandwich module to allow for an increase in radiator area for operation at higher sun concentration. Though the focus of this work was primarily on the former, a novel design embodying the latter was created, for which a patent application was published, U.S. 20130099599A1. It was observed that an array of modules that could still fulfill the implicit requirements of having a flat projected collection area to maximize solar energy collection and being able to serve as an antenna element could be formed using “step” shaped modules.

Step Module Concept

In the step module design, upper and lower radiator surfaces are added to provide for additional heat rejection. The length of these radiators is arbitrary, but as the distance from the heat source increases, the benefit of the additional radiator surface will tend to diminish. The location of the electronics was moved from being in close proximity to the hot solar panel to a cooler place on one of the radiator panels. To visualize this departure from the traditional flat sandwich module, dubbed the “tile” module to distinguish it from the newer concept, or “step” module, consider the depiction in Figure 11, which shows a close-up view of the photovoltaics and transmission antenna of the Modular Symmetrical Concentrator implementation from Figure 3.

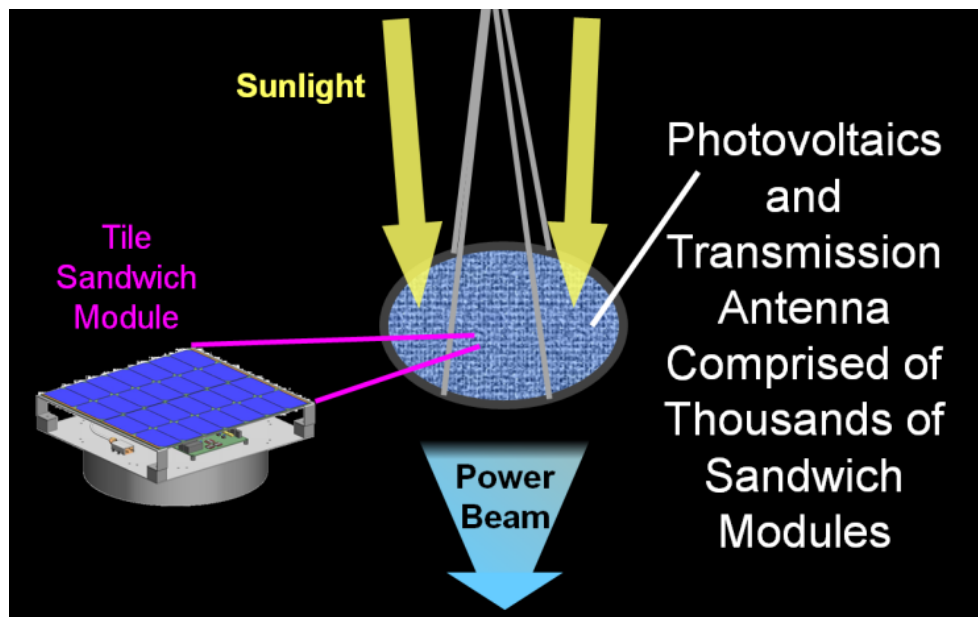


Figure 11: Photovoltaics and transmit antenna comprised of tile modules.

Contrast this with the photovoltaics and transmission antenna portion comprised instead of step sandwich modules as seen in Figure 12.

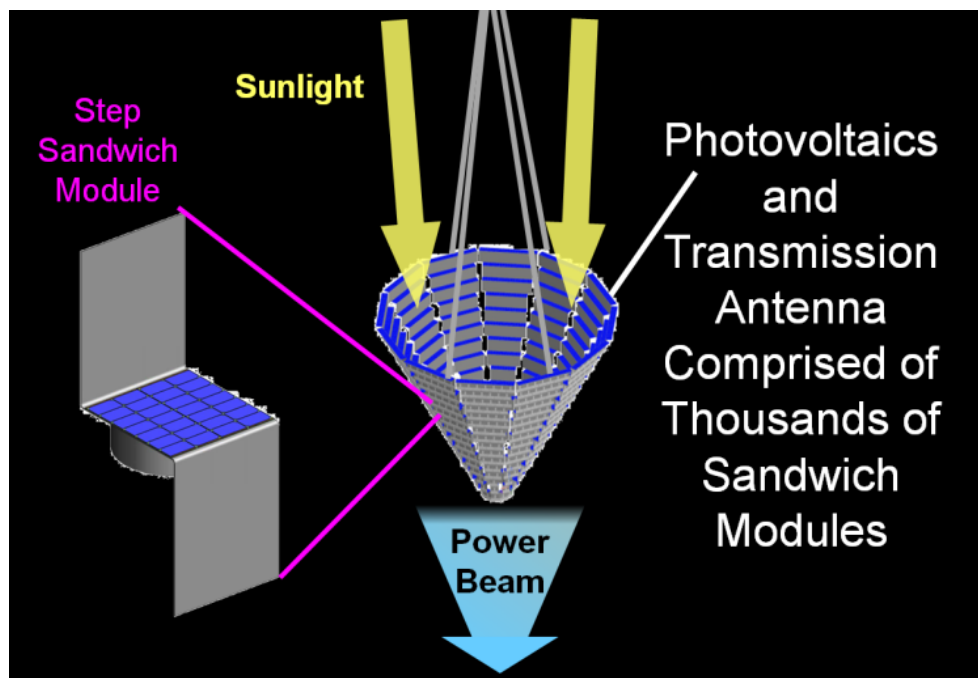


Figure 12: Photovoltaics and transmission antenna comprised of step modules.

Note that suitable transmit antenna apertures can be created using the step modules as elements to form structures in the shapes of cones, inclined ridged discs, and other shapes with varying radiator views of deep space for heat rejection [36]. An elongated spike formation at the tip of a cone could serve to increase radiator area further for additional heat rejection capability in the center of the array where the power density and waste heat would likely be greatest. In any case, from above or below the optical projection will very closely resemble the original flat disc, allowing it to be used essentially interchangeably with the rest of a given solar power satellite architecture that employs the sandwich module concept. Since the modular aspect is common to both the tile and step, techniques that envision self-organizing structures for assembly are still usable.

A thermal simulation performed in Thermal Desktop® showed that the step approach effectively lowered the maximum temperature of the module when compared with the tile module under the same test conditions. Furthermore, the DC and RF conversion electronics operate about 20°C cooler than in the tile module. The results of the thermal simulation can be seen in Figure 13.

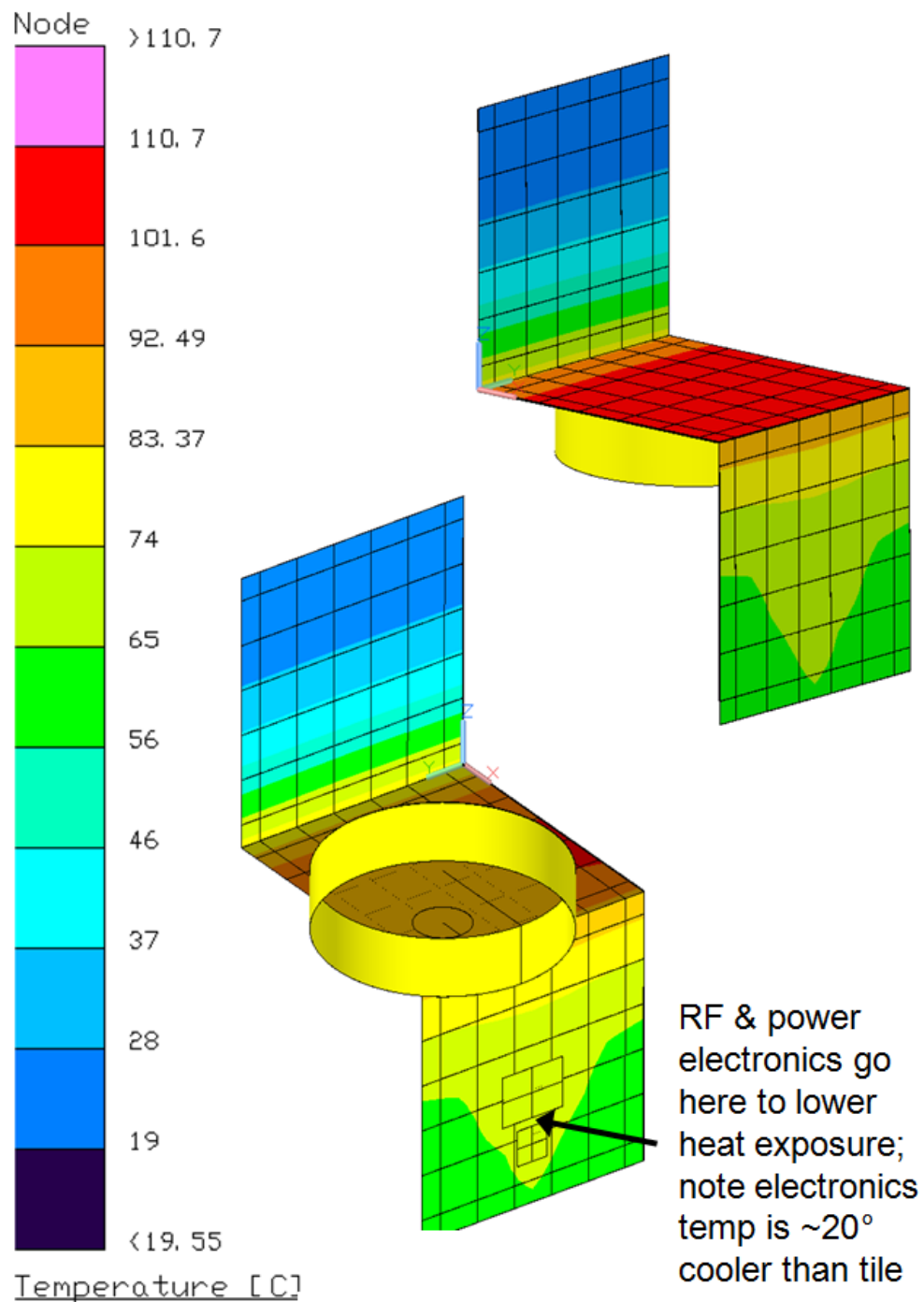


Figure 13: Thermal Desktop® simulation of a step module under 3 suns of illumination.

Both tile and step module concepts were pursued in order to evaluate the relative merits and disadvantages of each, and in particular to determine whether the thermal benefits of the step module were outweighed by the increase in mass required for the additional radiator area [37]. These results are presented in Chapter 4: **Results and Discussion.**

Critical Tradeoffs

Each layer of the module presented a plenitude of options for performing the required function. Prior to the design and fabrication of the prototypes, tradeoff studies were performed to assess the merits, disadvantages, and suitability of the various options for each layer for utilization in the modules.

Photovoltaics

For the module prototype, commercially available space-qualified photovoltaics (PV) were used. Though there exist many promising high efficiency technologies in laboratory settings, they were not available or practical for inclusion in the prototype because of prohibitive costs or lack of availability. PV cells commonly used for space are readily available from two companies: Emcore Corporation and Spectrolab Incorporated, a division of Boeing. Both offer triple junction cells with conversion efficiencies quoted near 30%. Spectrolab's Ultra Triple Junction (UTJ) GaInP₂/GaAs/Ge solar cells with a bare-cell efficiency of 28.3% were selected. The layer stackup and cell I-V curve (current and voltage measurements as a function of varying the load presented to the device's output terminals) from the datasheet are shown in Figure 14.

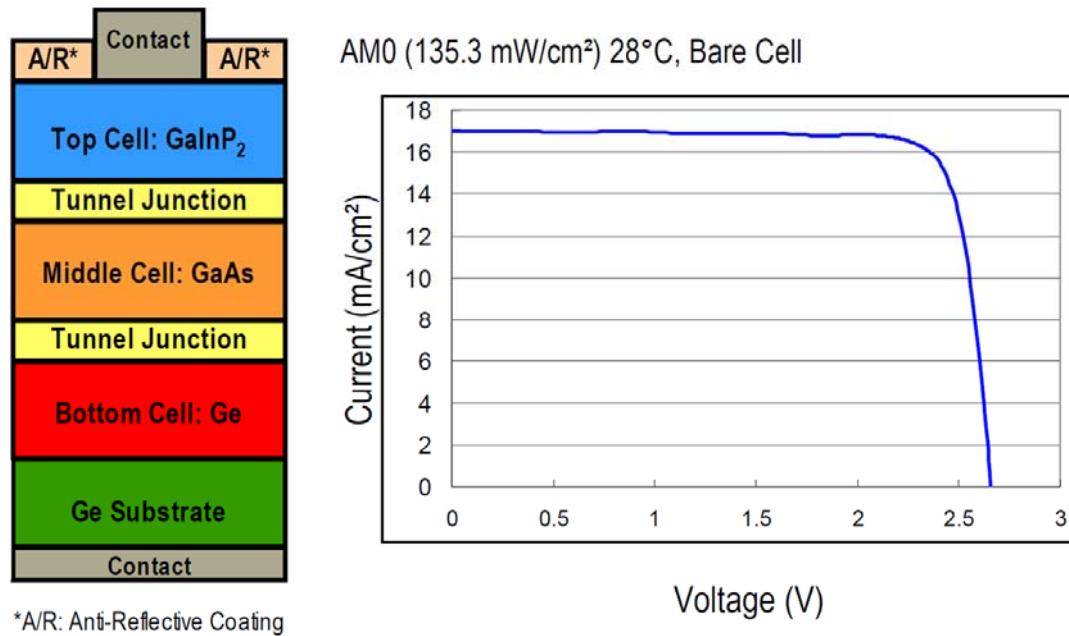


Figure 14: Layer stackup and I-V curve for the Spectrolab UTJ photovoltaic cells from the datasheet [38].

SpaceQuest, Ltd. produced the solar arrays and employed fabrication methods to foster high temperature tolerance during cell-to-substrate integration. The finished solar panels for both the tile and step modules utilized two 14-cell strings in parallel to provide the desired voltage and current. A tile module solar panel is shown in Figure 15 and a step module solar panel is shown in Figure 16.



Figure 15: Conversion module solar panel for a tile module.

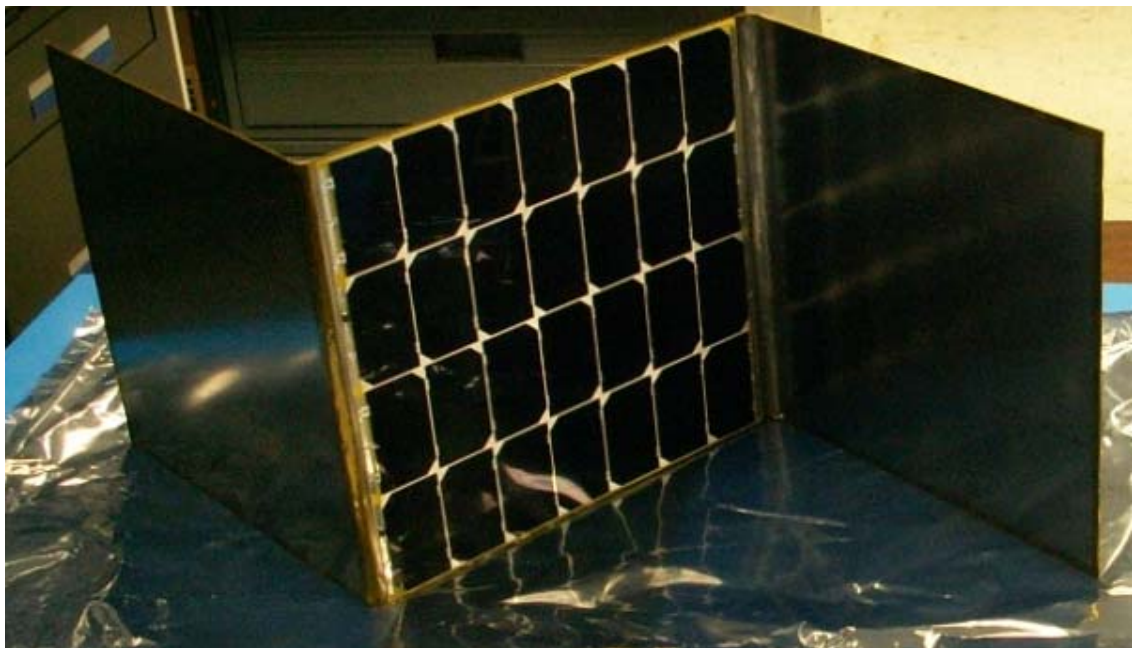


Figure 16: Conversion module solar panel for a step module.

Since each 26.62 cm^2 cell at its maximum power point outputs 2.35 volts and 434 millamps at one sun AM0 illumination and 28°C per the data sheet [38], the total projected panel output was 28.0 W near room temperature accounting for a 2% loss anticipated due to cell coverglass installation. Because the initial projected operating temperature in vacuum was 100°C , the expected output power was 22.5W, accounting for the temperature effects on voltage ($-6.5\text{mV}/^\circ\text{C}$ per cell) and current density ($1.2\mu\text{A}/\text{cm}^2/^\circ\text{C}$) [38].

Prior to integration with the prototype, the completed solar arrays were characterized by collecting I-V curves. A representative I-V and power data plot is shown in Figure 17.

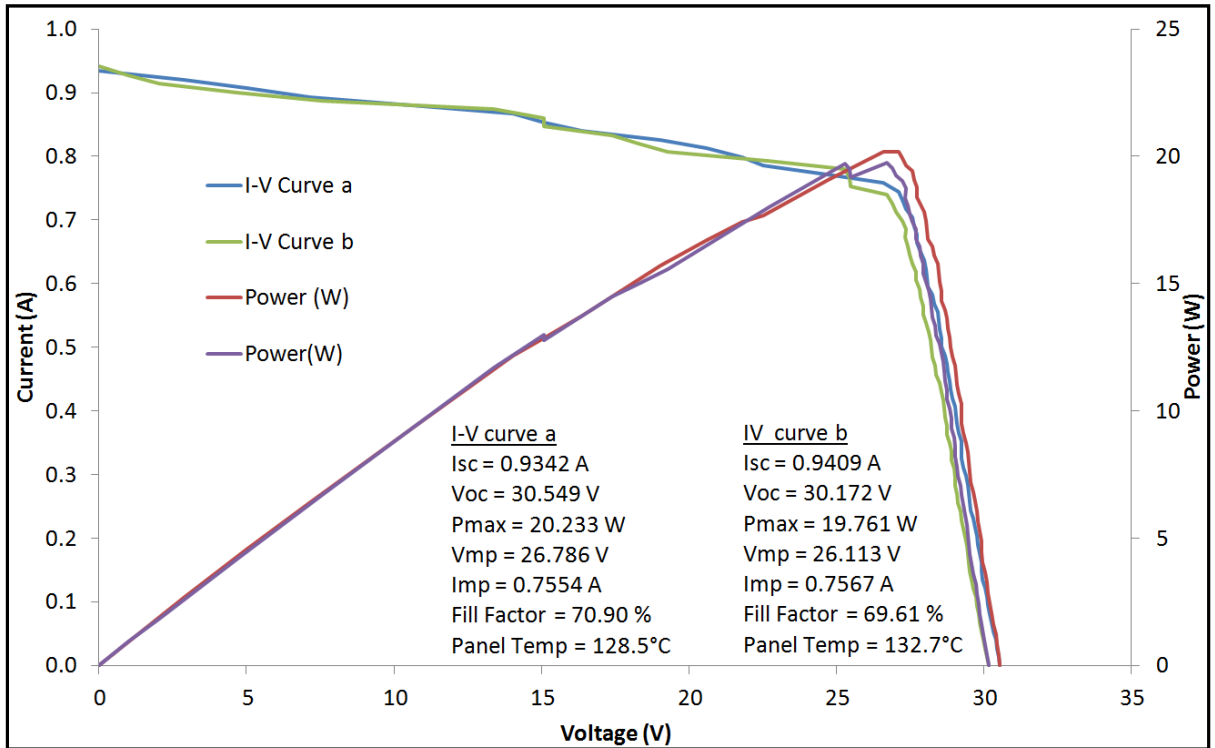


Figure 17: Representative array string I-V and power data plot collected with direct sun-simulated illumination.

The I-V curve collection also afforded an opportunity to observe the temperature effect on the cell and string voltage and power output. Considering Figure 18, it can be seen that even over a comparatively small span of about 20°C the open circuit voltage drops by 1.5 volts. The output power drop is on the order of half a watt. This particular set of I-V curves was taken on one of the strings of a tile module panel while the beam from the xenon lamp used as a sun simulator was partially blocked by a set of screens, resulting in an illumination level equivalent to just over one sun. The basis for the estimated illumination level is described in the “Light Field Characterization” subsection in Chapter 3: **Prototype Testing**.

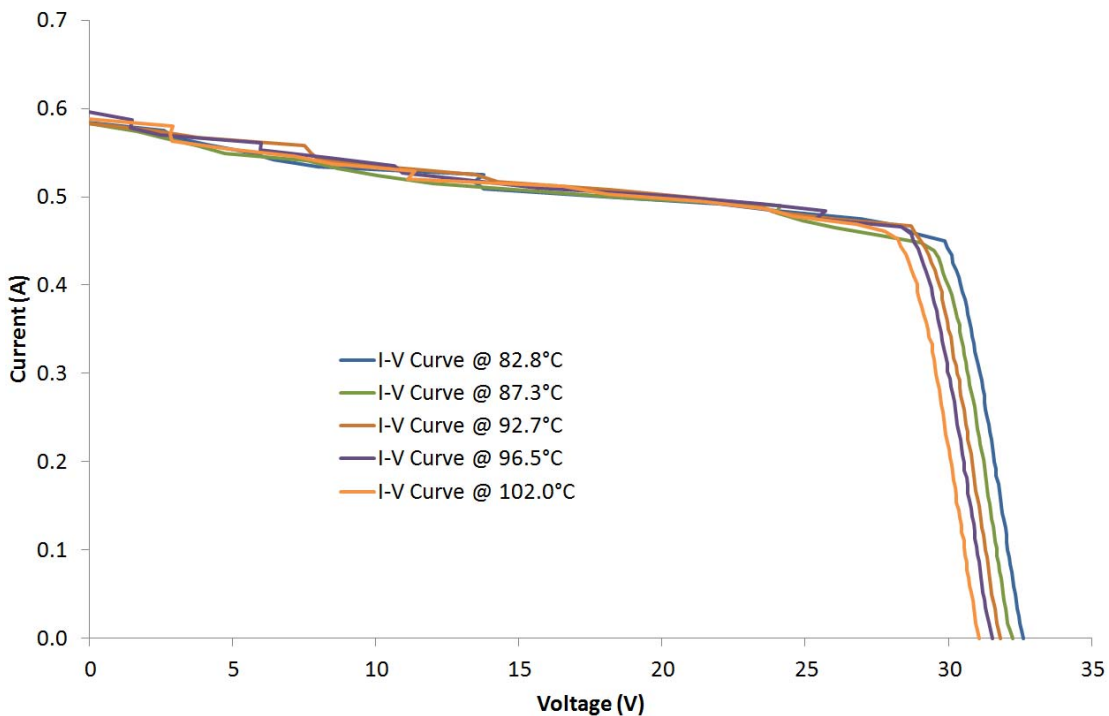


Figure 18: I-V curves showing the effect of temperature on panel open circuit voltage with lamp output attenuated by screens to produce about one sun.

Since the cells and assembly techniques employed were very similar to those used for actual satellites and space missions, no special modifications or accommodations were made to adapt the solar arrays for vacuum and illumination testing.

DC-to-RF conversion

The conversion electronics needed to simultaneously achieve cost, weight, efficiency, and output power requirements. Considerations and trade options are considered in greater detail in [39] and are outlined in Appendix A in Table 11. Because high power, high efficiency solid state devices had not been demonstrated at the likely greater than 30dB gain required to add the power to the input frequency to effectively utilize the available solar array power, the construction of a suitable amplifier chain was central to this layer of the module. Monolithic microwave integrated circuit (MMIC) options could be considered to implement this level of gain in the future.

Power to feed the multistage architecture was generated by power circuitry painstakingly designed to minimize conversion losses, in large part by directly driving the final stage amplifier. The resulting prototype board demonstrated a DC to DC conversion efficiency on the order of 97%, and is shown in the context of the integrated DC and RF electronics baseplate shown in Figure 19. This high efficiency was due in large part to driving directly the final stage RF amplifier.

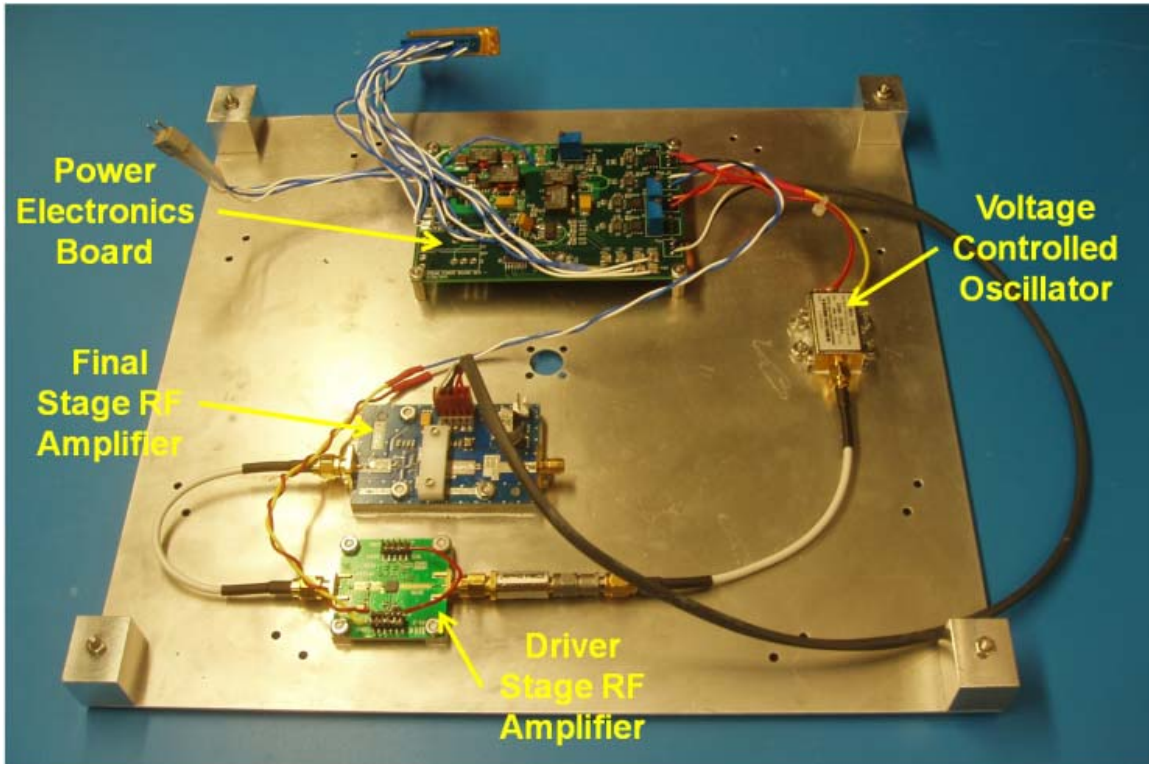


Figure 19. DC power and RF electronics baseplate for the tile module.

For the prototype, all RF components were “off-the-shelf” items operating at 2.45 GHz. They were selected to best match the expected output of the solar array at its peak power point under the projected operating conditions, with about 30 W for the one sun case. The frequency source was a voltage-controlled oscillator (VCO) with a 7.5 dBm output (the Mini-Circuits ZX95-2755+), which was filtered and attenuated prior to entering the GaAs driver stage (the Hittite HMC755LP4E). The driver stage provided about 31 dB of gain, and the signal was then fed into the final stage (the Cree CGH27015) where approximately 12 dB of additional gain was applied, resulting in an RF output power on the order of 15 W. When the final stage was

characterized on its own, greater than 55% Power Added Efficiency (PAE) in the region of interest was observed as seen in Figure 20.

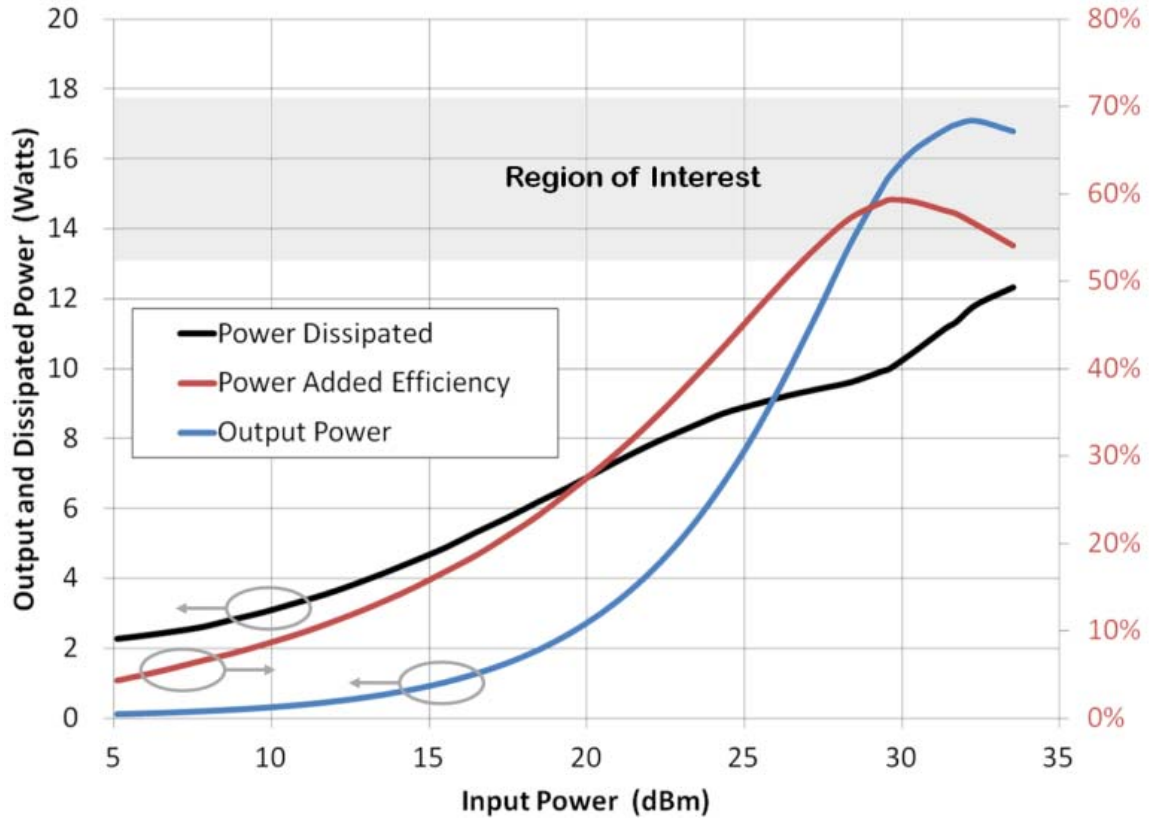


Figure 20. Characterization of Power Added Efficiency performance of final stage amplifier [35].

The projected maximum efficiency performance of the single chain used for the tile module is shown in Table 1. The measured efficiency matched the projection closely.

Table 1: Projected RF signal and efficiency chain performance for tile module.

	Source	BPF	Atten	Delay Line	AMP Hittite	Loss	PA CGH27015	Loss	
Vds	[V]	5.0			5.0		29.0		
Pdc	[W]	0.2			4.8		27.6		32.6
PAE	[%]	3%			21.0		55.0		47.4%
Gain	[dB]	0.0	-2.0	-6.0	-0.3	30.9	-0.1	12.1	-0.2
Pout	[dBm]	7.5	5.5	-0.5	-0.8	30.1	30.0	42.1	41.9
Pout	[W]	0.0	0.0	0.0	0.0	1.0	1.0	16.2	15.5
									TOTAL

Temperature and vacuum testing of the complete electronics prior to module integration showed only limited variation in the output total electronics efficiency, on the order of $45\pm2\%$. The range of temperature testing for the electronics chain alone in vacuum was from -20°C to $+95^{\circ}\text{C}$, with the final RF amplifier stage as the control point. The reduction from the results achieved with the final stage amplifier alone can be attributed to inefficiencies from the power electronics, driver stage amplifier, and cabling losses.

For the step module, the RF chain was instantiated in triplicate, the approximate integer number of suns under which simulations suggested the step module should be able to operate. This scaled with the multiplicative current increase associated with increasing sun concentration. The layout can be seen in Figure 21. The outputs of the three parallel RF chains were power-combined for routing to the antenna.

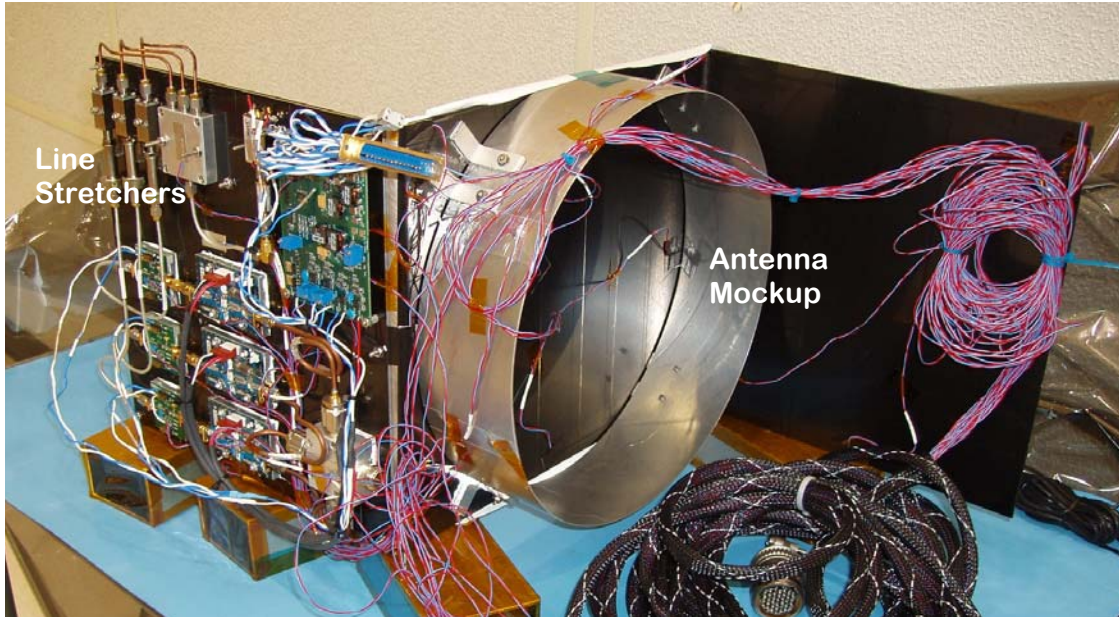


Figure 21: Step module prototype with antenna mockup, electronics shown at left.

Because the three legs were combined at the outputs of the final stage amplifiers, it was critically important to phase-match each leg to avoid heat dissipation in the power combiner. More importantly, a phase mismatch would also lower the total RF output power. A line stretcher preceding each driver input was used to tune the phases. The three line stretchers are visible in the upper left corner of Figure 21.

The bandwidth and harmonics of the output were monitored using a spectrum analyzer. These proved effectively invariant over different illumination and temperature conditions, with the center frequency shifting over less than a 5 MHz range. A representative spectrum analyzer screen capture is shown in Figure 22.

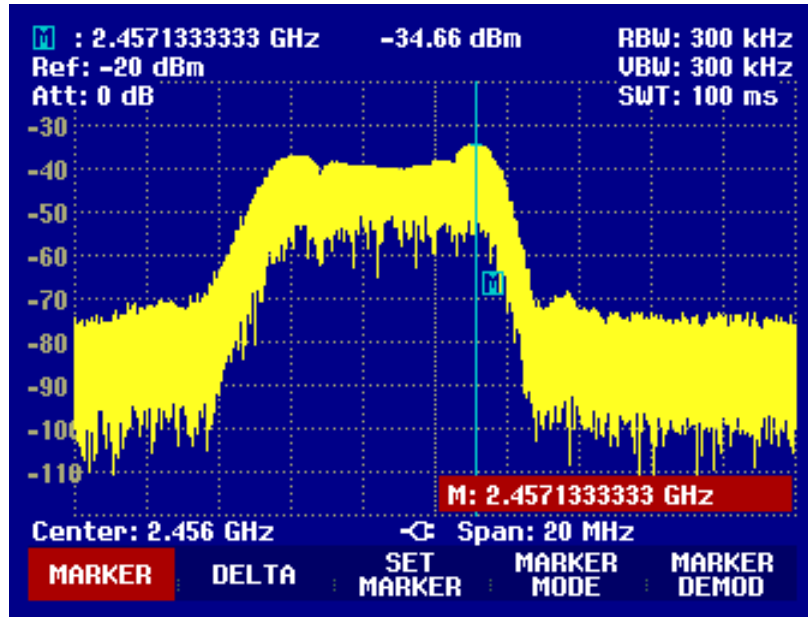


Figure 22: A representative spectrum analyzer screen capture from monitoring of the RF bandwidth, harmonics, and center frequency. This capture is for the step module while powered by a solar array simulator.

Since the electronics used were not space-qualified nor in some cases even built to withstand military specified temperature ranges, there was some risk associated with exposing them to vacuum and temperatures that exceeded their datasheet “Absolute Maximum” ratings. Though initial testing specifically avoided transgressing these limits, ultimately the limits on the voltage-controlled oscillator and driver stage amplifier were exceeded somewhat, with no apparent ill effects to their operation. Discussions with the manufacturers suggested that the “Absolute Maximum” limits cited in the datasheets were established to ensure reliability over long operating periods and for the driver amplifier to specifically support one million hour mean time between failures. All electronics components were assessed for suitability of operation in vacuum, and aluminum electrolytic capacitors found on the final stage

amplifier boards were removed and replaced with tantalum capacitors to eliminate the possibility of a component rupture during vacuum operation. No parts were assessed or screened for radiation tolerance (neither total radiation dose nor single event effects) and no reliability or other requirements were placed on them beyond their ability to function for module testing.

In an ultimate module for use in a spaceborne demonstration or operational space solar power system, electronics would also be implemented to effect the phase shifting needed for a retrodirective control scheme. Similarly, as previously shown in Figure 5, such a flight module would also require very narrow bandpass filtering on the output of the final stage to suppress amplified harmonics and thermal noise.

Antenna Elements

The antenna component needed to have a potential path in order to serve as an element in a large phased array that would comprise the spaceborne power transmitting aperture, or “spacetenna.” This aperture would be quite large and would scale with the frequency selected for operation. Some examples of transmit antenna sizes for different frequency and power density parameters can be seen in Appendix B: SPS System Design.

A wide variety of antenna types were considered for the microwave transmission face of the module. Ultimately, a short backfire antenna was chosen by virtue of its high directivity, high efficiency, ability to act as an effective thermal radiator, and because it was nearly an ideal physical size for the selected operating frequency and solar array dimensions. A CAD depiction showing the surface current distribution

appears in Figure 23 and the simulated gain pattern for a single antenna element is shown in Figure 24.

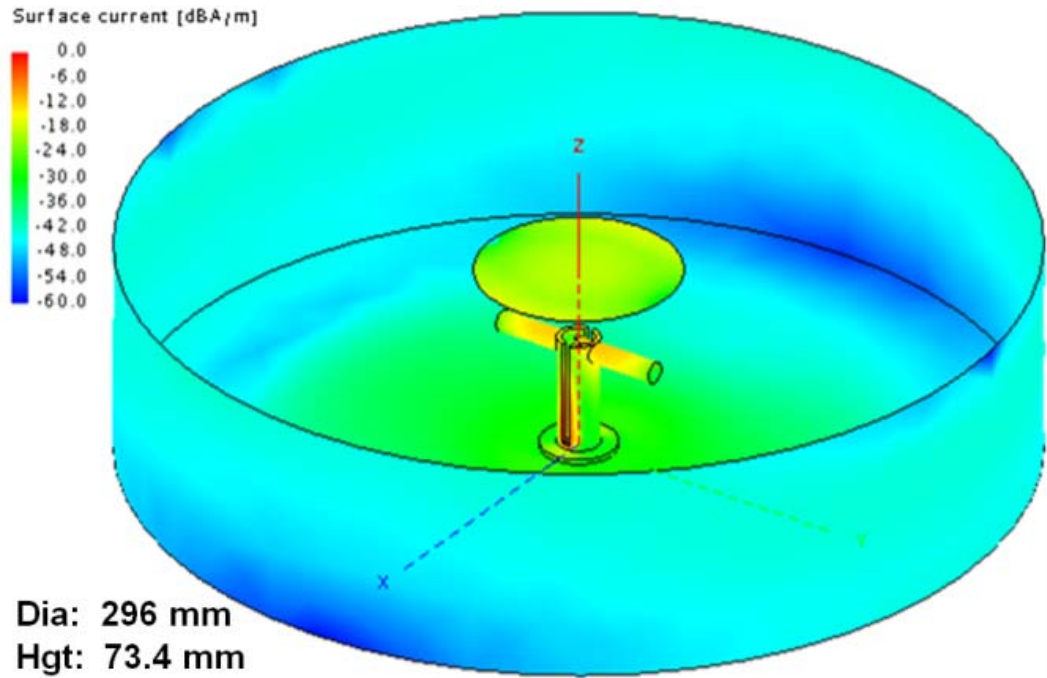


Figure 23: Simulated surface currents of short backfire antenna [40].

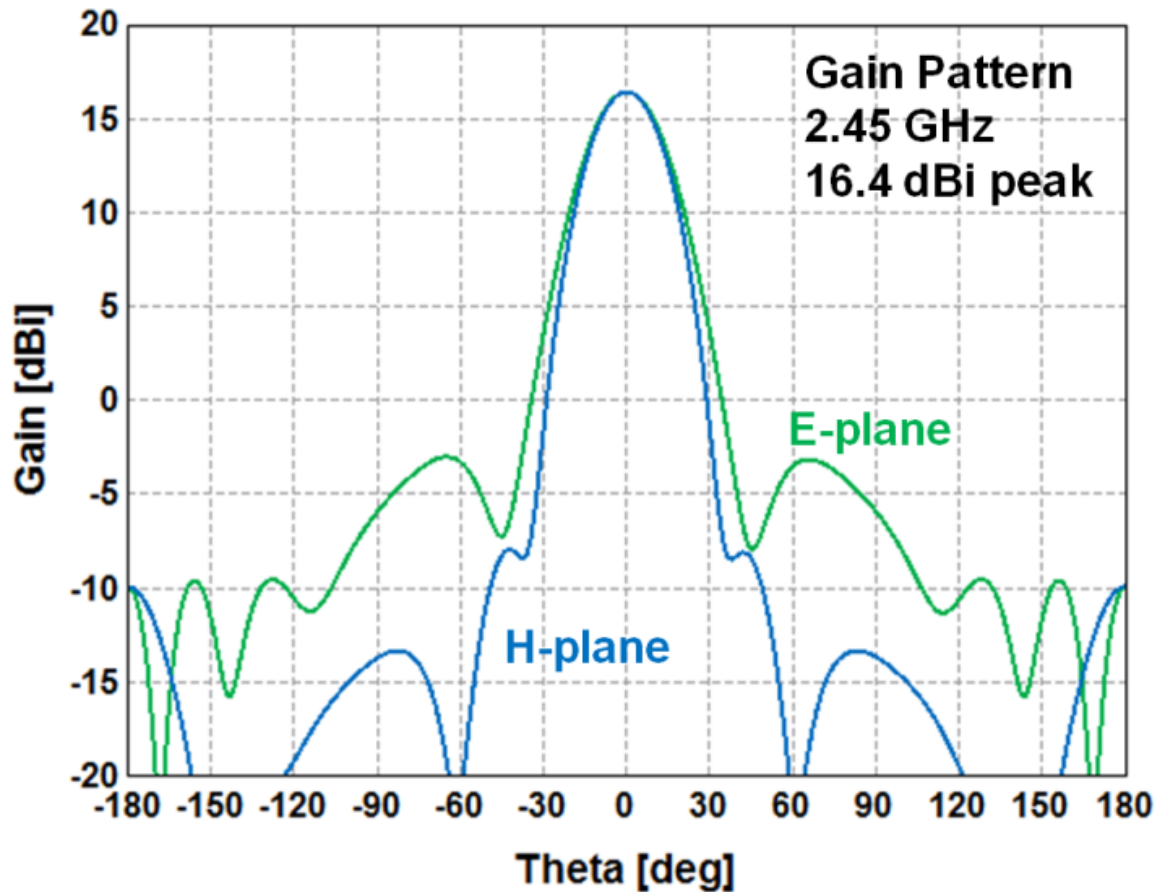


Figure 24: Simulated gain pattern for a short backfire antenna at 2.45 GHz [40].

The element pattern was designed to suppress the grating lobes that would otherwise result from having spacing between elements that exceeds a wavelength. In an SSP system, this antenna element would be one of hundreds of thousands in a filled array. Both the tile and step modules employ the short backfire antenna design described above.

Module Architectures

Most previous sandwich module concepts have taken a hexagonal shape, ostensibly to maximize the usage of the volume of a cylindrical launch vehicle fairing. A preliminary analysis of current launch vehicle fairing volumes and throw weights suggested that a module of any reasonably achievable density will exceed the launch vehicle throw weight before exceeding the fairing volume. Because of this, module shape was selected based on other factors, such as photovoltaic cell coverage, though it is reasonable to anticipate that fairings for launches of SSP elements would be custom designed to maximize launch economy. Since currently available PV cells are essentially rectangular, a square or rectangular panel surface can be more efficiently filled than a hexagonal one. The module thickness is driven by the need to accommodate the DC-to-RF conversion electronics and the antennas, as well as by its ability to manage the transport and radiation of waste heat.

Thermal Control Methods

There are many effective and novel means for transferring heat from one area to another: diamond or graphene heat spreaders, pyrolytic graphite structures, microchannels, and two-phase heat pipes, among others. Regardless of the transport method, the waste heat needs to be radiated from the module. An appropriately anodized antenna surface closely approaches the emissivity of a black body. The area available for radiation of heat can be increased with judicious module design. In the tile module prototype for this effort, thermal grease between RF electronics modules and the substrate was employed, multilayer insulation (MLI) blankets were used to protect the power electronics from excess solar array heat, and black Kapton® tape

was used to maximize emissivity. Two thermal zones were created: one for the solar array which could tolerate and operate under higher temperatures, and a second lower temperature zone for the electronics to preserve their operating efficiency and to extend their reliability. The integrated tile module with some of the thermal features visible is shown in Figure 25.

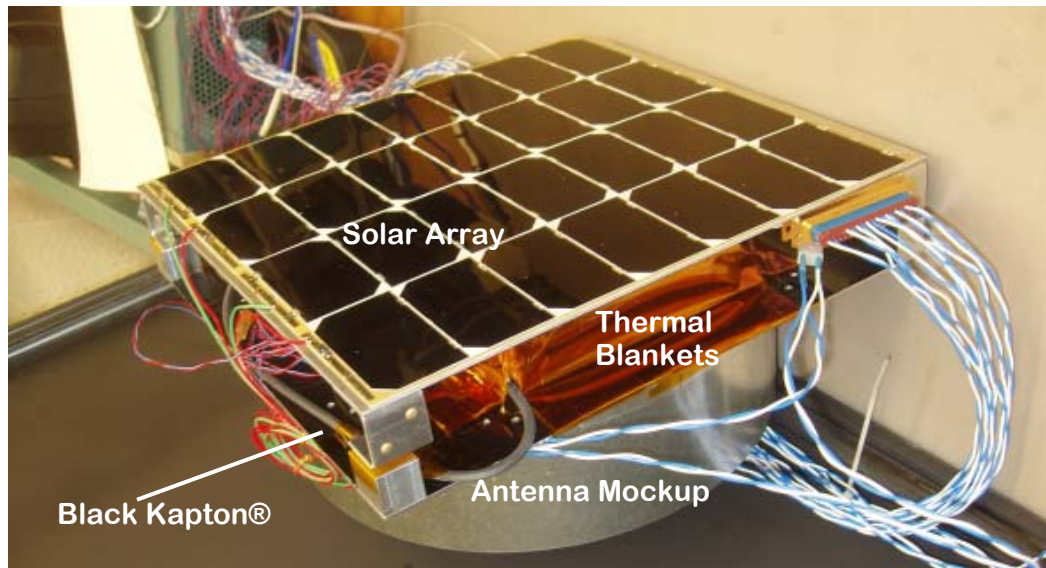


Figure 25: Integrated tile module showing from top to bottom: solar array, conversion electronics with multilayer thermal blankets and black Kapton® tape, and antenna mockup.

For the step module, a layer of graphite sheeting was applied to the module substrate in an effort to facilitate heat transport. Black Kapton® to increase emissivity and thermal grease to enhance thermal conductivity between the electronics, baseplate, and substrate were again employed.

Design Iteration

The original tile module design proceeded through a series of design iterations, beginning with a large hexagonal shape and migrating to a rectangular shape because of the considerations described in the “Module Architectures” subsection. The size of the solar array was initially larger, but was reduced to more closely match the output levels of the anticipated RF amplifier components, as well as to fit within the confines of the available test chamber. Minor mechanical updates were made almost constantly as the antenna design progressed and went through a long series of iterations of its own. Once the solar array was ordered, as the costliest and longest lead element, it effectively constrained subsequent design changes. Each layer was deliberately kept separable, to the extent that the thermal control approach would allow, in order to permit replacement or revision of damaged or underperforming components. Thus, the module design was in itself maintained as modularly as possible. The step module was kept similar to the tile module in most regards to allow for more direct and meaningful comparisons to be made, though it required a different substrate to achieve the step shape and additional RF chains to handle the higher output power levels.

Module Fabrication

Except for the solar array and commercial electronics components, the modules were fabricated and integrated on-site at the Naval Research Laboratory using in-house machinists, technicians, and engineers. This allowed for rapid turnarounds in the event the design changed, and also enabled close oversight of the modules’ build

progress. Multiple copies of critical assemblies were fabricated to support quick replacement of components in the event of hardware failures or other problems.

Chapter 3: Prototype Testing

Since effective testing of the prototypes was fundamental to meeting the research goals, a treatment of the testing philosophy, facility, and approach is presented here. Because of the three layers and their various constitutive elements, testing was done progressively so that anomalies might be discovered prior to integrated module testing where problems would present larger setbacks with respect to time, and the ability to alter the architecture would be constrained.

Progressive Testing

As the various layers of each module type were completed, they were tested separately to at least a functional level prior to full module integration. This allowed individual characterization of each section of the modules in the event there was an unexpected interaction between the layers. In certain cases, this also provided an opportunity to use and learn lessons from test configurations that would be used for or would feed into final testing. For instance, an early RF electronics chain was tested in vacuum with the fused silica chamber window, verifying the approach to sealing the chamber, and allowing a chance to perform insertion loss measurements and attenuation compensation of the RF power measurement.

Upon their completion, the integrated modules were characterized under ambient pressure and vacuum conditions. An overview of the process for the tile module leading up to this point is shown in Figure 26. “Mass Properties” indicates a point at

which the subassembly or module was weighed and checked for dimensions so that figures of merit could be calculated.

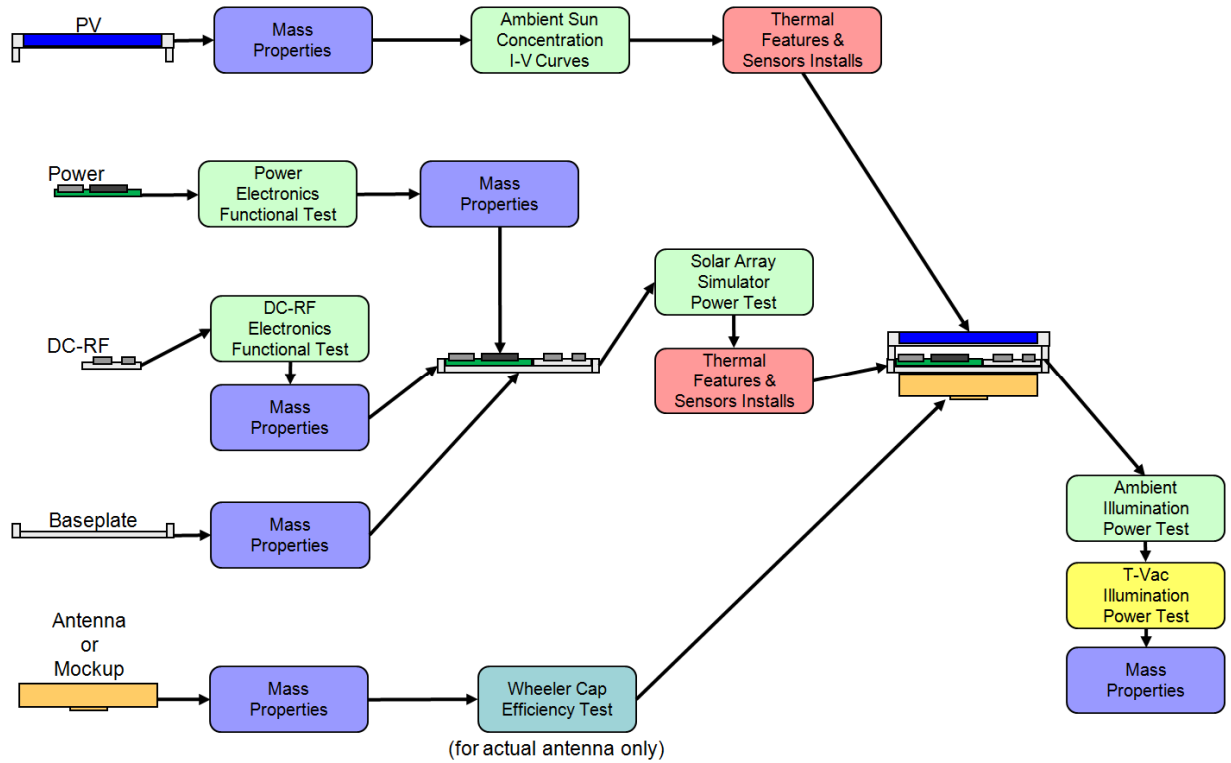


Figure 26: Tile module integration and test flow overview.

Antenna mockups were used in place of the actual antennas during testing. Though it was initially considered to test with an output antenna radiating inside the vacuum chamber to a rectenna or power sensor to capture the transmitted microwave energy from the modules, routing the RF output via a coaxial cable through the chamber bulkhead was deemed sufficient to meet the research objectives. This avoided the need to install specialized, high-power, vacuum-rated RF absorbing material and eliminated the uncertainty that would have been introduced through the possibility of not being able to capture all of the emitted RF energy.

The prototype testing facility can be considered in three functional segments: (1) sun simulation, (2) space environment simulation, and (3) additional supporting equipment. These segments are addressed in turn, and the overall test configuration is discussed as well.

Sun Simulation

A critical subsystem of the test ensemble was that for the simulation of solar illumination. Comprised of two major sub-elements, one or two xenon lamps, and a series of attenuating screens, this subsystem produced the lighting conditions that a sandwich module might be expected to operate under while in space.

Xenon Light Source

A variety of sun simulation sources are available for various purposes. Ranging from simple arrays of common halogen lamps to xenon lamps with sophisticated filtering systems, a solution was needed that could provide intensity in excess of one sun (AM0) over a sizable area. A 4,000W xenon short arc lamp system, Model 6806 made by LP Associates, Inc. was ultimately selected for solar panel illumination. This lamp system, seen in Figure 27, has a parabolic reflector and is primarily used as a spotlight for sky and theatrical lighting.



Figure 27: 4,000W xenon light source with power supply.

The lamp sports good beam collimation but uneven beam uniformity. Its focus could be adjusted via a motor drive that slightly changed the angle of the parabolic

reflector. It was set up initially to provide approximately a 56cm diameter beam, which was found experimentally to offer a reasonable balance of beam size, intensity, and uniformity. The resulting uniformity was adequate for testing but resulted in excess heat generation on the solar panel versus the expected illumination condition in space. Excess heat was also generated by overrepresentation of power content represented by the spike evident in the 850nm to 1050nm spectral range as seen in Figure 28; this spike in the spectrum is not present for sunlight in space.

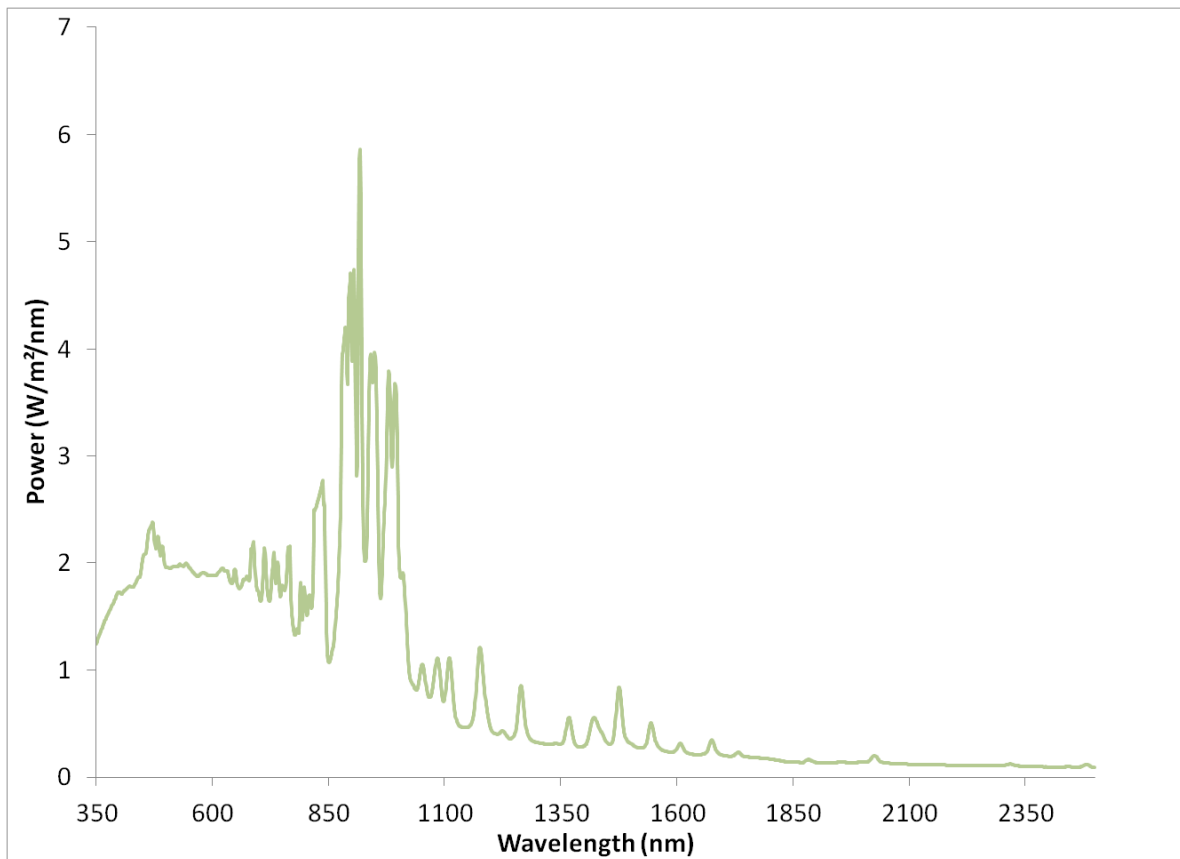


Figure 28: Spectrum of 4,000W L.P. Associates xenon lamp.

Light Attenuating Screens

Combinations of five different light attenuating screens were used to control solar concentration. The screens were hung from a metal rack in the path of the xenon lamp's beam. Table 2 shows the amount of light blocked and passed for each of the five screens individually.

Table 2: Screen designations with blockage and throughput percentages from manufacturer specifications.

Screen	Allowed
A	75.0%
B	65.9%
C	60.2%
D	50.7%
E	25.4%

At a given focus setting, the xenon lamp produced a peak intensity that could then be approximately scaled by the various percentages shown. The screens themselves can be seen in Figure 29.

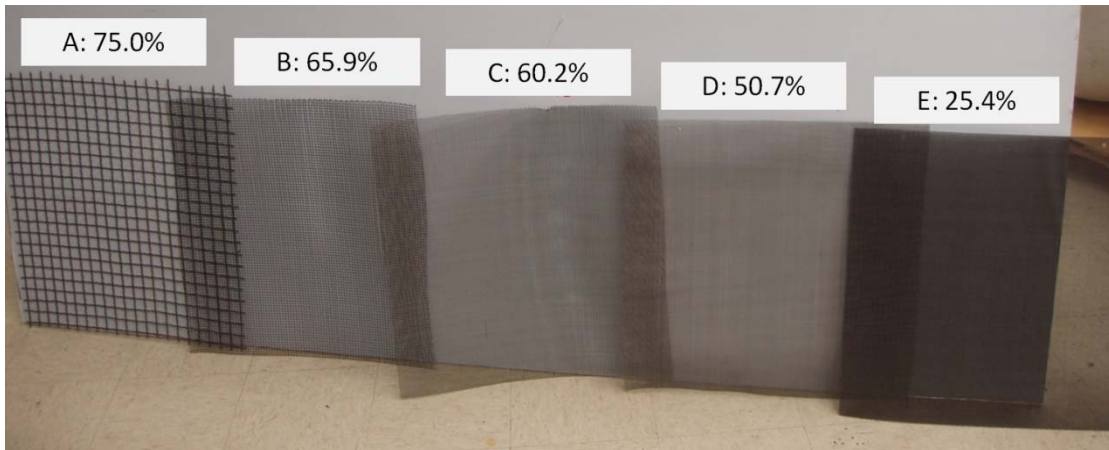


Figure 29: The five light attenuating screens labeled with percent open area.

As the wire screens reduced the light intensity by an essentially constant amount over the entire beam, they did not materially address the matter of uneven beam power uniformity. Some investigation and thought was given to developing customized patterns, screens, lenses, or some manner of adaptive optics that could compensate for the beam unevenness, but each of these options appeared beyond the scope and wherewithal of the project. Instead, the light field was measured to quantify the power nonuniformity and determine its impact on module characterization.

For the focus setting used for initial tile module testing, Table 3 shows the equivalent peak, minimum, and average solar concentration for each screen in terms of number of suns, where one sun is for AM0, 135 mW/cm^2 . These values changed as a function of the focus adjustments that occurred as testing progressed to slightly increase the illumination level on the module prototype. A 5% reduction in light power due to passage through the fused silica window is not reflected. This reduction factor was derived by comparing power measurements with and without the window.

Table 3: Screen designations and sun concentrations for initial tile module testing focus settings.

Screen	None	A	B	C	D	E
Peak	3.17	2.71	2.18	2.04	1.69	0.92
Average	2.23	1.90	1.56	1.44	1.21	0.66
Minimum	1.39	1.23	1.00	0.87	0.76	0.41

Light Field Characterization

Determining the evenness of the field and the absolute intensity of the light field had particular challenges. Ultimately, the evenness of the field and the absolute intensity of the light source were measured and characterized using a Newport thermopile sensor optical power meter with a customized heat shield and an Ophir-Spiricon beam profiling system with a large Lambertian surface. The thermopile sensor's output was compared against an Eppley global cavity radiometer by exposing both to similar conditions under an Oriel solar simulator. The reported power densities matched within 13.5% [41].

Digital image captures from the beam profiling system were taken of the unobstructed field in a plane in proximity to that in which the prototype module would be located, and again several times with the thermopile sensor in various points in the light field. The absolute intensity measurements from the thermopile sensor were logged and later referenced to the pixel locations in the unobstructed field image to create a mapping to show the relative sun intensities across the entire field.

The light field evenness and intensity characterization was done to ensure that the solar cell strings were exposed to a known minimum illumination condition, as the least-illuminated solar cell in a string current-limits the output of the entire string. Because the sun simulator had large intensity variations across the area of illumination, the efficiency calculations used the known minimum average illumination level. In order to ensure a minimum level of illumination of one sun (for AM0, 135 mW/cm²) over the entire solar array, some portions were exposed to greater levels. As a result, the thermal conditions were more oppressive in the testing than they would be in space, where the lighting conditions would be uniform. During a portion of the testing, the light field variations were exacerbated when the lamp focus was tightened to increase total intensity. A raw screen capture of the entire central light field of one lamp is shown in Figure 30.

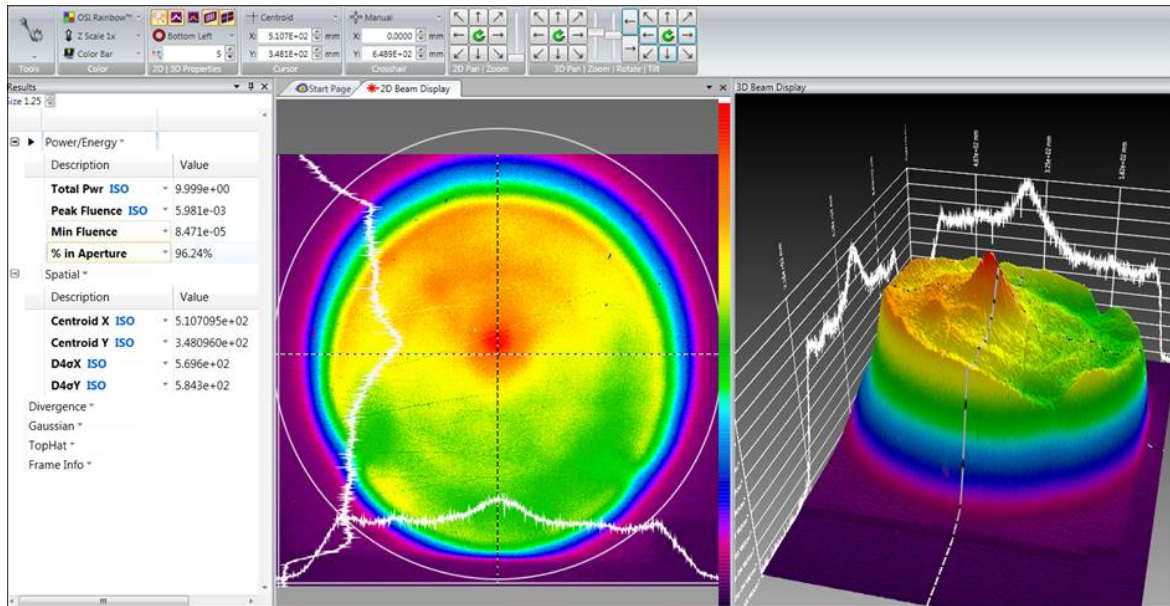


Figure 30: BeamGage software screen capture.

An example map of the beam uniformity was processed to show the equivalent numbers of suns averaged over each solar cell's area (Figure 31). Though it appears the intensity of the field could be better centered, this was the portion of the beam that offered the best uniformity. The anomalies in the upper left and lower right around the perimeter were due to a slight mismatch between the framing of the panel area on the Lambertian surface and the actual capture area in the BeamGage software.

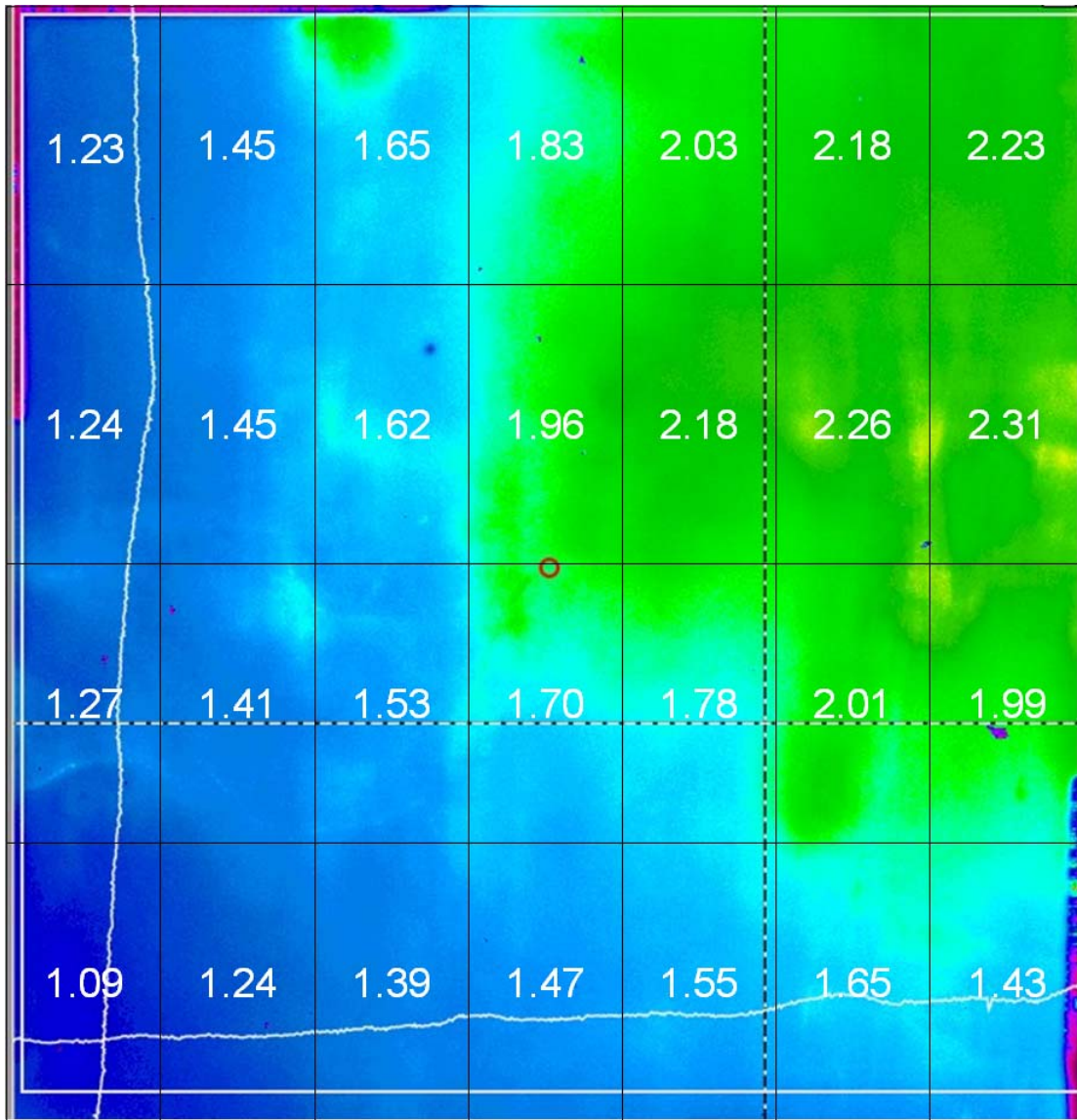


Figure 31: A light field portion matching the solar array size that has been processed to show the number of suns of intensity incident on each cell area, adapted from [42].

For step module testing, a second xenon lamp was added to increase the overall intensity. This helped even the uniformity of the field somewhat, but the inability to closely pack the lamp housings resulted in an incidence angle on the solar array face

slightly deviating from normal. This resulted in negligible cosine and refraction losses. A mapping showing the sun intensities per cell when two lamps were used is shown in Figure 32.

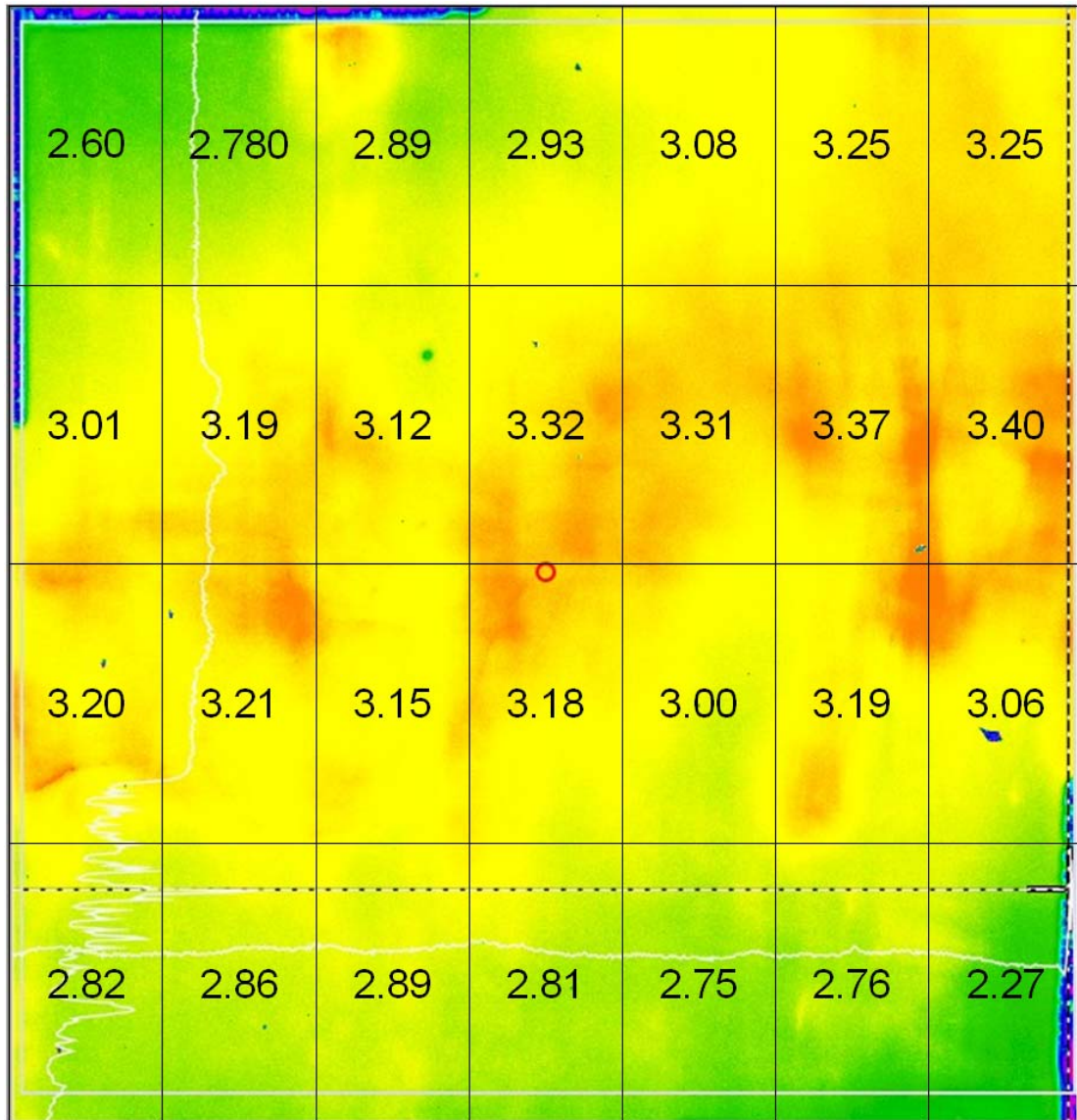


Figure 32: Two lamp beam mapping showing equivalent number of suns of intensity over solar cell areas, adapted from [42].

As with the single lamp light field map, the anomalies in the upper left and lower right around the perimeter were due to a slight mismatch between the framing of the panel area on the Lambertian surface and the actual imaging software capture area.

While considerable effort was put into minimizing the unintended variation of the factors affecting the light field, not all factors could be absolutely controlled. Variables that were identified and addressed to the extent possible included:

- Lamp pointing
- Lamp distance
- Lamp warm-up duration
- Bulb age
- Focus setting
- Screen used
- Screen positioning
- Vacuum window presence
- Reflections from adjacent apparatus (pipe, chamber)
- Light incidence angle on solar array

Further sources of error that could be introduced during the capturing and processing of the light field to derive the illumination intensity included:

- Imperfections of the Lambertian surface
- Pixel variability in the beam imaging camera

- Inconsistency of optical power measurements due to sensor misalignment
- Misalignment of the measured light field and the light field exposed to the module
- Difference in the distance between the Lambertian surface and the solar array
- Inability to account for imperfections in the fused silica window

Because of these factors, there are errors in the light field mappings that were difficult to bound with high accuracy, but the repeatability of the results from the beam mappings and module output power during testing instilled sufficient confidence in the findings.

Space Environment Simulation

As a major goal of the research, testing in a space-like environment was of paramount importance. While vacuum chambers are readily available in a range of research and manufacturing environments, it is not common to find chambers with windows larger than 30 cm in diameter, and not all chambers are equipped for the extreme temperature range found in space. As part of its spacecraft development facility, the Naval Research Laboratory's Naval Center for Space Technology offers a range of small and very large vacuum chambers that can achieve pressures lower than 10^{-6} torr and temperature ranges at least as large as -150°C to +100°C. However, at the start of this effort, none routinely incorporated a vacuum window of suitable size. Because of this, a very large thermal vacuum and sun concentration test facility at NASA's Glenn Research Center known as "Tank 6" was considered. This facility offered a large chamber volume and sun concentrations up to eleven suns over small

areas. However, limited project resources and the anticipated need to frequently enter into and exit from the vacuum state, which typically scales in time needed and general arduousness as a function of the vacuum chamber's size, required the creation of an alternative. This alternative needed to feature a sizable vacuum window that could transmit the solar spectrum effectively.

Fused Silica Window

Fused silica effectively passes the solar spectrum, as seen by comparing its transmission curve from Figure 33 and the solar radiation spectrum seen in Figure 34.

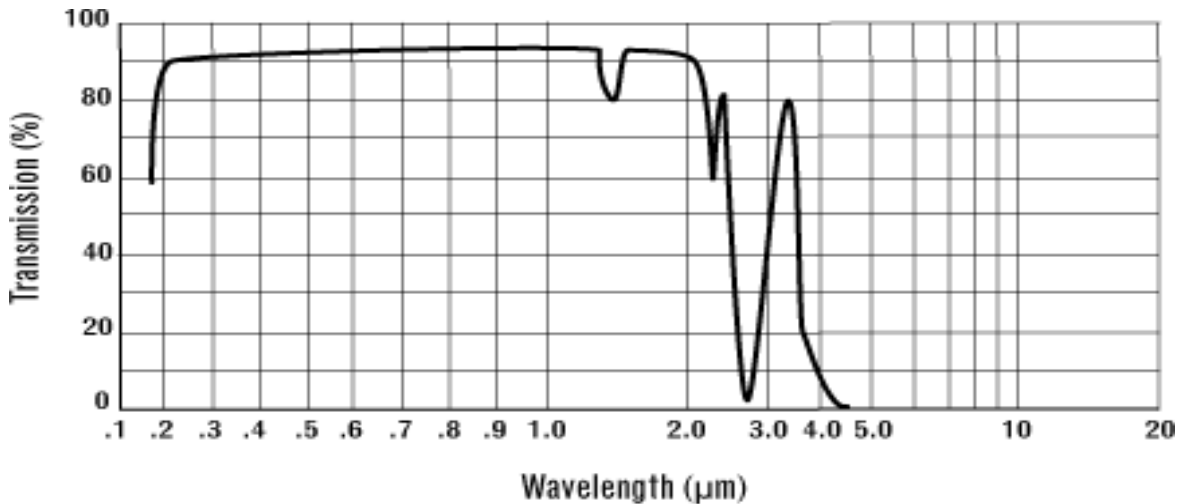


Figure 33: UV Grade Fused Silica Transmission Curve [43]

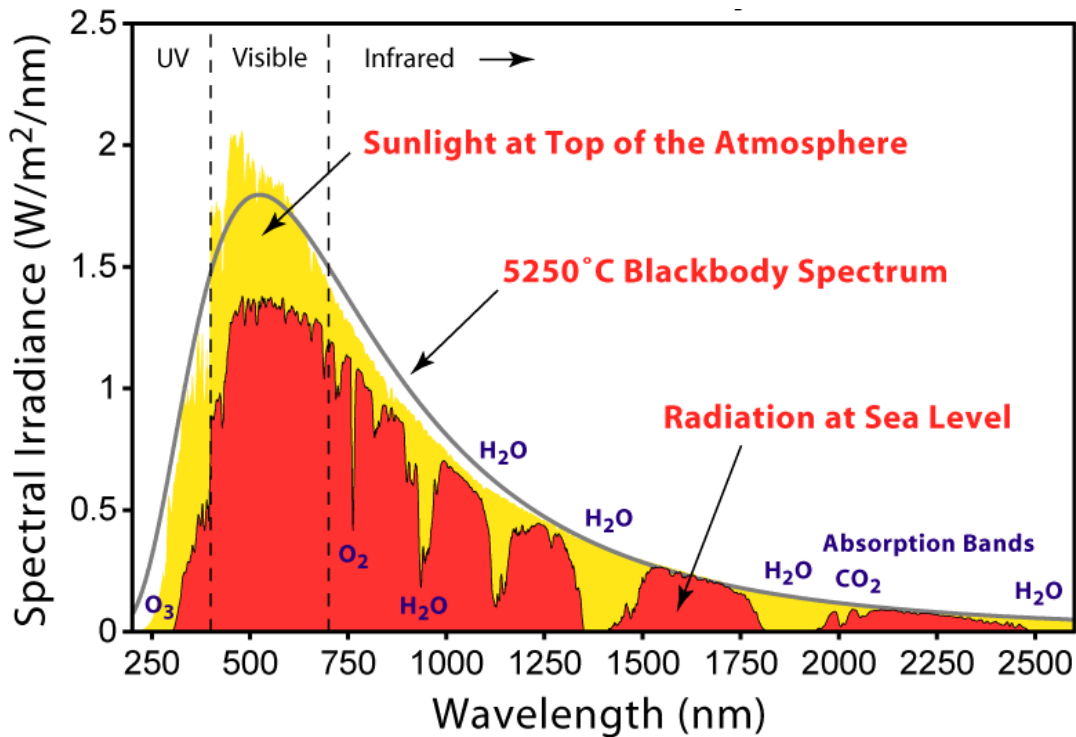


Figure 34: Solar Radiation Spectrum [44]

Though magnesium fluoride (MgF_2), or to a lesser extent, calcium fluoride (CaF_2) windows would have offered marginally better transmissivity, procuring a new window made of one of these materials of the required diameter and thickness was beyond the project's budget.

Fortunately, providence had it that a 68.6cm diameter / 4.5cm thick fused silica window that was designed to fit one of NRL's much larger chambers, and which had lain forgotten and unused for many years, was usable with a smaller chamber in lieu of the vessel's hinged door. This window, though it contained a few small blemishes and imperfections, proved effective and sufficient for the project's purposes. The window is shown in Figure 35. The markings showing the locations of the flaws were removed prior to testing, and the window was cleaned with isopropyl alcohol.



Figure 35: The fused silica window used with the vacuum chamber.

Ideally, an appropriate anti-reflective coating would have been identified and applied to the exterior face of the window to further enhance its transmissivity, but this was not done due to resource limitations. I-V curve collection testing with the window showed that it reduced the energy generated by the solar array strings on the panel from 4.1 to 5.8 percent versus without the window. This difference is principally due to reflection, as the window itself closely tracked room temperature, even when two lamps were used.

During testing, the front door to the chamber was restrained open or removed so as to accommodate the fused silica window. The window was then placed on a custom-designed and fabricated pair of supports affixed to the front of the vacuum chamber mounting structure and then clamped into place, as shown in Figure 35.

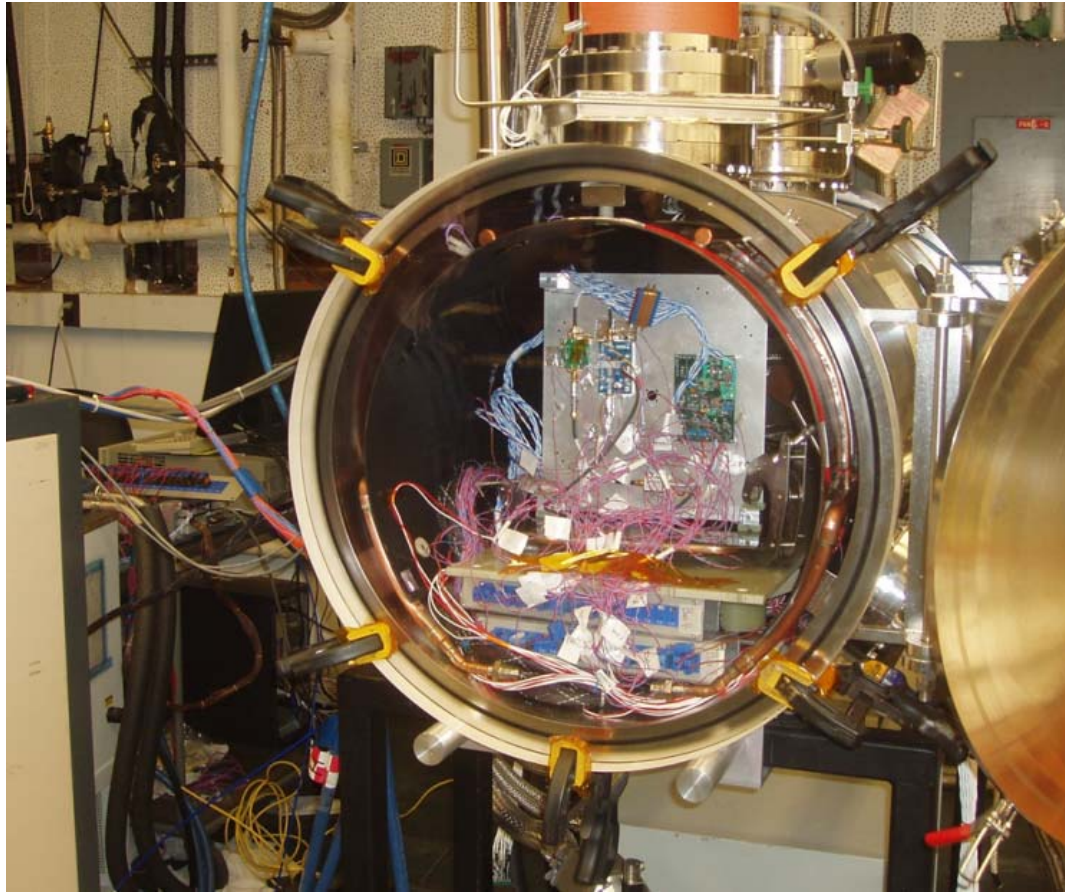


Figure 36: DC and RF electronics in thermal vacuum chamber with fused silica window sealing chamber opening.

As the air was pumped out of the chamber, the window sealed against the chamber O-ring gasket because of the pressure difference with the ambient surroundings.

Thermal Vacuum Chamber

The thermal vacuum chamber used was a liquid nitrogen-cooled vessel from Meyer Tools & Manufacturing (Part # 5928-01) capable of an internal shroud temperature range from -180°C to +100°C and of achieving a vacuum pressure of 1×10^{-8} torr. The vacuum is created by first using a mechanical roughing pump to approach the 10^{-4}

torr regime, and then a cryogenic pump is employed to get to “high vacuum”, the 10^{-6} to 10^{-7} torr range or lower. The standard configuration prior to fused silica window installation is shown in Figure 37.



Figure 37: Thermal vacuum chamber prior to fused silica window installation.

The configuration that was used for testing in thermal vacuum conditions is shown in Figure 38. Here the fused silica window sealing the front of the chamber is nearly invisible, allowing essentially full illumination by the 4,000W xenon light source with only limited spectral filtering. The tile module prototype is suspended from the top of the chamber by insulated wire connect to a fiberglass support piece to minimize conductive heat transport during testing.

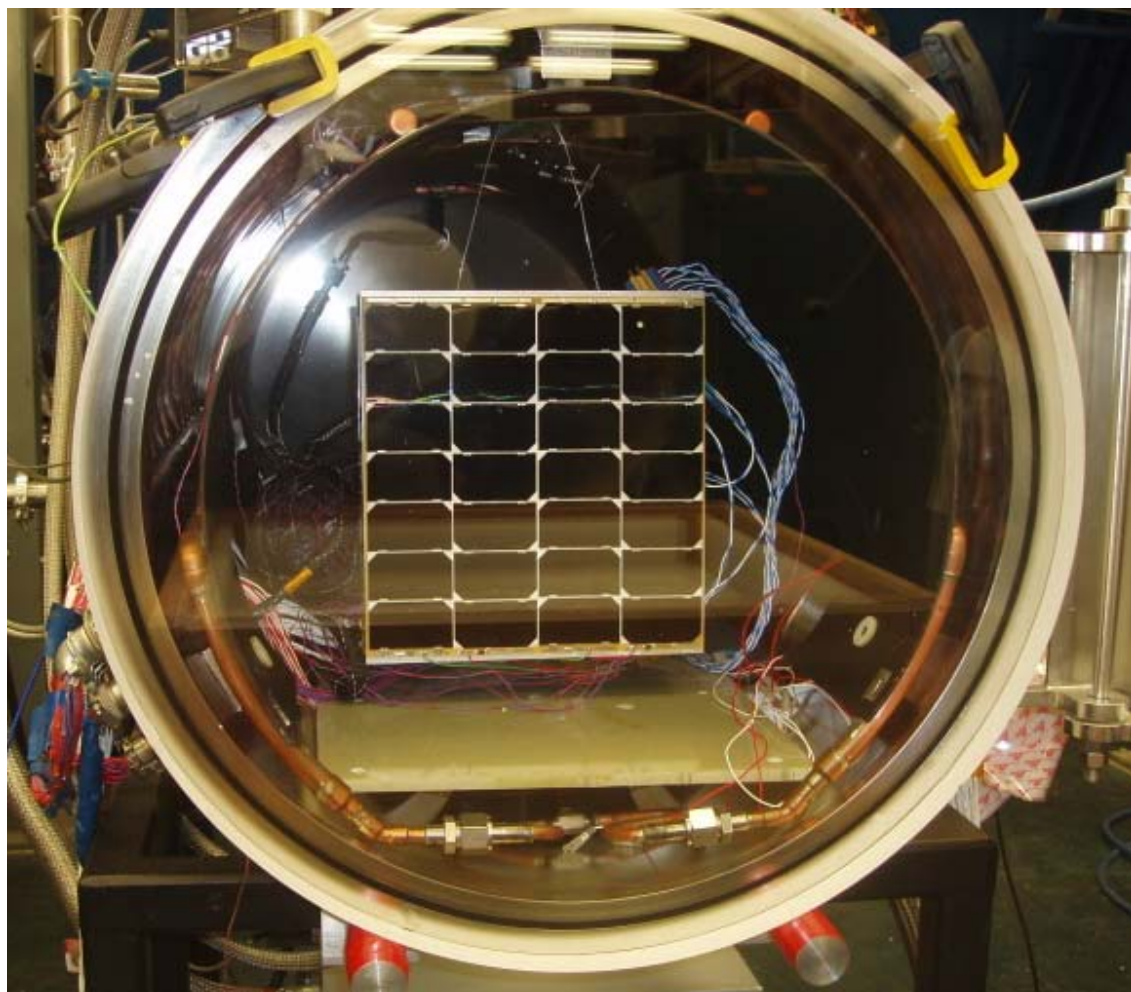


Figure 38: Module prototype in thermal vacuum chamber with fused silica window sealing chamber opening and vacuum chamber internals visible.

During testing, once high vacuum had been reached, a solenoid-controlled valve was opened to allow liquid nitrogen to flow through the plumbing surrounding the chamber's internal shroud. As the shroud temperature dropped, the illumination level was increased to prevent the module under test from dropping below about 5°C. Once ramped to the target temperature of -150°C to simulate the view of deep space, the shroud was maintained within $\pm 5^\circ\text{C}$ of this temperature with periodic flows of liquid nitrogen. The liquid nitrogen shroud cooling apparatus is shown in Figure 39. Note the container for receiving the nitrogen once it has circulated through the shroud to prevent excess nitrogen buildup in the test area.



Figure 39: Liquid nitrogen shroud cooling apparatus.

Though -150°C is about 123°K , which differs greatly from the background temperature of deep space of about 3°K , this shroud temperature is effective in measuring the module's likely heat radiating ability because the difference of the temperatures of the shroud and module to the fourth power differs negligibly whether 123°K or 3°K is used for the shroud temperature. For example, using:

$$P = \varepsilon\sigma AF(T^4 - T_{env}^4) \quad (2)$$

Where F is introduced to represent a constant view factor between the radiating body and the environment (ranging from 0 to 1) and T_{env} is the temperature of the environment. In the case of $T = 300^{\circ}\text{K}$ (approximately room temperature), for $T_{env} = 123^{\circ}\text{K}$ or 3°K , the $(T^4 - T_{env}^4)$ factor changes by less than 3%. This difference decreases further with increasing T . Due to uncertainties about the vacuum chamber shroud's capabilities, initial Thermal Desktop® simulations assumed a shroud temperature of -100°C (173°K); even this only changed the factor by about 11%.

As the window end of the chamber was illuminated by the xenon lamp, it effectively simulated the thermal environment due to the sun. The opposite end of the chamber was not covered by a liquid-nitrogen-cooled shroud and thus maintained a temperature near the ambient room temperature. This heat input, though small compared to the heat input from the sun simulation, would not be present to the same degree in an actual space environment since the earth's diameter only appears to occupy about 18° of the field of view from geosynchronous orbit. Even if the module were at the extreme window end of the chamber, the opposite end would occupy a

28° portion of the field of view. This only increase as the module is moved farther from the window end of the chamber.

The step module is shown in a pictorial depiction of the configuration in Figure 40. Note that for the actual testing the radiating surfaces faced the sides of the chamber, rather than the top and bottom, in part because the bottom of the chamber had a fiberglass platform that was not cooled by liquid nitrogen, and thus was not a good target for simulating the space condition.

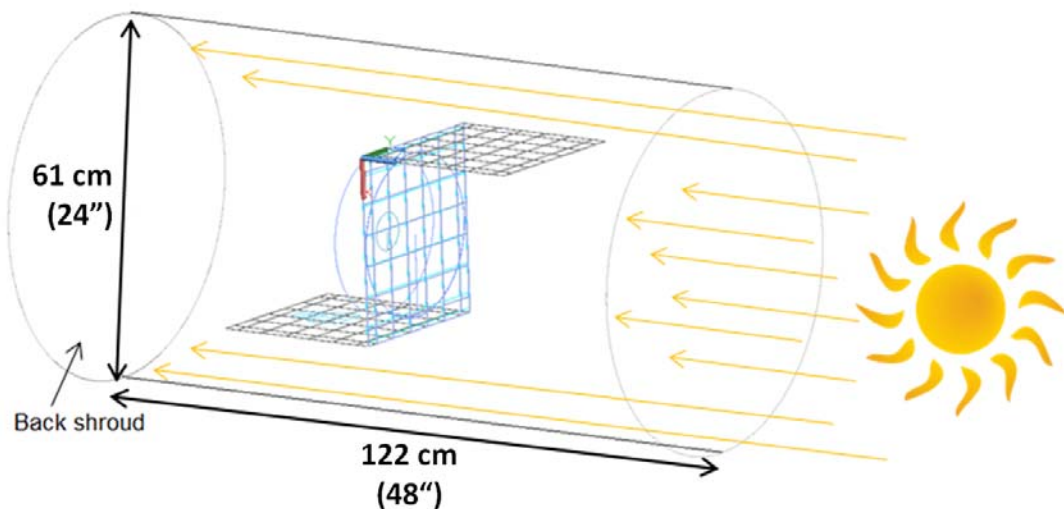


Figure 40: Depiction of step module in vacuum chamber configuration[45]

The step module installed in the chamber for testing is shown in Figure 41.

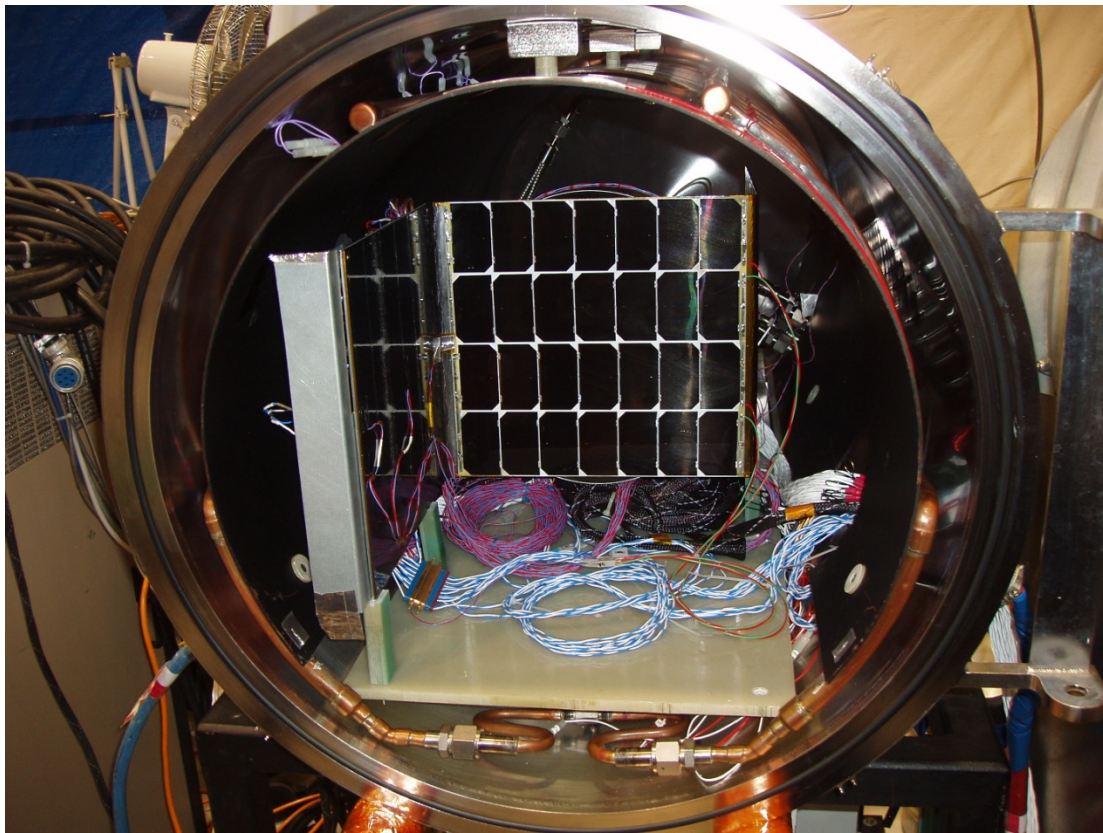


Figure 41: Step module installed in vacuum chamber for testing prior to installation of the fused silica window.

Summary Comparison of Space, Simulated Space, and Ambient Environments

Since it is not possible to recreate with exact fidelity the space environment on earth, an examination of the differences of the simulated space environment and the actual space environment is warranted. The comparison can provide insights into the effects of the environmental differences on module performance and allow for reasonable extrapolations. On the whole, the conclusion to be drawn is that the simulated space environment presents a more challenging heat rejection environment

to sandwich modules as compared to the actual space environment. Table 4 shows in summary form a comparison of some of the parameters of interest.

Table 4: Comparison of Space and Simulated Space Environments for Sandwich Module Operation

Parameter	Individual Sandwich Module in an Array in Geosynchronous Orbit	Individual Sandwich Module in Simulated Space Environment	Effect of Difference Between Space and Simulated Space
Minimum Temperature of Surroundings	-270°C	-150°C	Heat radiation is less effective to warmer surroundings
View of Minimum* Temperature Area	Approximately 3π steradians	Approximately 2π steradians	Reduced view to colder surroundings reduces heat radiation ability
Pressure	10^{-11} torr	$< 3 \times 10^{-6}$ torr	Negligible
Illumination Spectrum*	Sunlight in space filtered by reflectors used	Xenon lamp spectrum filtered by fused silica window	Higher spectral component between 850 nm and 1000 nm of xenon will result in increased heating
Illumination Uniformity*	Likely $\pm 5\%$ with adaptive optics	$\pm 20\%$ to $\pm 40\%$ depending on lamp focus setting	Higher variation in uniformity results in a more adverse thermal environment

*Depends in part on the ultimate satellite system implementation

Supporting Equipment and Configuration for Module Testing

The test support equipment used for module data collection is shown in Figure 42. The same equipment was also used with the DC and RF electronics prior to solar

array and antenna integration. Use of LabView software allowed for automated data collection and ease of test repeatability.

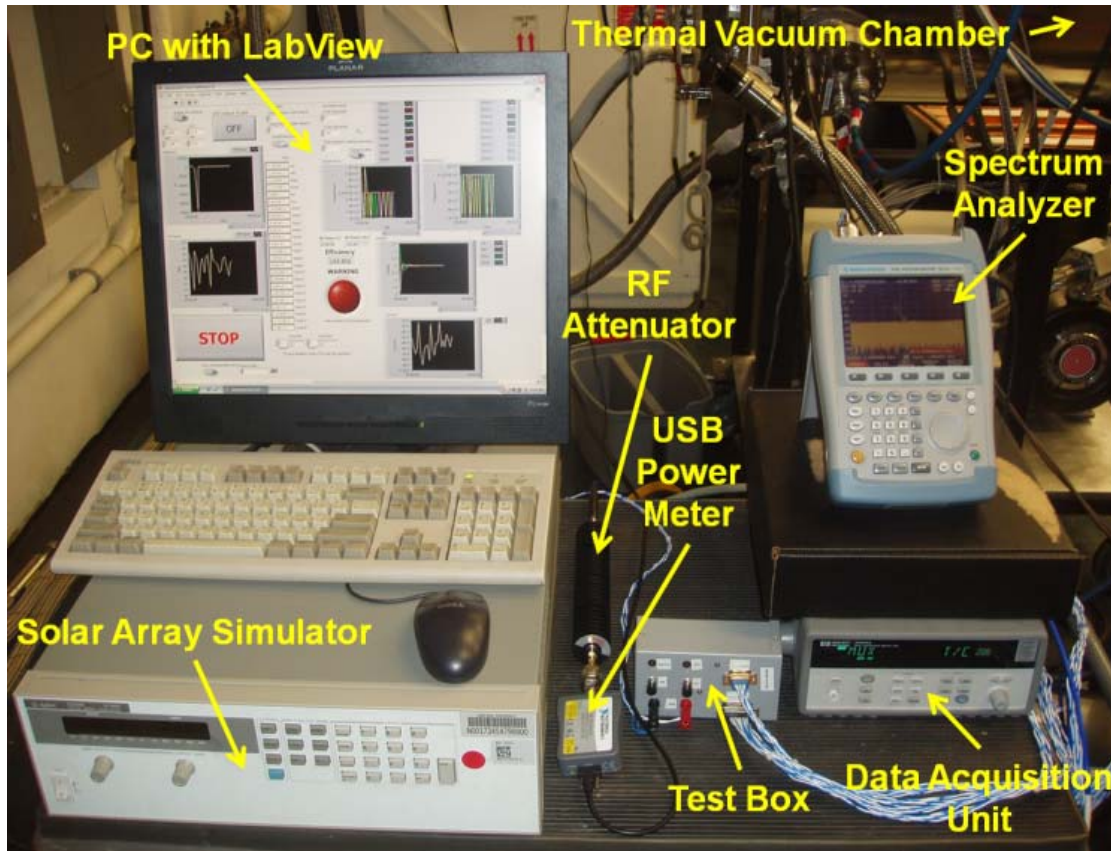


Figure 42: DC and RF electronics test support equipment.

Collected voltages included that of the solar array or solar array simulator output, the biases to the driver and final amplifier stages, and the voltage to the VCO. The current from either the solar array or solar array simulator output was measured using a galvanically isolated Hall effect current sensor. RF output power was measured via a true RMS power meter, and 18 temperature points from a range of locations in the tile module were measured with thermocouples. A subset of the temperature points measured for the tile module during vacuum testing is shown in Figure 43. The two plateaus are a result of different lamp focus settings.

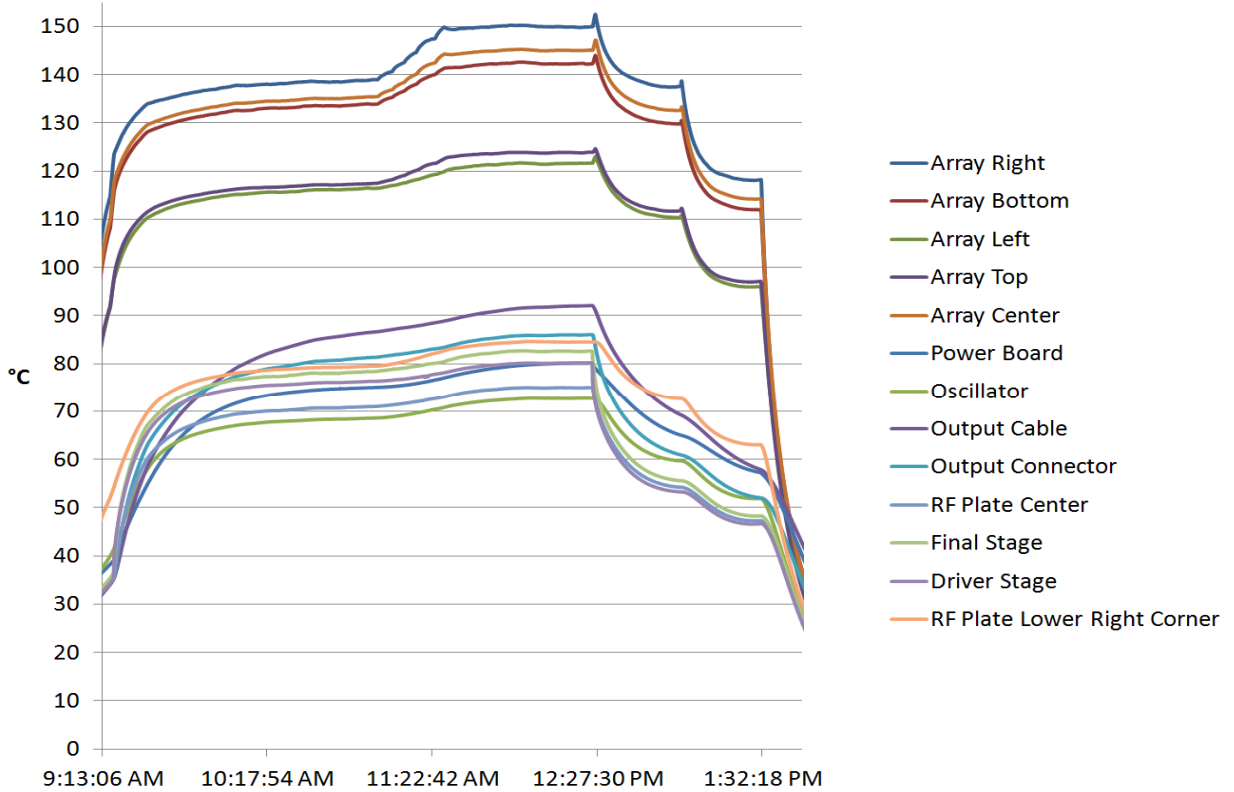


Figure 43: Subset of tile module temperature points collected during a representative vacuum test.

The step module included an additional 18 temperature measurement points to monitor the added RF components in the parallel chains and parts of the structure of interest. The output frequency bandwidth and harmonic levels for both modules were recorded using a spectrum analyzer. Because of the higher output power of the step module resulting from higher solar illumination, additional RF attenuation was put in the RF output path prior to the power meter to protect it from damage and to keep it within its dynamic range. The effect of this attenuation and the losses due to connectors, feedthroughs, and cabling were measured with a network analyzer. The insertion loss measurement for the step module configuration is seen as the value for S21 in Figure 44 as about -53.7 dB.

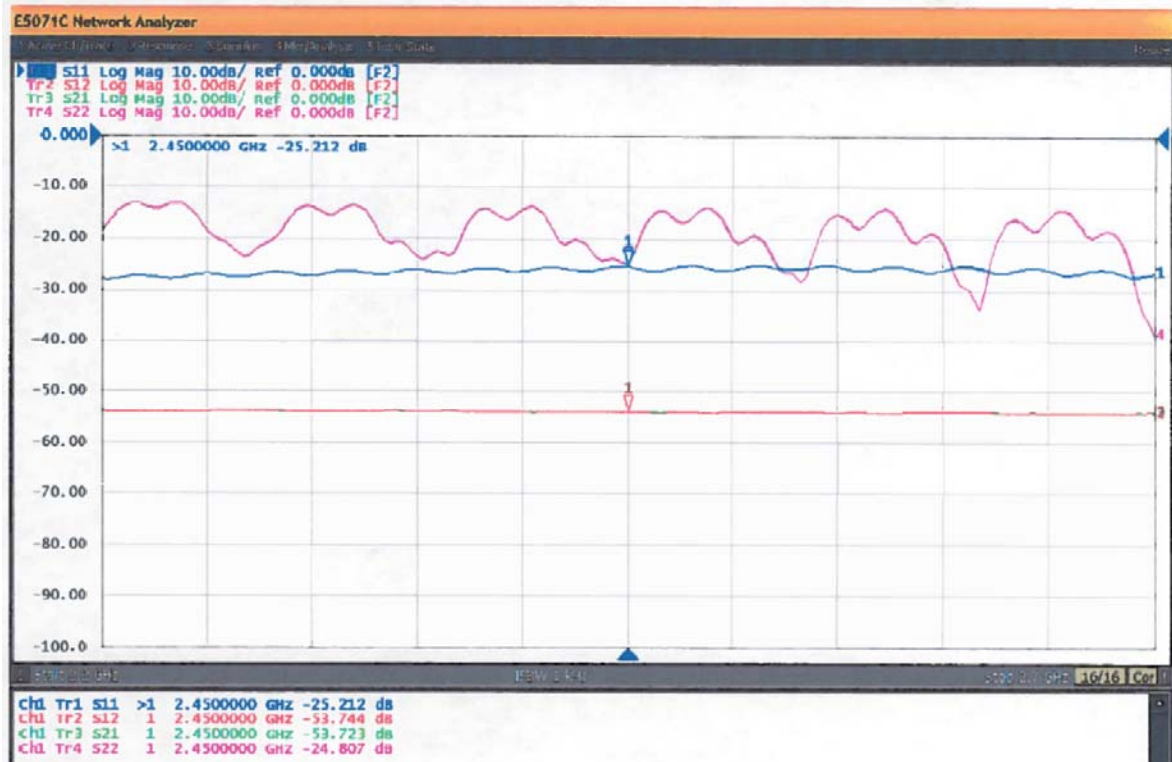


Figure 44: Insertion loss measurement of the step module RF power measurement configuration.

A photograph of the test configuration used for integrated module prototype testing in vacuum is shown in Figure 45. The large protective shroud served to protect test conductors and bystanders in the unlikely event of a catastrophic vacuum window failure, in which fragments of the large vacuum window could be anticipated to be drawn rapidly into the chamber and subsequently rebound out of the chamber opening at a high rate of speed. The shroud would have acted to contain the fragments. Testing proceeded uneventfully in this regard as the vacuum window remained intact.

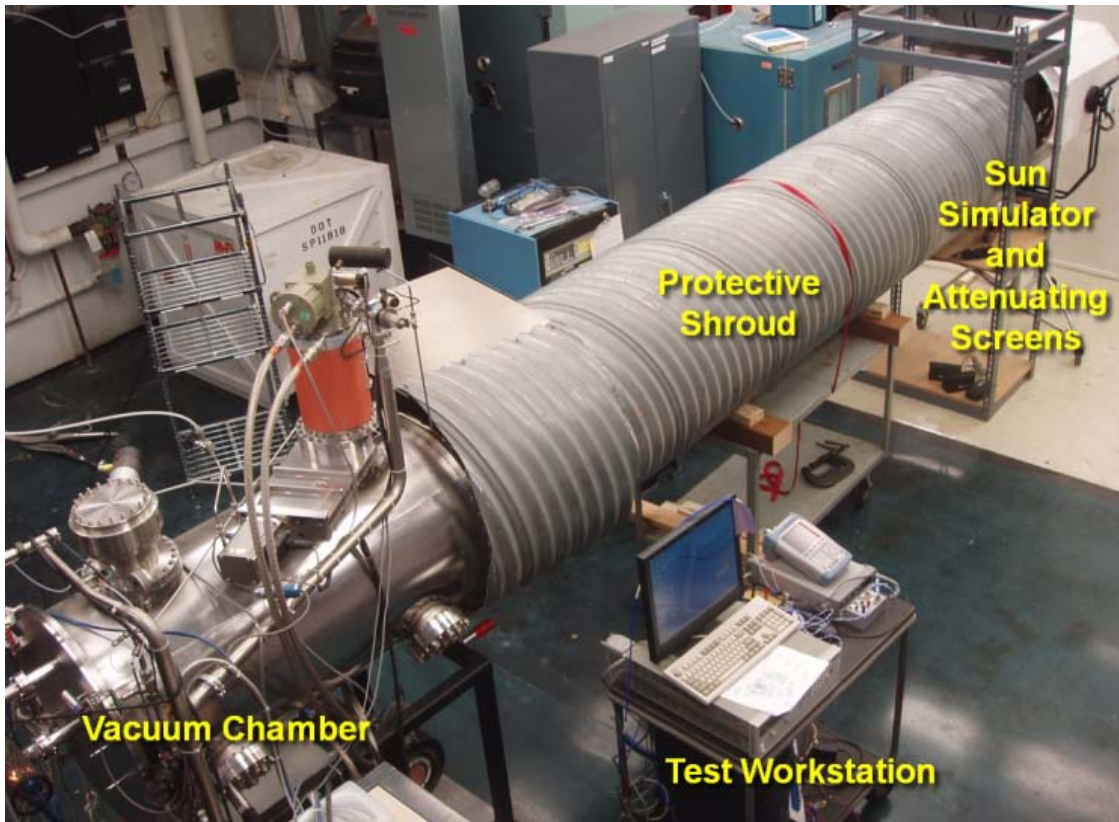


Figure 45: Test configuration for vacuum testing with illumination for the tile module [46].

Chapter 4: Results and Discussion

Overview

The results of the development and testing of the prototypes revealed the challenges of operating in a space-like environment, and the strong influence of the level of solar concentration on demonstrated efficiency and output power level. These results are reviewed, and their effect on and implications for the figures of merit are discussed.

Though this research specifically applies to modular photovoltaic collection / microwave power transmission solar power satellites, many of the findings are also relevant to other solar power satellite concepts and a range of space systems. The figures of merit outlined and economic thresholds posited aim to generalize some of the findings to these larger areas.

Effects of Varying Illumination Conditions and Vacuum

Ambient Testing with Varying Illumination

The electronics' demonstrated efficiency in the integrated module context for both the tile and step modules at ambient (atmospheric pressure) was on the order of $45\pm1\%$ with a solar array simulating power supply, well below the notional efficiency of 80% used in Figure 7. As can be seen in Figure 46, the efficiency of the RF chain when powered using the solar panel was just over 45% under optimal illumination conditions. This is within 2% of the predicted value of 47%. If the illumination level

was below a particular threshold, the efficiency dropped dramatically or was unstable, as can be seen when screens E and D are used, respectively. In this test, screen C gave the maximum sustained efficiency while minimizing the solar array temperature at about 95°C.

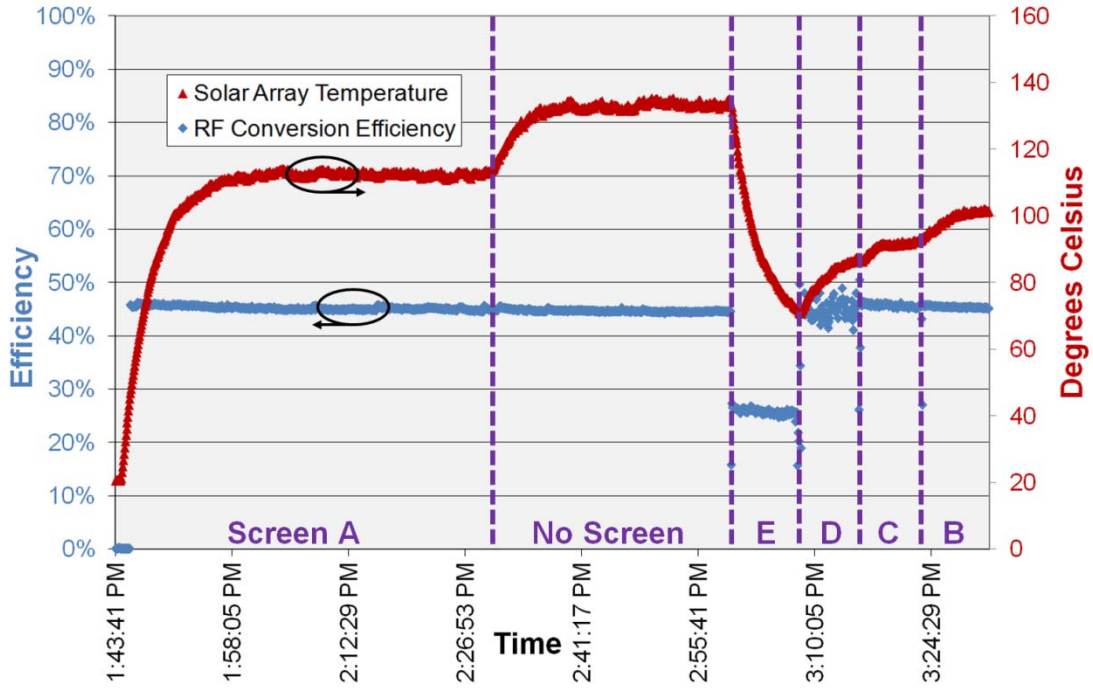


Figure 46: Tile module RF conversion efficiency and solar array temperature during testing at ambient pressure under various illumination conditions.

The amount of power generated by the solar array was greatest immediately after an increase in light intensity. This occurred because the cells had not yet heated up in response to the increase in incident light flux. Once thermal equilibrium was reached and the concomitant voltage drop on the then hotter cells stabilized, the solar array power remained constant. The output power of the electronics generally trended in concert with the solar array power output except in the instance where the array

power was insufficient to sustain operation of the electronics, as was the case with screen E. This behavior can be seen in Figure 47.

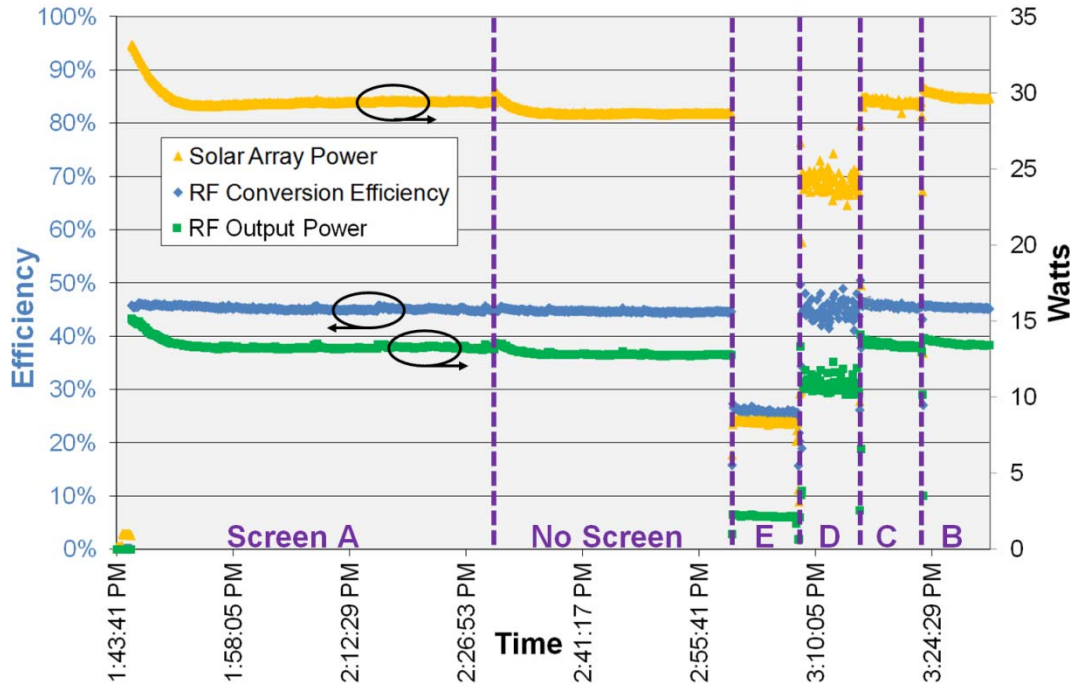


Figure 47: Tile module RF conversion efficiency, solar array power, and RF output power vs. time with various illumination conditions at ambient pressure

Vacuum Testing with Varying Illumination

Summarized results of both ambient and vacuum (10^{-6} torr or less) testing of the tile module are shown in Figure 48. Each of the five plot sections contains clusters of points employing the same marker type. These three markers represent (in order) the mean, minimum, and maximum values recorded during a thirty minute equilibrium period at the condition employed. This conveys the variability observed during testing at each condition. The plotted efficiency is the combined efficiency of both the power electronics and the elements in the RF amplifier chain.

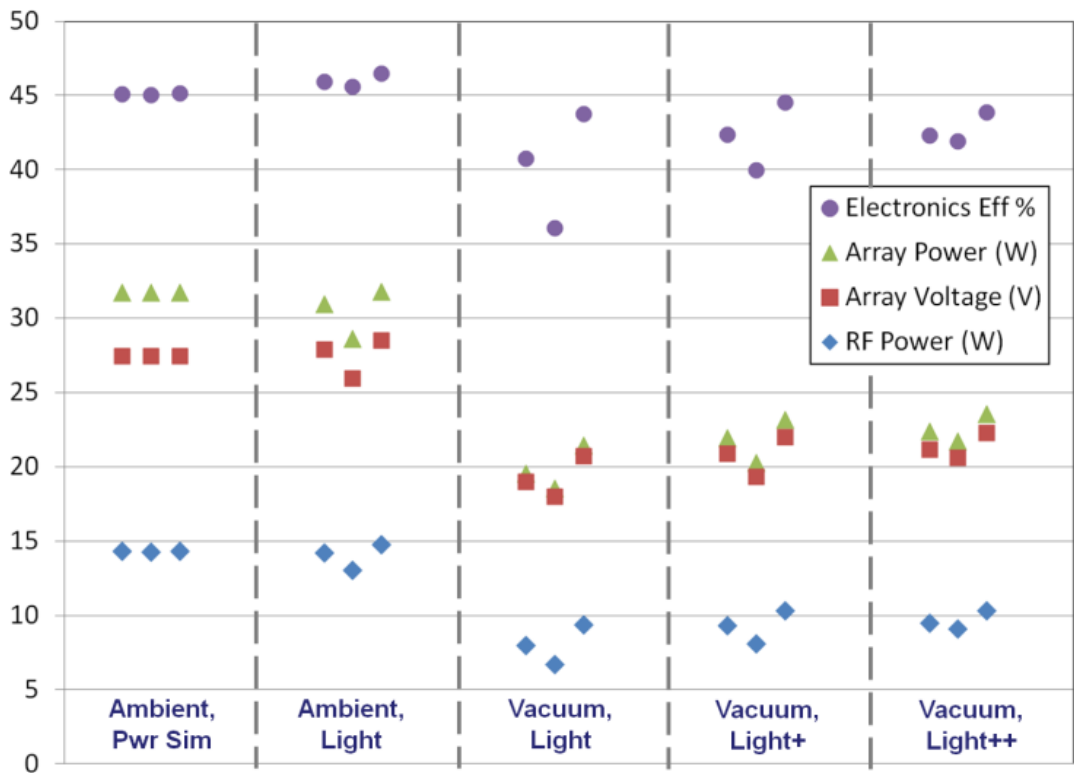


Figure 48: Tile module electronics efficiency, solar array output power, solar array voltage, and RF output power as a function of different operating conditions. Each cluster of three points represents the mean, minimum, and maximum.

The first of the five conditions, “Ambient, Pwr Sim”, was at ambient pressure and used the solar array simulator to provide power to the electronics. The solar array simulator was the DC power supply that was configured to act as a current source in the same way a solar array would. This allowed for operation of the module without the need to always illuminate the array, and also gave a point of comparison to operation with array illumination.

The second condition, “Ambient, Light”, was at ambient pressure with the array

illuminated using the Xenon sun simulator. Note that the voltage and power output of the array vary, which results in more RF output power variation of the electronics compared with when the electronics are powered by the solar array simulating power supply. This could be due to small brightness variations inherent to the xenon sun simulator. The ambient illumination test was performed in the vacuum chamber but without the chamber window in the beam and at atmospheric pressure.

In the third, fourth, and fifth conditions (“Vacuum, Light”; “Vacuum, Light+”; and “Vacuum, Light++” respectively) the module was operated in vacuum and powered by the light from the xenon sun simulator at three different light intensities. Immediately evident was a dramatic drop in solar array output power as compared to the ambient tests. Two factors likely contributed to this: (1) the power reduction due to the beam’s passage through the fused silica chamber window, and (2) in vacuum, the array operated at a much higher temperature because of the loss of the convective cooling mechanism which was available when it was operated at ambient pressure in air. The higher temperature resulted in decreased output voltage; about $6.5 \text{ mV}/^\circ\text{C}$ per cell, according to the vendor’s data sheet for the range 15 to 75°C . The power reduction forced the electronics to operate away from the maximum power point of the cooler array case and pulled down the output voltage. Because the effective load presented by the electronics decreases with decreasing voltage, the operating point on the array’s I-V curve is pulled even farther leftward from the maximum power point, meaning even a small shift in the available current or voltage will result in further degraded output power.

To compensate for these effects, the lamp intensity was increased by changing the

focus slightly. An unfortunate side effect of this adjustment was the beam uniformity degradation discussed previously. It can be observed that while the output power indeed increased, and simultaneously became more stable, the module temperatures increased as well. This effect can be seen in Figure 49. Solar array temps in vacuum rose to as high as 150°C versus about 100°C in ambient due to the lack of convective cooling, as would be expected in space.

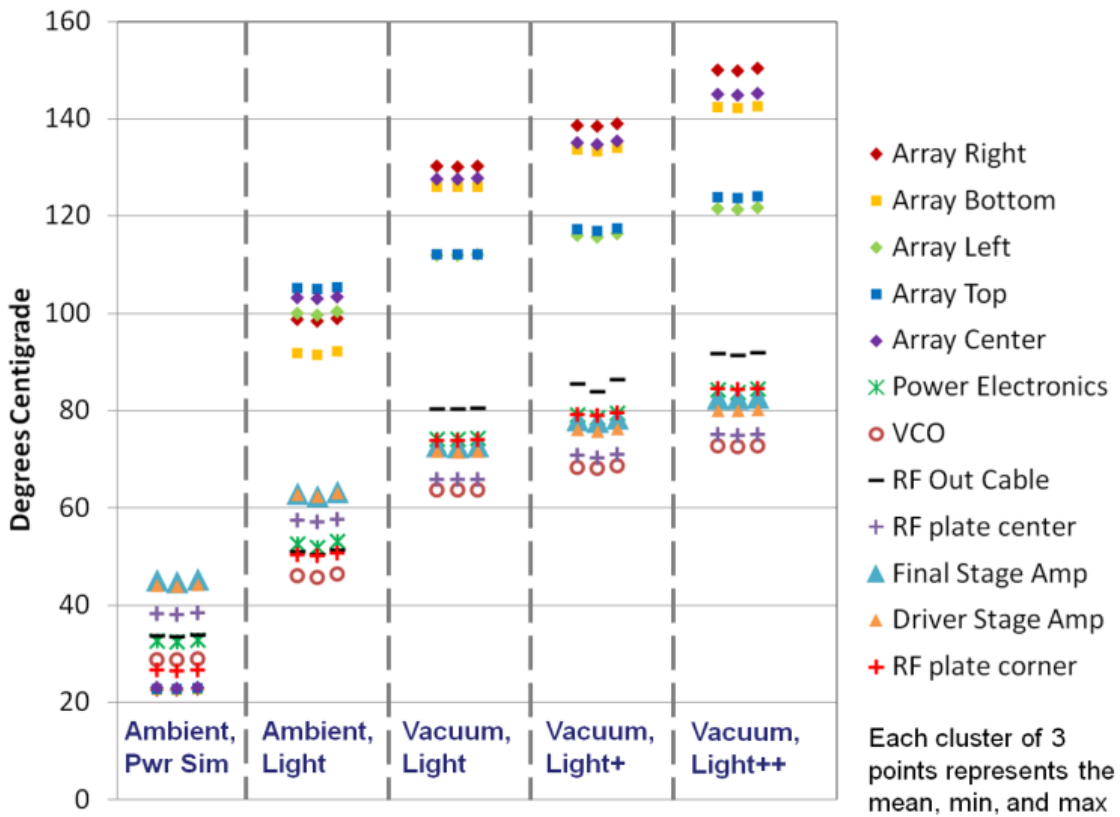


Figure 49: Tile module temperatures as a function of different operating conditions.

The voltage-controlled oscillator used as the frequency source and the GaAs driver stage amplifier both had maximum operating temperatures of 85°C according to their respective datasheets, though discussion with the GaAs driver vendor suggested that somewhat higher operating temperatures would likely merely degrade the device's operating lifetime. Other components had maximum operating temperatures of 125°C or higher. In the fifth condition, the maximum temperature for the driver stage amplifier was approached to within 5°C, making it the limiting component in terms of operating temperature. The highest observed solar array temperature was also in the fifth condition, “Vacuum, Light++”, at 150°C.

Key Figures of Merit and Results

Figures of merit are tied to economic considerations, but also can be used to help set targets for pushing technological boundaries. Outlined below are some of the likely figures of merit for a sandwich module or other conversion device for a solar power satellite that could provide a basis for performance goals or requirements, and to set the context for our results:

Collect/Transmit Area-Specific Mass [kg/m²]

This quantity is of significance because a typical solar power satellite's structure is likely to be dominated by large surfaces for collecting or redirecting sunlight, and in the microwave transmission case, large transmit antenna apertures. Previous estimates of area specific mass for only the transmitter portion of solar power satellite have ranged from about 4 kg/m² to 40 kg/m² [29]. An area-specific mass of 21.9 kg/m² for the overall tile module (including both collection and transmission

functions) was achieved based on a total mass of 1.91 kg and a projected area of $0.286 \text{ m} * 0.305 \text{ m} = 0.0872 \text{ m}^2$. This mass breakdown is shown in Table 5. Contributions to the total module mass from structural components, the solar arrays, and conversion electronics are compared in

Figure 50. Clearly, there is room for mass reduction, and a flight module could expect to improve on these results.

Table 5: Tile module mass breakdown, all measurements are in grams. Items marked with * indicate estimated contributions based on difference with total measured mass. Mass was measured using antenna mockup rather than actual antenna.

Item	Description	Qty	Measured	Total Measured
Top plate	12" x 11.26" Al6061-T6 sheet with 1/16"	1	392.25	392.25
Bottom plate	12" x 11.26" Al6061-T6 sheet with 1/16"	1	371.70	371.70
Elbow plate	2" x 1" Al6061-T6 sheet with 1/16" thickness	8	0.00	0.04
Rivet	P/N: MS20426-A03-4. Holds top plate and	16	0.09	1.46
SpaceQuest clip	Panel consisting of 14 PCB-mounted solar cells	2	110.30	220.60
4-40 bolt, short	Flat head bolt attaches Spacers and bottom	32	0.40	12.80
4-40 bolt, long	Attaches top and bottom plates	4	1.27	5.08
4-40 nut	Nut	36	0.46	16.56
4-40 washer	Washer	36	0.38	13.68
Spacer	Aluminum Spacer block between top and	4	22.70	90.80
Antenna*	Short backfire antenna	1	300.00	300.00
Voltage-Controlled Oscillator (VCO)	Source, 2.45 GHz	1	19.43	19.43
Hittite board	Driver stage power amplifier	1	20.42	20.42
CGH27015	Final stage power amplifier, Cree board	1	63.70	63.70
Attenuator	Male to female SMA	1	4.09	4.09
Band Pass Filter (BPF)	Male to female SMA	1	8.96	8.96
N female flange mount	Antenna feed to N-SMA cable connetor	1	5.31	5.31
N-SMA cable	Right-angle N to Male SMA connector.	1	22.56	22.56
SMA cable 1	6" Male-Male SMA cable. Cree board to hittie	1	9.73	9.73
SMA cable 2	6" Male-Male SMA cable. Hittie board to BPF	1	9.73	9.73
Power board and Wiring	Power PCB with 1/4" 4-40 stand-offs and	1	107.11	107.11
Antenna mounting bracket*	For securing antenna to module	8	2.00	16.00
Thermal grease and adhesives*	To establish thermal connections	1	100.00	100.00
Kapton tape, MLI, thermocouples*	Thermal features	1	100.00	100.00
				1912.01

Structural components	1420.37	74%
Solar array	220.60	12%
Conversion electronics	271.04	14%

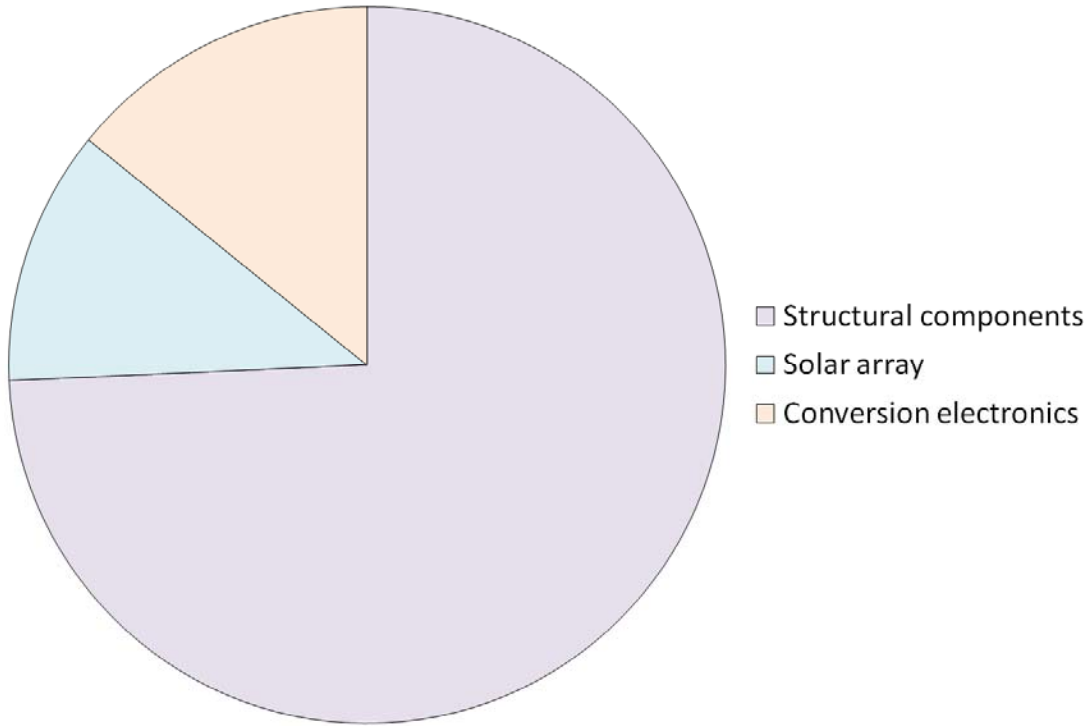


Figure 50: Mass contributions of major categories of tile sandwich module parts.

For the step module, an area-specific mass of 36.5 kg/m^2 for the overall module was achieved based on a total mass of 3.33 kg and a projected area of $0.286 \text{ m} * 0.319 \text{ m} = 0.0913 \text{ m}^2$.

Mass-Specific Transmitted Power [W/kg]

“Specific Power” is of typical interest for satellite solar arrays as it conveys the mass needed to provide a given power level. Mass-specific transmitted power is instead taken with respect to microwave transmit power to assess the amount of installed generating capacity that would result from a given number of launches for a solar power satellite. In this case, the necessary reflector system to illuminate the array of sandwich modules is neglected. This figure of merit is of prime interest as it

feeds into a range of solar power satellite economic analyses, and in particular the simplified economic model presented in Chapter 5: **Potential Economic Thresholds**. The tile module prototype gave a mass-specific power of 4.5 W/kg at about one sun minimum illumination with solar array temperatures ranging from 122-150°C under vacuum of about 10^{-6} torr. The step module prototype gave a mass-specific power of 5.8 W/kg at about 2.2 suns minimum illumination with estimated solar array temperatures ranging from 225-300°C under vacuum of about 10^{-6} torr. The solar array temperatures are estimated because the initial instrumentation of the step module only measured the temperatures on the back side, and these proved dramatically divergent from temperatures later measured on the front side under slightly different conditions.

Combined Conversion Efficiency

The efficiency of the module is of great interest in that higher efficiencies help alleviate thermal dissipatation problems by constraining the amount of heat that needs to be rejected.

Though the solar cells are quite efficient, there is a penalty, the “packing factor”, in any solar panel implementation for the areas on the panel that are not covered with cells. Hence, the panel efficiency is lower than the cell efficiency. The manufacturer’s quoted cell efficiency is for the bare cell; addition of a cover glass will reduce cell efficiency by about 0.5%, depending on the cover glass thickness. Also, unless the array is operated at the maximum power point on its I-V curve, the effective efficiency will be lower than the panel’s maximum. In vacuum testing, we were operating farther from the maximum power point than originally intended; this

was the largest detriment to the effective panel efficiency. Operating the array at elevated temperatures also significantly degraded the efficiency.

From a functional standpoint, the power electronics efficiency was high, due in large part to directly driving the final stage RF amplifier from the solar panel. DC-DC converters were only employed where needed to produce supply and bias voltages. This efficiency was measured under realistic operating conditions at the subassembly level.

The RF chain efficiency is reasonable, but does not approach the upwards of 80% efficiency demonstrated by some researchers. If the electronics had operated near the peak power point of the array while in vacuum, the demonstrated figure would likely have been about 3% to 4% higher, as it was under ambient conditions, and the total module output power would also have increased by 3 or 4W since the effective solar array efficiency would have increased as well.

The antenna efficiency shown here is the product of simulation.

As seen in Table 6, the total combined efficiency in vacuum for the tile module was on the order of 8% with 9W power output. At ambient pressure with no chamber window, these figures were 11% with 14W power output.

Table 6. Efficiencies for the 2.45 GHz prototype tile module in vacuum at about one sun illumination (117W input over 0.087m²).

Element	Goal	Achieved	Power Out (W)
Solar Panel	24%	19%	22
Power Electronics	95%	97%	22
RF Chain	50%	44%	9
Antenna	95%	95%*	9
COMBINED MODULE	11%	8%**	9

*From simulation

**Using simulated efficiency for antenna

Efficiencies were similar for the step module, with the exception of the solar panel, which was found to be nearer 17%. This efficiency degradation can probably be attributed to the elevated operating temperature. However, the power output doubled to 18 W and the resulting combined module efficiency was 7%.

The biggest shortcoming of the step module is that it did not operate for very long. After about an hour of operating the soldered terminals on the ends of the strings began to detach, opening up one of the strings. Subsequent inspection showed also that two of the cells were beginning to detach from the RTV. It was later determined that the lower through-plane heat conductivity of the graphite sheeting was acting in effect as a heat shield and preventing much of the heat from being moved to the radiators, hence generating the much greater operating temperatures than predicted by initial simulations with no graphite layer. Additionally, it was observed that the test

setup was such that the radiator surface opposite the electronics plate was being illuminated by one of the xenon lamps, retarding its heat rejection effectiveness.

Though the step module did exhibit a better W/kg figure than the tile module, its short operating life indicates that the design needs revision before it can be seriously considered as a viable alternative to the tile module.

Additional Figures of Merit and Module Qualities of Interest

Other figures of merit of possible interest for conversion module prototypes and certainly for flight units would include [47]:

- Survival temperature range [$^{\circ}\text{C}$]
- Continuous operation duration [hours]
- Solar concentration acceptance [number of suns]

While not necessarily figures of merit, other module qualities of possible interest include:

- Adaptability for control of the microwave power beam
- Susceptibility to space radiation environmental effects
- Susceptibility to solar wind and space weather effects
- Rate of degradation due to solar ultraviolet light exposure
- Space environment charging behavior
- Susceptibility to parts aging effects

- Avoidance of radio frequency multipactor effects
- Launch acoustic and vibration environment tolerance
- Electromagnetic compatibility and interference susceptibility
- Manufacturability
- Ease of integration with other modules in space
- Ability to transfer heat from other modules
- Ability to transfer electrical power from other modules
- Outgassing qualities that could affect PV performance
- Structural rigidity
- Reliability
- Durability
- Serviceability

Each of these qualities and the more fundamental figures of merit discussed previously may be used as inputs to economic models to find feasibility thresholds for different solar power satellite system implementations.

Chapter 5: Potential Economic Thresholds

Generalized Comparison of Energy Sources

Since interest in alternative energy sources began, a number of means of economic comparison have been devised. Among the most widely used is that of Levelized Cost of Energy, (LCOE). Many different ways of calculating LCOE have been proposed and used. Most can be reduced to a representation resembling the following [48]:

$$LCOE = \frac{TLCC}{\sum_{n=1}^N [Q_n / (1 + d)^n]} \quad (3)$$

With TLCC = total life-cycle cost, Q_n = energy output in year n, d = discount rate, and N = the analysis period. If the discount rate is set to zero and it is assumed that the values for all years are identical, the expression can be further simplified to:

$$LCOE = \frac{TLCC}{Q_{total}} \quad (4)$$

That is, the Levelized Cost of Energy is the total life-cycle cost divided by the total energy output. This is commonly expressed in \$/kWh or \$/MWh. By framing an economic assessment of space solar power in these terms, it can be compared in a general sense to other energy alternatives.

Economic Analyses for Solar Power Satellites

Solar power satellite economic analyses have been performed since the concept was originally proposed, some in considerable depth [49]. Recent analyses have addressed sandwich-based solar power satellite system implementations specifically [50]. Though a detailed system level economic analysis is beyond the scope of this work, valuable conclusions can be drawn from looking at a few important variables and making some simplifying assumptions.

Several authors have contended that the most cost-effective means of putting a solar power satellite system in place would be to use extraterrestrial materials [51][52]. Though this may be the case, it is probable that pathfinding demonstrations for solar power satellites would require the launch of the components from earth. For this reason, the simplified economic analysis presented here will assume launch of the system mass from earth.

Space solar power economic models can potentially utilize a wide range of inputs and produce a comparably wide range of outputs. For a straightforward analysis, the inputs from Table 7 can be considered to generate an approximate Levelized Cost of Energy:

Table 7: Minimal inputs for a space solar power cost model

Input	Unit
Mass-specific transmitted power of conversion element, MSP	W/kg
Total on-orbit service life, TSL	years
Cost of launch to low earth orbit, COL	\$/kg
Cost of conversion element space segment, CSS	\$/kg

Additional system variable that could be considered for economic analyses include:

- Solar concentration factor
- Space segment conversion efficiencies (PV, DC-RF, antenna)
- Area-specific mass (PV, sandwich module, reflectors)
- Mass of space segment elements (energy conversion, structures, attitude control system, propellants)
- Transmit antenna diameter
- Transmission frequency
- Orbital assembly costs
- Orbital altitude
- Satellite constellation size
- In-space transportation costs
- Space segment operation and maintenance costs
- Launch vehicle mass and volume capacities (low earth orbit, geosynchronous orbit, geosynchronous transfer orbit)

- Launch segment costs
- Launch rate
- System deployment time
- Non-space segment system efficiencies (beam coupling, tropospheric effects, rectenna, grid transmission)
- Power desired at receiving station
- Power density desired at receiving station (center, perimeter)
- Receiving station diameter
- Receiving station real estate costs
- Ground segment operation and maintenance costs
- Cost of energy trends
- Non-recurring development costs
- Manufacturing costs
- Financing costs
- Development incentives

Note that depending on the system requirements, a given quantity might be treated as an input or an output. For instance, for an implementation that imposes constraints on the available collection area on the ground, such as power for a forward operating base for military purposes, that quantity would be an input. For an implementation where minimizing total power cost is more important, ground collection area might be comparatively unrestricted.

For a simple model based on the quantities in Table 7, the following relation can be constructed:

$$LCOE = \frac{COL+CSS}{MSP*TSI} \quad (5)$$

Though this relation neglects many of the variables listed above that would contribute to the cost of system implementation, it serves as a means of establishing a lower bound for cost estimates. Notable omitted contributions include low earth orbit to geosynchronous orbit transportation costs, ground segment costs, operations and maintenance costs, and any costs associated with the space segment other than those for the conversion elements, that is, the sandwich modules.

Cost of launch to low earth orbit, COL, could reasonably be expected to vary greatly with the demand for launches. An enterprise associated with developing a solar power satellite system would likely create an unprecedented demand for launch capacity, in all likelihood driving prices downward. An ultimate lower bound for this cost element has been outlined in [14, p. 37] and posits \$3.30/kg, assuming an energy cost of \$0.10/kWh. A review of launch prices from United States launch providers circa 2012 finds a range of unit prices between about \$2,000/kg and \$12,000/kg, varying largely as a function of maximum payload mass delivered to low earth orbit, with larger payload masses resulting in lower launch costs. Though most space launch providers are coy about openly publishing their launch prices, SpaceX claims a “paid in full standard launch price” of \$135M for the Falcon Heavy to put 53,000 kg in a 28.5° inclination low earth orbit [53]. This equates to a unit price of about \$2,500/kg.

The cost of the conversion element portion of the space segment, CSS, can be estimated in a number of ways. A common rule of thumb for low-volume space missions has been \$10,000/kg. Since mass production of sandwich modules would offer improved economies of scale, the resulting cost could be expected to be lower. The material cost of the prototypes developed for this effort was on the order of \$20,000 per unit, with the majority of the cost being the high-efficiency solar cells. With a mass just under 2 kg for the tile module, the result closely matches the predictions from the rule of thumb. For comparison, commercial solar panels featuring about 15% efficiency are available for approximately \$10/kg. Another high volume mass-produced item with greater complexity than a solar panel that offers an instructive comparison is the high definition television. These retail at unit prices on the order of \$50 to \$75 per kg; undoubtedly the manufacturing unit price is lower.

As noted in the results chapter, the mass-specific transmitted power, MSP, achieved in this effort for the tile module, with minimal attention to opportunities for mass reduction, was 4.5 W/kg.

The total service life, TSL, of existing satellites varies widely. Satellites have been known to have operating lifetimes measured in decades, with ATS-3 and LandSat-5 (34 and 28 years of operation, respectively) exhibiting the greatest longevity. Operating lifetimes in excess of ten years are very common. While space can be a hostile environment from temperature, radiation, and vacuum standpoints, it is devoid of hazards due to moisture, vandalism, and those of terrestrial weather and geophysical origins. A common life-limiting factor is propellant supply, which might

be avoided for solar power satellites by employing a geosynchronous Laplace plane orbit which requires no station-keeping propellant.

Four cases are examined with different assumptions for each of the four inputs to the simplified Levelized Cost of Energy model. These are:

- Case 1 – Using currently demonstrated values
- Case 2 – Assuming incremental improvements
- Case 3 – Assuming aggressive improvements
- Case 4 – Assuming revolutionary improvements

The values used in resulting \$/kWh output for each case are shown in Table 8. As would be expected, increases in mass-specific power and total service lifetime have the greatest effect in decreasing the Levelized Cost of Energy. In the absence of any improvement in the other figures of merit, a LCOE of about \$0.10 per kWh could be achieved if mass-specific power increased to 700 W/kg, or if the service life could be extended to 3,300 years, or if the combined cost of launch and space segment hardware development could be reduced to \$80/kg. As a point of reference, the mass-specific power of the UTJ solar cells used for the prototypes (neglecting any DC-to-RF conversion or structure) is on the order of 450 W/kg, though it is possible the cell substrate could be removed and replaced with a lighter material. Silicon and thin-film solar cells are less efficient, but have mass-specific power figures reported as high as 700 to 3,000 W/kg, respectively. Regardless, improvements in several rather than a single figure of merit are likely needed.

Table 8: Four cases with varying assumptions to generate Levelized Cost of Energy values for solar power satellites.

Inputs	Case 1	Case 2	Case 3	Case 4
Mass-specific power (W/kg)	5	20	80	200
Total service life (years)	20	25	30	35
Cost of launch (\$/kg)	2,500	1,000	500	100
Cost of space segment (\$/kg)	10,000	5,000	1,000	100
<hr/>				
Output				
Levelized cost of energy (\$/kWh)	15.84	1.37	0.07	0.0033

The results from each of the four simple solar power satellite model cases are shown in context against conventional energy sources in Table 9. Data for the conventional energy sources is from [54]. These figures do not include the effect of any tax credits or other incentives that may be applied to encourage the development of particular energy sources.

Table 9: Comparison of simple solar power satellite Levelized Cost of Energy cases with conventional sources in \$/MWh. Conventional energy data from the U. S. Energy Information Administration [54].

Plant Type	Capacity Factor (%)	Levelized Capital Cost	Fixed O&M	Variable O&M (including fuel)	Transmission Investment	Total System Levelized Cost
Natural Gas: Advanced Combined Cycle	87	17.9	1.9	44.4	1.2	65.4
Natural Gas: Conventional Combined Cycle	87	17.5	1.9	48.0	1.2	68.6
Hydro	53	76.9	4.0	6.0	2.1	89.0
Wind	34	83.3	9.7	0.0	3.7	96.7
Conventional Coal	85	65.8	4.0	28.6	1.2	99.6
Geothermal	92	76.6	11.9	9.6	1.5	99.6
Advanced Coal	85	75.2	6.6	29.2	1.2	112.2
Advanced Nuclear	90	88.8	11.3	11.6	1.1	112.8
Biomass	83	56.8	13.8	48.3	1.3	120.2
Advanced Coal with CCS	85	93.3	9.3	36.8	1.2	140.6
Solar PV	25	144.9	7.7	0.0	4.2	156.8
Solar Thermal	20	204.7	40.1	0.0	6.2	251.0
Solar Power Satellite Case 1	90	15,844.0	0.0	0.0	0.0	15,844.0
Solar Power Satellite Case 2	90	1,368.9	0.0	0.0	0.0	1,368.9
Solar Power Satellite Case 3	90	71.3	0.0	0.0	0.0	71.3
Solar Power Satellite Case 4	90	3.3	0.0	0.0	0.0	3.3

Cases 3 and 4 appear to be competitive with current energy alternatives, but the assumptions in the simplified model imbue considerable uncertainty. It is probably fair to assert that currently demonstrated capabilities are at least two orders of magnitude removed from utility grid viability, given existing assumptions.

However, the situation for “premium, niche markets” [14] may be more viable. In military scenarios, the delivered cost, or “fully burdened cost,” of fuel has ranged as high as \$400 per gallon for situations where several stages of helicopter delivery are required [55]. The Congressional Research Service surveyed reports from the Defense Logistics Agency that cited studies done by the Army, Air Force, and

Marines and found a range from \$3 to \$50 per gallon depending on the mode of delivery, unsurprisingly with ground transportation means tending to be cheaper and air means more expensive [56]. This energy is much more expensive than utility grid users are accustomed to, and it presents a clearer potential opportunity in the near term for power provision via solar power satellite. Table 10 presents a comparison of the simple solar power satellite model results against the fully burdened cost of fuel kWh kerosene-based jet fuel (such as JP-8) equivalents. For this comparison, an equivalency of 37.5 kWh per gallon of kerosene-based jet fuel was used [57]. This was motivated by the fact that most of the U.S. Department of Defense uses JP-8 kerosene-based fuel: standardization across vehicles eases the logistical burden. JP-8 also contains about 10% more energy per unit volume than gasoline, enhancing the energy per unit delivered.

Table 10: Comparison of fully burdened cost of fuel kWh kerosene-based jet fuel equivalents to solar power satellite levelized cost of energy model results.

\$/(Gallon of JP-8)	\$/kWh
3.75	0.10
7.51	0.20
15.02	0.40
22.53	0.60
30.03	0.80
37.54	1.00
45.05	1.20
52.56	1.40
60.07	1.60
...	...
450.51	12.00
...	...

← 0.07 SPS Case 3

← 1.37 SPS Case 2

← 15.84 SPS Case 1

Patently apparent from Table 10 is that the solar power satellite model results fare much better from a cost feasibility standpoint. Even in Case 1 where only existing levels of technology are assumed, the result comes close to being competitive with the most extreme fully burdened fuel cost situation, and SPS Cases 2 and 3 are well within the realm of the reported fully burdened cost range. The same caveats as applied with respect to the simple solar power satellite model's limitations should be observed, and the further challenges with respect to power density, portability, and resource access control inherent in military applications described in [12] should be considered as well. Perhaps most importantly, though electrical generators used by

the military do run on JP-8, much of the JP-8 is consumed by vehicles that might not be easily converted to run on electricity in the near term, such as helicopters and fixed wing aircraft. A paradigm shift in how military vehicles are powered would thus likely be required for true feasibility, as greater than 70% of DoD energy use is as petroleum-based fuels, and of that greater than 90% is for vehicular purposes [56]. While there has been tacit interest in electric and hybrid vehicles for military use, most notably for ships and tactical ground vehicles, the switch to an all-electric approach is deterred by the classic problem of battery energy density being a fraction of that of petroleum-based fuel. Though electricity from solar power satellites could conceivably be used in a military or other niche application to generate synthfuels via a Fischer–Tropsch or derivative process, fuel feedstocks would still be required. For military applications in particular, it should also be considered that a rectenna receiver could present a large, though possibly robust, target for enemy attack.

Chapter 6: Conclusions

Summary

A review of the vast body of prior work related to solar power satellites reveals many intriguing concepts. The wireless power transmission required for most proposed concepts is well understood, and techniques for the safe retrodirective control of the microwave beam have been developed and demonstrated by others. Focus on solar power satellite architectures that exploit modular elements that could be created through mass production has stimulated interest in the sandwich module and was the genesis of this effort. Thermal analyses and testing showed that the sandwich module design and its operation posed significant challenges. This sandwich module prototyping and characterization effort demonstrated the fundamental functional feasibility of such units for use in a space environment, but also illuminated the integration and testing challenges, as well as the limits of currently achievable systems.

The module prototype development and subsequent testing performed achieved the goals from the project's outset. The results affirm that thermal concerns are paramount in sandwich module design, and suggest that even novel approaches, such as the step module, to the sandwich architecture will need to be carefully implemented to effectively address this problem. Prototypes were successfully tested in vacuum under simulated sunlight illumination.

Implications of Present Work

This work has contributed to an empirical foundation for informing debates on the technical and economic viability of a prominent class of proposed space solar power systems. By creating a functional, actual sandwich modules and testing them under realistic conditions, a lower bound has been set on what could be possible for this element in a solar power satellite system.

The tile module demonstrated a collect/transmit area-specific mass of 21.9 kg/m^2 , a mass-specific transmitted power of 4.5 W/kg , and a combined conversion efficiency of 8% in vacuum. The step module demonstrated a collect/transmit area-specific mass of 36.5 kg/m^2 , a mass-specific transmitted power of 5.8 W/kg , and a combined conversion efficiency of 7% in vacuum. These figures represent points of departure for future improvements to sandwich module performance.

Future Work

There are many opportunities for future work beyond this effort. Insights gleaned during the course of the project point not only to sandwich module implementation improvements, but also to avenues of further investigation in testing, as well as to other concepts for utilizing sandwich modules in a large array. Some possible directions are outlined below.

Specialized Test Facility Development

To make substantive progress in assessing the performance of sandwich modules or other devices that are designed to operate in vacuum under solar illumination

equaling or exceeding one sun AM0 intensity, it will be critical to have a facility capable of accurately and consistently reproducing these conditions realistically. A major challenge of this work was addressing this point, and it became clear that currently this is something for which there are limited options. In particular, the production and measurement of an even light field poses significant difficulty at high intensity levels. While not directly related to the work done in developing the module, this is assuredly an area in which future work is needed.

Production and measurement of a uniform light field are of paramount importance. Possible means of enhancing field uniformity in conjunction with bright, uneven sources include the use of reflectors employing adaptive optics, or using custom-fabricated or adjustable screens. Alternatively, an existing commercial sun simulator such as the Spectrosun® X-25, or an array of such simulators, could be used to achieve the desired intensity while providing good uniformity. This approach might require making smaller module prototypes to ensure that they are fully illuminated. The illumination system (e.g., lamp location and pointing) should be robustly resistant to accidental changes, and any changes in intensity should be easily and effectively repeatable in the event there is a need to repeat testing under identical conditions following a configuration change. The facility should also have an integrated field uniformity measurement system capable of rapid field uniformity measurements during the course of testing to ensure the field is consistent and that any changes can be accurately characterized. This likely means utilizing a Lambertian surface large enough to intercept the beam that can be easily inserted repeatably for field measurements and then removed. Similarly, optical power meter measurements

need to be consistent and repeatable, and the beam profiling imager needs to remain fixed throughout testing.

Using a comparatively small vacuum chamber in this effort proved invaluable, as it allowed reasonably quick iterations without the need to spend a great deal of time transitioning between ambient and vacuum pressures and ambient and cold temperatures. Future efforts should exploit the agility afforded by this approach; perhaps an even smaller chamber could suffice.

An effective test facility offers utility not only for the testing of sandwich modules, but could be used to test other possible solar power satellite technologies, such as solar dynamic heat engines or sun pumped lasers. Such a facility could also be used in the simulation of the solar illumination environment that space probes to locations inside the earth's orbit would experience, such as nanosatellite missions to Venus, Mercury, or the sun.

Antenna Characterization

The focus of this research was not on the antenna performance beyond the fact that the antenna would act as a workable transmit element and simultaneously perform as an effective thermal radiator for heat rejection. Future testing efforts should delve into more detail in regards to sandwich module antenna radiation patterns, sidelobe suppression performance, and performance in array configurations. For radiating antenna characterization, an anechoic chamber facility like that pictured in Figure 51 will be required.

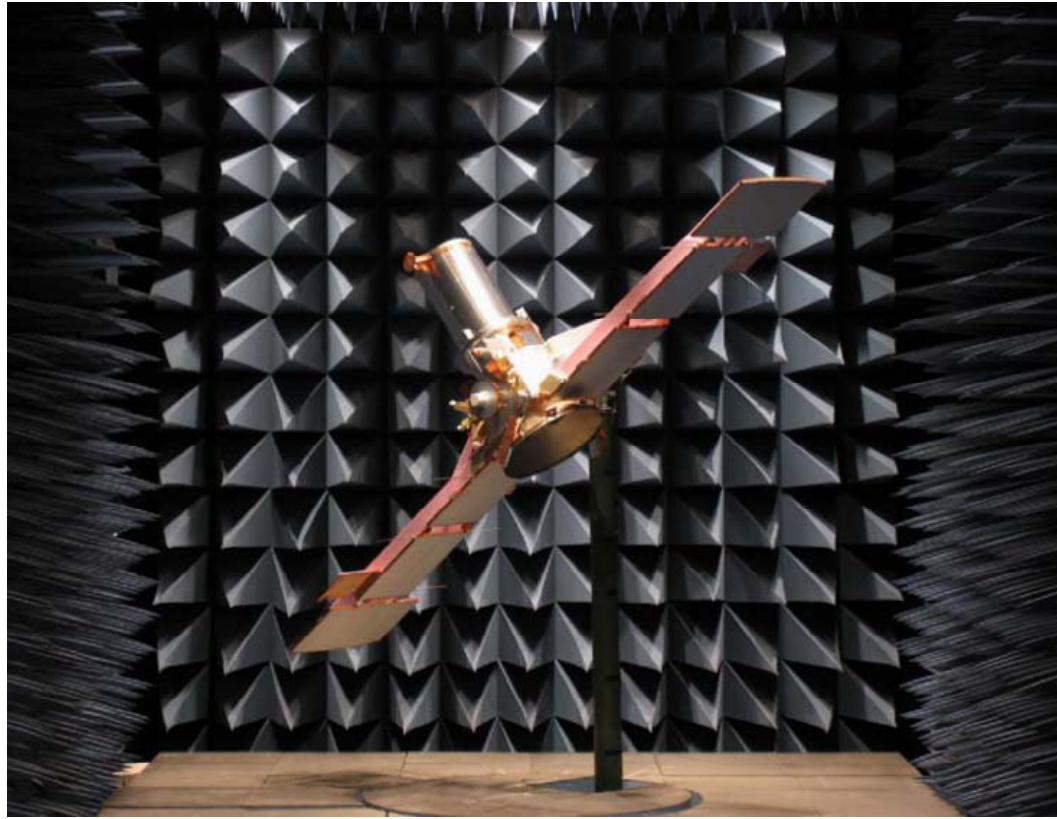


Figure 51: NRL RF Anechoic Chamber [58]

Testing a biaxially symmetric array of transmitting elements, both tile and step configurations, would help determine how closely the design goal of suppressing the array sidelobes was achieved. Varying the phase input between array elements would also demonstrate the degree of steerability inherent in such an array. The antenna array and RF electronics might be modified to incorporate a pilot signal receive antenna and phase control electronics, respectively.

Mass Reduction

Easily evident from the prototypes produced are opportunities for mass reduction. In many cases, given components were used for expedience at the expense of added

mass. Development of a monolithic microwave integrated circuit (MMIC) to perform many if not all of the functions in the RF chain would reduce mass and through judicious design would almost certainly increase efficiency as well.

The largest contributor to mass among the categories of structural components, solar array, and conversion electronics was that of structural components by a wide margin. This area likely offers tremendous opportunities for mass reduction through use of novel materials such as composites or carbon nanotube-based materials. These might have the added benefit of fostering heat transport. Mass reductions realized through minimizing structural component mass would perhaps offer the biggest benefit to the step module because of its comparatively large structural mass percentage.

The solar array could also be reduced in mass using techniques to remove much of the cell substrates. Fabrication methods that dispense with the room temperature vulcanizing (RTV) cell adhesives would reduce mass and could extend the maximum temperature range of the array. Thin film solar cells might be employed as an alternative, though to date their efficiencies have been lower than triple junction cells.

Thermal Management Improvements

Though in each of the prototypes thermal features were implemented, there is much room for improvement. In both modules, the black Kapton® tape used to increase surface emissivity could be replaced with black anodization, which could more tightly couple the heat transfer from the substrate to the radiating surface. Alternatively black high emissivity or carbon nanotube impregnated paint could be used.

Heat transfer within the module could be improved as well. Though in both the tile and step modules separate thermal zones were maintained to allow the electronics to operate at cooler temperatures than the solar array, this might not be necessary if either the photovoltaics were more efficient and generated less heat, or if the electronics could operate at higher temperatures. Even if it still proved most beneficial to maintain separate thermal zones, there would still be a potential need to spread heat more effectively within them. In particular, rapid heat spreading from the final stage and driver stage amplifiers would lower their junction temperatures and promote higher efficiency and enhanced reliability. Possible methods to accomplish this might include films or substrate layers of ceramics (such as AlSiC), metallics or metal particle infused epoxies, diamond, graphite, or graphene. Care would need to be exercised to ensure that the problems associated with the differences in through-plane and in-plane heat conductivity encountered with the use of the flexible graphite layer with the step module were not replicated. Alternatively, active means such as two-phase heat pipes could be used. Implemented completely within a module, they could be used in a manner which would preserve the simplicity and element replaceability aspects that hold attraction for modular approaches.

Where appropriate, RF cabling could be better thermally connected to structure, or replaced with stripline, microstrip, coplanar waveguide, waveguide, or another RF transmission means. Depending on the implementation, these could offer superior thermal performance and reduced RF losses within the module.

With the solar array itself, there are a number of possible areas of improvement for thermal performance. Depending on the ultimately targeted level of solar

concentration, different degrees of additional temperature tolerance could be pursued. A few simple and straightforward improvements suggested by the solar array vendor, SpaceQuest, that could be implemented include using higher melting point solder and higher temperature tolerance RTV or silver epoxy for substrate bonding. Alternatively, a completely adhesiveless approach could be explored; this has been demonstrated by Deployable Space Systems in non-flight prototypes. Using optics to concentrate at the cell level might also be implemented, in either a linear Stretched Lens Array (SLA) fashion as demonstrated by Entech, or using a Fresnel dome or lens concentrator as shown by Semprius. These approaches could offer not only thermal and reduced advantages, but lower costs as well by requiring much smaller photovoltaics. Concentrating sunlight at the cell level is sometimes avoided because it levies tighter array pointing requirements, but this is less of a concern in solar power satellite contexts like SPS-ALPHA, the Integrated Symmetrical Concentrator, and the Modular Symmetrical Concentrator because of the extant optical train. In fact, a higher pointing requirement could be an advantage as it may reduce the intensity variability resulting from variation in orbital position and directly impinging sunlight.

In any of these cases, subscale testing with coupons or small prototypes is recommended prior to implementation at the module level. Several alternative approaches, whether they use different heat spreading techniques, cell architectures, or fabrication approaches, should be carefully instrumented and tested with actual proof articles in realistic vacuum and illumination conditions to check performance before expansion to wider usage. Thermal simulations may not be capable or dependable indicators of the effectiveness of a given approach in practice, though

they should be undertaken in advance regardless to highlight possible shortcomings of a given approach.

Thermal Instrumentation Improvements

Of utmost importance in evaluating the effectiveness of a given thermal management technique is proper instrumentation. Though the prototypes created were monitored with many thermocouples during the course of testing, it became clear that the insights provided by several additional judiciously placed thermal sensors would have offered great value. In particular, no thermocouples were initially placed on the front side of the solar array, as it was perceived these might obstruct light that would otherwise impinge on the cells. Because of this, there was a dependence on the assumption that front side array temperatures would closely track the backside array temperatures. Partially through testing of the step module, it was discovered that this assumption was not valid, particularly at high temperatures. In light of this, some means of monitoring array front side temperatures is warranted. This could be in the form of a thermocouple or thermocouples mounted in the narrow gaps between cells, or perhaps via the embedding of thermocouples behind the cells during the solar panel build process. Attention would need to be paid in either case to possible differences between the thermocouple temperature and the temperature of portions of the array of interest. For instance, once a thermocouple was installed on the front side of the step module array, it was held in place with Hysol TRA-BOND 2115 epoxy, but the surface of this epoxy has different optical properties than both the cells and RTV adhesive used to bond the cells to the panel substrate. As a result, the thermocouple likely read higher temperatures than were present on the cells or RTV.

Another possible means of temperature measurement beyond the use of additional thermocouples or other contact temperature sensors is to use an infrared thermal sensor or infrared thermal imager. For later rounds of step module testing, these remote thermal measurement devices were taken advantage of to correlate front and back panel temperatures. However, they were only usable at ambient pressure because once the vacuum window was put in place, the devices would read the window's temperature rather than the module's. The units used were handheld and thus made it difficult to ensure consistency in the location and precision of temperature measurements. Both the infrared thermal sensor and thermal imager required compensation for the emissivity of the surface being measured to attain more accurate measurements, suggesting that they are a good adjunct source of temperature measurements but should not be relied upon as a sole source. Ideally both contact and remote temperature measurement means should be used together in a consistent, repeatable manner, and if possible with an effective way to use the remote measurement devices inside the vacuum chamber.

Efficiency Enhancement

A key path to resolving the thermal challenges is maximizing efficiency in each layer of the module, to be discussed presently.

While the power electronics in the prototype were highly efficient, the RF chain did not push the state-of-the-art for efficiency at 2.45 GHz. This was partially due to the need to implement a multistage architecture to achieve the required gain. The RF chain efficiency could likely be increased by 10% or more with a more monolithic approach. Similarly, even in the few short years since the commencement of the

project, there have been notable gains in the least efficient element in the sandwich module, the solar cells. Both commercially available space grade cells and cells in the laboratory have since marked efficiency increases, with current performance in excess of 30% and 40% respectively. Potentially promising technologies include space-qualified third generation triple junction cells, rigid/flexible inverted metamorphic multijunction (IMM) cells, concentrating cells, and quantum dot cells. Implementation of a new module leveraging more efficient layers could result in higher performance and fewer thermal challenges.

Additional Module Functionality

This effort deliberately neglected the implementation of a retrodirective beam control system, phase adjustors, and output filtering for simplicity. Each of these would be required in a module in an operational system and should be demonstrated first in a prototype. The addition of this functionality could begin either with electronics or with the antenna, as described above. At the electronics level, the task of maintaining a high level of conversion efficiency could be a challenge. Determining the most effective means and points in the RF chain or chains to apply phase control and amplification would need to be determined. Implementing a suitable output filter to suppress harmonics and the effects of amplified thermal noise to avoid creating radio frequency interference (RFI) could also pose difficulties.

Alternative Sandwich Module Approaches

Further investigation into sandwich module designs that depart from a flat configuration is warranted. Though the step module prototype demonstrated only

limited success, the effort showed the potential of this approach. This concept and its variants should be explored as possible means of enhancing sandwich module thermal performance and improving figures of merit.

Perhaps further afield, sandwich modules that employ a means of transferring power or heat to adjacent modules could be investigated. Power networks to reroute power to optimize transmit array radiation patterns could be employed, though this could also be accomplished via optical routing with judicious reflector design. Modular heat pipes or other assemblable heat transfer methods could be leveraged to move heat from the center of the transmit array to the perimeter where additional heat radiation devices could disperse it, though accommodation should be made for the module replacement strategy. Perhaps heat could be routed around areas where modules are in need of replacement. Communication networks to link modules for relay of states and statuses might be added to optimize array thermal and transmission performance or to ease troubleshooting.

Entire layers of the sandwich could be replaced with alternative conversion means, such as a heat engines for power generation in lieu of photovoltaics, or compact vacuum electronics in place of the solid state amplifier chain. Lasers could be used as an alternative to microwave power transmission, replacing the RF conversion electronics and antenna layers with a laser and optical train. Perhaps solar pumped lasers could be used, avoiding the need for any electrical conversion stages.

Since there does not currently exist a comprehensive design for the concentrating optics envisioned for use with the sandwich module array, work could be done in its development. Alternatively, a gossamer sandwich module under lower sun

concentration could be devised to take advantage of thin-film photovoltaics and ultra-compact RF electronics in an effort to truly push the mass-specific power envelope.

Subsequent research could go in many directions, further illuminating the need for a broad-based series of research campaigns to gain clarity concerning the technological opportunities and limitations associated with prospective solar power satellites.

Appendix A: Microwave Power Transmission

Many researchers and engineers are accustomed to using the Friis transmission equation to model microwave links for communication applications. It relies on far-field assumptions to find the received power, P_r

$$P_r = \frac{P_t A_t A_r}{\lambda^2 D^2} \quad (6)$$

It also assumes that the antennas of the system are correctly aligned in geometry and polarization. A_t and A_r are the areas of the transmit and receive antenna apertures respectively, P_t is the transmitted power, λ is the wavelength of the transmitted power, and D is separation between the two antennas [10]. For communications, it is only necessary to collect enough transmitted energy at the receiver to ensure the signal to noise ratio is sufficient to operate the link to meet the required performance. This is generally only an infinitesimal fraction of the power transmitted. In the case of power transmission, it is desirable to collect a significant portion of the transmitted power, typically in excess of 80%. To accomplish this, antenna aperture sizes must be selected that are quite large relative to the antenna separation and wavelength. Because the Friis transmission equation relies on transmitter and receiver far-field assumptions for determining the collection efficiency at the receiving antenna, it is no longer applicable for this purpose, but in a revised form it can be used to determine transmitted power density. For large apertures, the far field distance is greater than twice the square of the antenna's largest dimension, d , divided by the wavelength

$$D > \frac{2d^2}{\lambda} \quad (7)$$

For the separation between the surface of the earth and geosynchronous orbit (GEO), about 36,000 km, this condition fails for a transmit antenna diameter of 1,500 m and an operating frequency of 2.45 GHz, thus rendering equation (1) inapplicable. The link is more accurately modeled using the methods outlined by Goubau and Schwering [59] with

$$\tau = \sqrt{A_t A_r} / \lambda D \quad (8)$$

where τ is a parameter that relates the system parameters to collection efficiency. Collection efficiency is plotted as a function of τ in Figure 52, and a point is shown to reflect Degenford's experiments [60]. Each τ value has a unique transmitter amplitude taper that maximizes the collection efficiency. Maximum efficiency also requires a phase-calibrated transmitter [59]. The optimum power distribution for the transmit aperture closely resembles the Gaussian distribution [61]. Using the GEO, 1500 m, and 2.45 GHz assumptions above with a 7.5 km diameter receiving area, Equation (8) provides a τ of about 2. Referencing Figure 52, the collection efficiency is greater than 95%.

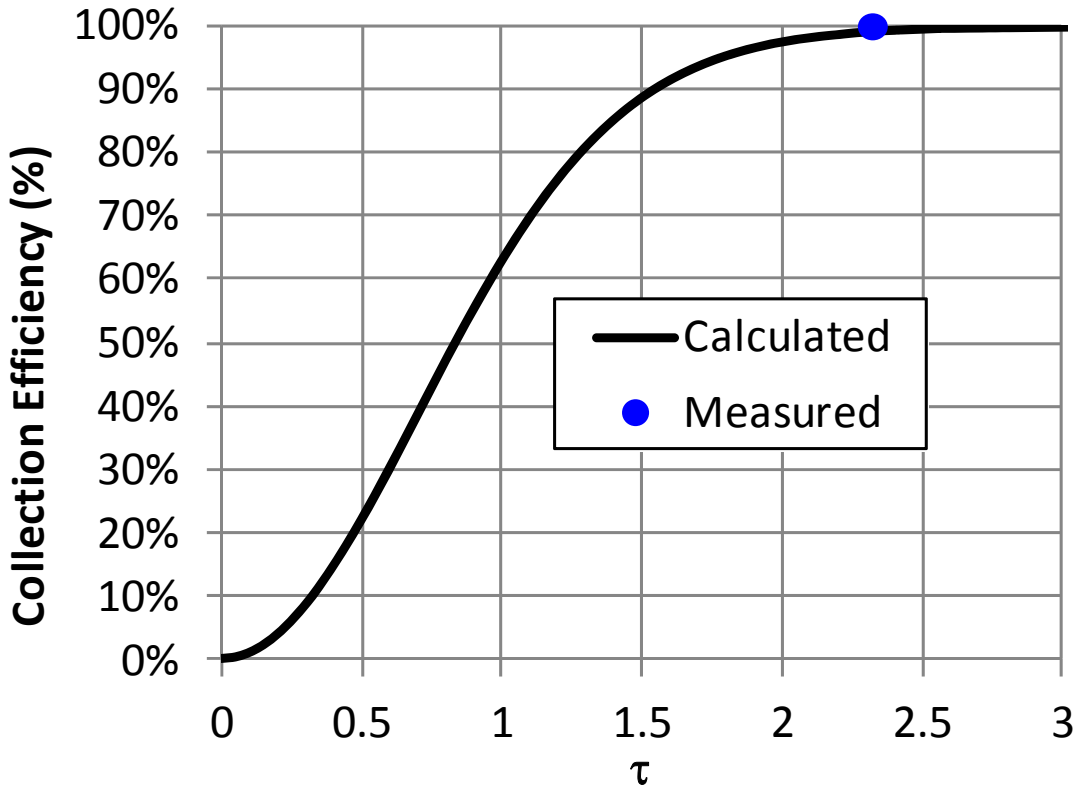


Figure 52. Power collection efficiency as a function of τ with optimum power taper over the transmitting aperture [61].

It may be desirable to limit the power density at the receiver site to meet safety requirements. On the other hand, in military and other applications where the area available for reception is limited, it may instead be necessary to constrain the receiver aperture size. These parameters may be traded with transmit power and wavelength in the system design.

Higher frequencies are attractive to reduce the transmit and receive antenna aperture sizes, but other factors besides link coupling must be considered. These include atmospheric attenuation, desired power density on the ground, and device efficiencies at the selected frequency. Atmospheric and rain attenuation increase

significantly above 10 GHz, resulting in a tradeoff between antenna size and link availability. Figure 53 shows total, water vapor, and dry air clear sky attenuation in dB from sea level at the given surface conditions to zenith (that is, straight up through the entire atmosphere) as a function of frequency [62].

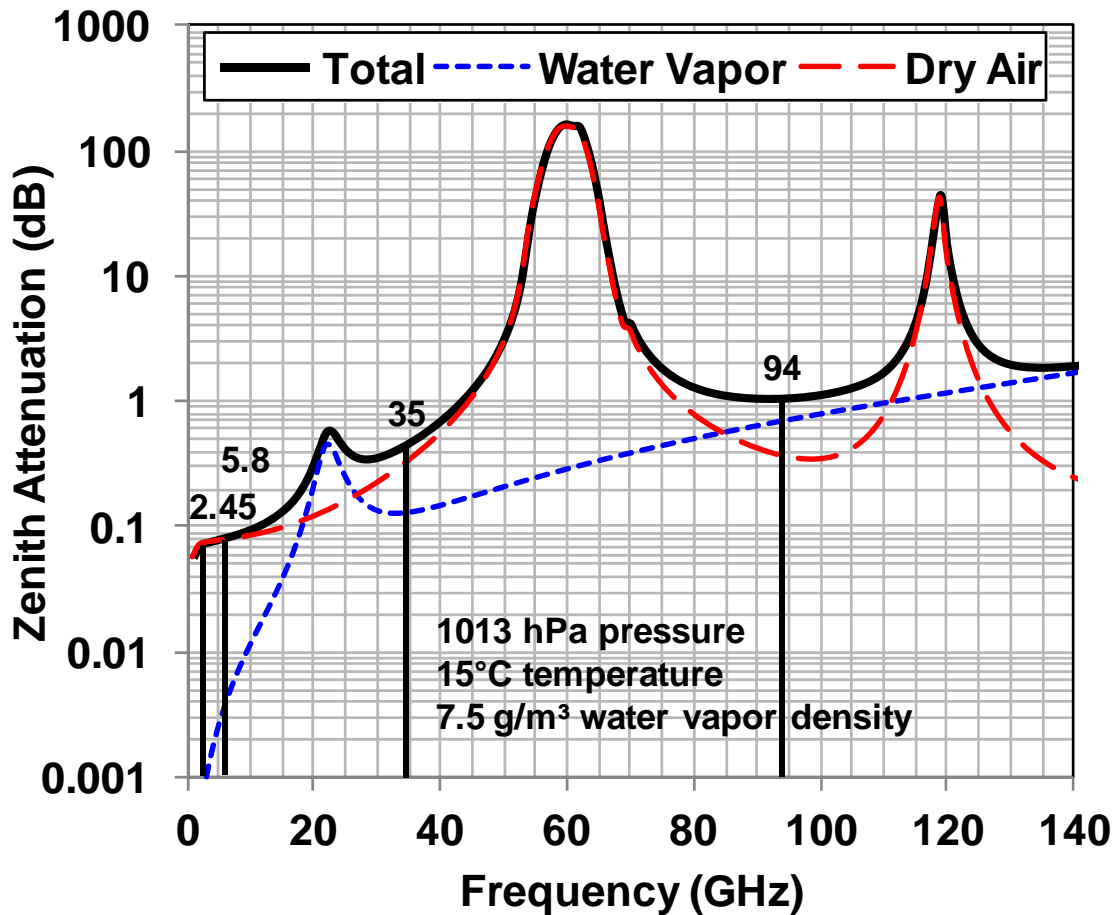


Figure 53. One-way sea level to zenith (straight up through the entire atmosphere) attenuations in clear sky conditions [35].

To date, the most commonly examined frequencies for microwave power beaming for space solar power are 2.45 GHz, 5.8 GHz, 35 GHz, and 94 GHz. The first two have received the most attention, largely by virtue of their being Industrial, Scientific,

and Medical (ISM) designated bands. ISM bands are slots in the spectrum that do not require a license at low power because they were originally conceived as frequencies reserved for spurious microwave emissions from industrial processes [63]. The 35 GHz and 94 GHz frequencies offer smaller aperture sizes, and fall within clear sky atmospheric transmission windows, but device efficiencies are generally lower than for the lower frequencies, and rain attenuation will be greater.

Transmitter Efficiency

For simplicity, this discussion focuses on lower frequency options, and principally 2.45 GHz because of the prevalence and ready availability of devices at this frequency. Table 11 shows a comparison of some possible amplification and DC to RF conversion options. Note that these figures, with the exception of the multiple beam klystron data, represent values from data sheets of mass-produced parts and do not reflect higher efficiencies achieved with experimental devices in the laboratory, which will be discussed momentarily.

Those devices with high input voltages would require high voltage power supplies, the efficiencies of which are not factored in the efficiency stated, though they are generally in excess of 90%.

Table 11. Comparison of selected means of amplification and DC to RF conversion.

Method	GaN SSPA	Magnetron	TWT	MBK
Efficiency	43-70%	44-73%	66-70%	50%*
Mass (kg)	<0.1	0.9-4.3	0.7-3.0	1.0*
Power Output (W)	25-220	900-5,000	20-300	1,000*
Input voltage (V)	28-50	4,000-20,500	5,000-20,000	2,000-4,000*
Manufacturers	Cree, TriQuint	Toshiba, Hitachi	L3, Thales	CCR

SSPA=Solid State Power Amplifier, TWT = Traveling Wave Tube, MBK = Multiple Beam Klystron. Values (except for MBK) taken from data sheets of potential models in the 2-10GHz frequency range, some available from Richardson Electronics. Masses exclude voltage conversion components. *rough estimates

Volumes and densities of systems incorporating each of these means vary and are difficult to compare directly because of variations in supporting electronics, though in general solid state options will tend to be the most compact. Additional options not shown include gyrotrons, klystrons, and extended interaction klystrons [12].

Solid State Power Amplifiers (SSPAs) have recently been encroaching on applications where formerly only traveling wave tube amplifiers (TWTAs) were feasible. SSPAs offer system designers significant benefits and challenges to system integration. Besides being small and lightweight, SSPAs can be a factor in reducing the cost of a system requiring significant power levels. In particular, in an array configuration large numbers of moderately powered devices can be coherently combined to form a large filled array to provide a microwave beam of substantial power. Although gallium nitride (GaN) offers the benefits of higher operating temperatures and power densities over other semiconductors, it also brings challenges that arise from its generally lower gain per stage compared with gallium arsenide (GaAs) and other devices, requiring a multistage architecture.

In the intervening years since the DOE/NASA studies first considered solid state conversion, solid state amplifiers have shown significant performance improvements, and results have been reported by Schmelzer and Long of a GaN HEMT Class F amplifier configuration with greater than 80% power added efficiency (PAE) at 16.5 watts output power [64]. Their results were obtained with commercial Cree transistors operating at 2 GHz on hybrid printed circuit boards. If efficiencies resembling these could be implemented in a conversion module, the task of keeping the junction temperature lower would be simplified. A key point to recognize is that while the efficiency of the single device that Schmelzer and Long was impressive, the level of electronic RF gain likely needed in a conversion module would probably exceed the gain value they achieved by more than 20 dB, depending on the frequency source employed. Similarly, while Yamanaka's group achieved 70% PAE for 7 W output at 5.8 GHz, their gain was only about 10 dB [65]. Note that Yamanaka's effort specifically targeted the SSP application. Recent surveys of progress in GaN illuminate the broad scope of work being done in this area [66].

Rectification at the Receiver

At the receiving site, the incoming microwaves are converted to DC by using a rectenna, a device that combines an antenna, input filters, a rectifying diode, and an output filter. Rectenna efficiencies in excess of 80% have been demonstrated by several authors [67], [68] at 2.4 GHz and 5.8 GHz, and even as high as 91% [61], though not all authors define efficiency in the same way. A functional depiction of a rectenna is shown in Figure 54. For the conversion module prototyping efforts described herein, a receiving rectenna array was not constructed, as the principal

focus of the research is in addressing the issues associated with the transmit module layer integration.

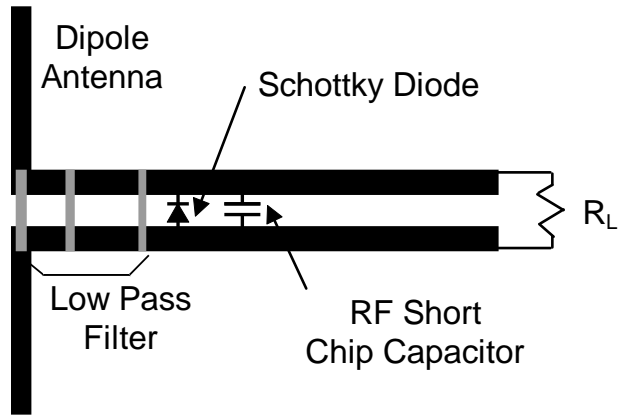


Figure 54. Rectenna components [68].

Rectenna systems have been studied in great depth for many decades, and recent interest in energy harvesting has led to a significant resurgence in work in this field. Microwave power beaming has been demonstrated by dozens of groups around the world since 1963, often to power small aircraft. In 1975, over 30 kW was transmitted across 1.6 km and converted back to DC power with a rectenna efficiency greater than 84% [61]. Brown has described wireless power transmission technology at 2.45 GHz as “ready for use when it is needed [61, pp. 69].”

Appendix B: SPS System Design

Creating a detailed point design of every subsystem inherent in an SPS implementation would require a large team including specialists in many disciplines. For the purposes of this research, it was sufficient to use existing system designs from previous studies, allowing for the possibility that there would almost certainly be some departure from them in a future system. Many of the studies are largely implementation agnostic and focus only on the collection area and parameters of the microwave power transmission system. Compared in Table 12 are designs from the Japanese space agency (JAXA) and the NASA-DOE effort analyzed in conjunction with the International Union of Radio Science study report. The table has been adapted from one that appears in the URSI report.

Table 12: System designs examined by the URSI report [69]

Model	Old JAXA model	JAXA1 model	JAXA2 Model	NASA-DOE model
Frequency	5.8 GHz	5.8 GHz	5.8 GHz	2.45 GHz
Diameter of transmitting antenna (TX)	2.6 km	1 km	1.93 km	1 km
Amplitude taper	10 dB Gaussian	10 dB Gaussian	10 dB Gaussian	10 dB Gaussian
Output power (beamed to earth)	1.3 GW	1.3 GW	1.3 GW	6.72 GW
Maximum power density at TX center	63 mW/cm ²	420 mW/cm ²	114 mW/cm ²	2.2 W/cm ²
Minimum power density at TX center	6.3 mW/cm ²	42 mW/cm ²	11.4 mW/cm ²	0.22 W/cm ²
Antenna spacing	0.75 λ	0.75 λ	0.75 λ	0.75 λ
Power per one antenna (Number of elements)	Max. 0.95 W (3.54 billion)	Max. 6.1W (540 million)	Max. 1.7 W (1,950 million)	Max. 185 W (97 million)
Rectenna Diameter	2.0 km	3.4 km	2.45 km	10 km
Maximum Power density at rectenna	180 mW/cm ²	26 mW/cm ²	100 mW/cm ²	23 mW/cm ²
Collection Efficiency	96.5 %	86 %	87 %	89 %

As a point of reference, FCC [70] and IEEE [71] guidelines on RF exposure limit those in occupation and controlled access environments for frequencies between about 1.5 GHz and 15 GHz to around 5 mW/cm² to 10 mW/cm², averaged over 6 minutes. For the general public or in uncontrolled environments, the limits are about 20% of the occupational and controlled levels. With a 10 dB fall off from the receiver center, the JAXA1 and NASA-DOE models approach the uncontrolled limit at the receiver edge.

References

- [1] S. Fetter, "Space Solar Power: An Idea Whose Time Will Never Come?," in Physics and Society, 33(1), pp 10-11, 2004.
- [2] T. Murphy, "Space-Based Solar Power," *Do the Math* blog, posted on 2012-03-20 at <http://physics.ucsd.edu/do-the-math/2012/03/space-based-solar-power/>, 2012.
- [3] A. Globus, "In Defense of Space Solar Power," from <http://space.alglobus.net/papers/FetterResponse.html>, 2009.
- [4] *Satellite Power System (SPS) FY 79 Program Summary*, DOE/NASA Satellite Power System Concept Development and Evaluation Program, Washington, DC, DOE/ER-0037, 1980.
- [5] D. R. Corson, et al, "Electric Power from Orbit: A Critique of a Satellite Power System," National Academy of Sciences, Washington, DC, ISBN 0-309-03183-4, 1981.
- [6] J. C. Mankins, "A Fresh Look at Space Solar Power: New Architectures, Concepts and Technologies," presented at the 38th International Astronautical Federation, Brighton, England, 1997, Paper IAF-97-R.2.03.
- [7] *Laying the Foundation for Space Solar Power: An Assessment of NASA's Space Solar Power Investment Strategy*, Committee for the Assessment of NASA's Space Solar Power Investment Strategy, Aeronautics and Space Engineering Board, National Research Council, Washington, DC, ISBN: 0-309-07597-1, 2001.
- [8] *Earth & Space-Based Power Generation Systems - A Comparison Study*, Contract No. 17682/03/NL/EC to ESTEC, 2005.
- [9] M. Moria, H. Nagayamab, Y. Saitob, H. Matsumoto, "Summary of studies on space solar power systems of the National Space Development Agency of Japan," in *Acta Astronautica* Vol. 54, 2004, pages 337-345.
- [10] *Report of the URSI Inter-Commission Working Group on SPS*, URSI Inter-Commission Working Group on SPS, 2007.
- [11] *Space-Based Solar Power As an Opportunity for Strategic Security*, Phase 0 Architecture Feasibility Study, National Security Space Office, Washington, DC, Release 0.1, 2007.

- [12] W. N. Johnson, et al., "Space-based Solar Power: Possible Defense Applications and Opportunities for NRL Contributions," Washington, DC, NRL/FR/7650--09-10,179, 2009.
- [13] National Space Society Space Solar Power Library, [Online]. Available <http://www.nss.org/settlement/ssp/library/index.htm>
- [14] J. C. Mankins, "Green Energy from Space Solar Power - The First International Assessment of Space Solar Power: Opportunities, Issues and Potential Pathways Forward," International Academy of Astronautics, 2011.
- [15] P. E. Glaser, F. P. Davidson, K. Csigi, K., *Solar Power Satellites – A Space Energy System for Earth*, West Sussex, England, Praxis Publishing, 1998.
- [16] D. M. Flournoy, *Solar Power Satellites*, SpringerBriefs in Space Development, 2012.
- [17] A. Lindenbaum, "PowerSat Files Patent That Accelerates Viability Of Space Solar Power (SSP) Satellite Systems," PowerSat press release, undated, [Online]. Available http://www.powersat.com/patent_release.html
- [18] Mitsubishi Electric Solarbird Overview [Online]. Available <http://www.mitsubishielectric.com/bu/space/rd/solarbird/index.html>
- [19] U. Wang, "Solaren to Close Funding for Space Solar Power," Greentechmedia December 4, 2009, [Online]. Available <http://www.greentechmedia.com/articles/read/Space-the-Next-Frontier-For-Renewable-Power/>
- [20] M. Reddy, "Energy's final frontier?," INSEAD Knowledge, September 15, 2010, [Online]. Available <http://knowledge.insead.edu/Entrepreneurship-Space-Energy-100917.cfm?vid=464>
- [21] W. Shockley, H. J. Queissner, "Detailed Balance Limit of Efficiency of p-n Junction Solar Cells," in *Journal of Applied Physics*, 32(3), 1961.
- [22] W. Brown, "Beamed Microwave Power Transmission and its Application to Space," in *IEEE Transactions on Microwave Theory and Techniques*, 40(6), pp.1239-1250, Jun1992.
- [23] *The Final Proceedings of the Solar Power Satellite Program Review*, Lincoln, Nebraska, April 22-25, 93 pp., 1980.
- [24] *Reference System Report*, DOE/NASA Satellite Power System Concept Development and Evaluation Program, Washington, DC, DOE/ER-0023, 1978.

- [25] H. P. Davis, *Space-Based Solar Power, An Update*, Solar High Study Group, SolarHigh.Org, August 23rd, 2012.
- [26] J. C. Mankins, "The Promise and the Challenge of Space Solar Power," NASA Headquarters Advanced Systems briefing, pp. 13, 2003.
- [27] J. C. Mankins, "SPS-ALPHA: The First Practical Solar Power Satellite via Arbitrarily Large PHased Array" [Online]. Available http://www.nasa.gov/offices/oct/early_stage_innovation/niac/mankins_sps_alpha.html
- [28] O. E. Maynard, " Solid State SPS Microwave Generation and Transmission Study," NASA CR-3338, Vol. I, Phase II Final Report prepared for MSFC under contract NAS 8-33157, 230 pp., Nov 1980.
- [29] J. McSpadden, J. C. Mankins, "Space Solar Programs and Microwave Wireless Power Transmission Technology," *IEEE Microwave Magazine*, 3(4), pp 52, Dec 2002.
- [30] H. Matsumoto, "Research on solar power satellites and microwave power transmission in Japan," *Microwave Magazine, IEEE* , vol.3, no.4, pp. 36- 45, Dec 2002.
- [31] M. Mori, H. Matsumoto, N. Shinohara, K. Hashimoto, "Solar Power Radio Integrated Transmitter (SPRITZ) Unit for SPS," 2002 URSI General Assembly, poster 1441.
- [32] N. Shinohara, "Beam Control Technologies With a High-Efficiency Phased Array for Microwave Power Transmission in Japan," *Proceedings of the IEEE*, vol.101, no.6, pp.1453, June 2013.
- [33] S. Etani, M. Iwashita, N. Kaya, "Development on the Sandwich Panel for the Practical Solar Power Satellite," in *Proceedings of the 28th International Symposium on Space Technology and Science*, Okinawa, Japan, 2011, Paper No. 2011-q-9s.
- [34] S. Spencer, B. Nguyen, P. Jaffe, "Thermal Analysis of Space-Based Solar Power System Study Photovoltaic DC to RF Antenna Module (PRAM)," in Proceedings of the 10th Annual International Energy Conversion Engineering Conference, Atlanta, GA, 2012, pp. 636.
- [35] P. Jaffe, J. McSpadden, "Energy Conversion and Transmission Modules for Space Solar Power," *Proc. IEEE*, vol.101, no.6, pp.1424-1437, June 2013.

- [36] Jaffe, P., Nurnberger, M., Brown, M., “THERMALLY EFFICIENT POWER CONVERSION MODULES FOR SPACE SOLAR POWER,” U. S. Patent Application 20130099599, Apr. 25, 2013.
- [37] P. Jaffe, et al, “Sandwich Module Prototype Progress for Space Solar Power,” in *Acta Astronautica*, accepted, to be published.
- [38] Spectrolab datasheet, “28.3% Ultra Triple Junction (UTJ) Solar Cells,” [Online] Available <http://www.spectrolab.com/DataSheets/cells/PV%20UTJ%20Cell%205-20-10.pdf>
- [39] P. Jaffe, J. Hodkin, F. Harrington, “Development of a Sandwich Module Prototype for Space Solar Power,” in *Proceedings of the IEEE Aerospace Conference*, Big Sky, MT, 2012.
- [40] Jaffe, P., Person, C., Nurnberger, M., Nguyen, B., Scheiman, D., Han, A., Stewart, G., Moses, M., “Space Solar Power Sandwich Module Testing and Performance Characterization,” in *Proceedings of the 64rd International Astronautical Congress*, Beijing, China, 2013, Paper No. IAC-13.C3.2.1, to be published.
- [41] D. Scheiman, private communication.
- [42] A. Han, “IV Curve and Beam Mapping Report for Step Module”, unpublished.
- [43] Rocky Mountain Instrument Co., [Online] Available <http://rmico.com/technical-notes/transmission-curves/>
- [44] [Online] Available http://en.wikipedia.org/wiki/File:Solar_Spectrum.png
- [45] B. Nguyen, “PRAM_Thermal_WeeklyMeeting_04242012.ppt”, unpublished.
- [46] P. Jaffe, D. Scheiman, K. Hemmendinger, “Testing a Small Energy Conversion Module Under Multiple Suns in Vacuum,” *Journal of the Institute of Environmental Sciences and Technology*, accepted, to be published.
- [47] P. Jaffe, J. Hodkin, F. Harrington, “Development of a Sandwich Module Prototype for Space Solar Power,” IEEE Aerospace Conference, Big Sky, UT, 2012, pp 4.
- [48] W. Short, D. J. Packey, T. Holt, “A Manual for the Economic Evaluation of Energy Efficiency and Renewable Energy Technologies,” NREL/TP-462-5173, Mar. 1995.
- [49] M. K. Macauley, J. F. Davis, “An Economic Assessment of Space Solar Power as a Source of Electricity for Space-Based Activities,” Resources for the Future Discussion Paper 01–46, Oct. 2001.

- [50] I. McNally, M. Ceriotti, G. Radice, “Systems Analysis of the Sandwich Solar Power Satellite,” in *Proceedings of the 63rd International Astronautical Congress*, Naples, Italy, 2012, Paper No. IAC-12.C3.1.9.
- [51] D. L. Akin, “A Systems Analysis of Space Industrialization,” D.Sc. dissertation, Massachusetts Institute of Technology, United States, 1981.
- [52] P. A. Curreri, M. K. Detweiler, “A Contemporary Analysis of the O’Neill – Glaser Model for Space-based Solar Power and Habitat Construction,” NSS Space Settlement Journal, Dec. 2011.
- [53] SpaceX website, [Online]. Available: <http://www.spacex.com/about/capabilities>
- [54] “Levelized Cost of New Generation Resources in the Annual Energy Outlook 2012,” U.S. Energy Information Administration, 2012.
- [55] *More Capable Warfighting Through Reduced Fuel Burden*, Report of the Defense Science Board, p.19, May 2001.
- [56] M. Schwartz, K. Blakeley, R. O'Rourke, “Department of Defense Energy Initiatives: Background and Issues for Congress,” CRS Report R42558, p.6-7, Jun. 2012.
- [57] *Energy Information Administration/Household Vehicles Energy Use: Latest Data & Trends*, p.160, 2005.
- [58] *NRL Major Facilities 2008*, (2008).
- [59] C. Okress, *Microwave Power Engineering*, Academic Press: New York, vol. 1, 1968, pp. 241-255.
- [60] J. E. Degenford, M. D. Sirkis, W. H. Steier, “The Reflecting Beam Waveguide,” *IEEE Transactions on Microwave Theory and Techniques*, 12(4), pp. 445- 453, Jul 1964.
- [61] W. C. Brown, “Beamed Microwave Power Transmission and its Application to Space,” *IEEE Transactions on Microwave Theory and Techniques*, pp. 1241, Jun. 1992.
- [62] Recommendation ITU-R P.676-9, “Attenuation by atmospheric gases,” 2012. Available: <http://www.itu.int/>
- [63] “The ISM Bands – A Review of the Essentials,” Signal Processing Group, Inc., undated PDF from:

[Online]. Available: <http://signalpro.biz/ism1.pdf>

[64] D. Schmelzer, S. Long, "A GaN HEMT Class F Amplifier at 2 GHz With >80% PAE," in *IEEE Journal of Solid-state Circuits*, 42(10), 2007.

[65] K. Yamanaka, Y. Tuyama, H. Ohtsuka, S. Chaki, M. Nakayama, Y. Hirano, "Internally-matched GaN HEMT High Efficiency Power Amplifier for Space Solar Power Stations," in *Proceedings of Asia-Pacific Microwave Conference 2010*, Paper No. WE3A-1.

[66] R. S. Pengelly, S. M. Wood, J. W. Milligan, S. T. Sheppard, W. L. Pribble, "A Review of GaN on SiC High Electron-Mobility Power Transistors and MMICs," *IEEE Transactions on Microwave Theory and Techniques*, 60(6), pp. 1764, Jun 2012.

[67] W. C. Brown, J. Triner, "Experimental Thin-film, Etched-circuit Rectenna," 1982 IEEE MTT-S International Microwave Symposium Digest, 1982, pp. 185.

[68] J. McSpadden, L. Fan, K. Chang, "Design and Experiments of a High-Conversion-Efficiency 5.8-GHz Rectenna," *IEEE Trans on Microwave Theory and Techniques*, 46(12), pp. 2053-2060, Dec 1998.

[69] *Report of the URSI Inter-Commission Working Group on SPS*, URSI Inter-Commission Working Group on SPS, pp. 13, 2007.

[70] R. Cleveland, D. Sylvan, J. Ulcek, "Evaluating Compliance with FCC Guidelines for Human Exposure to Radiofrequency Electromagnetic Fields", Federal Communications Commission, OET BULLETIN 65, Edition 97-01, 1997.

[71] *IEEE Standard for Safety Levels with Respect to Human Exposure to Radio Frequency Electromagnetic Fields, 3kHz to 300 GHz*, IEEE C95.1-2005, 2005.